Pardee Dam – Foothills Fault System Study,

Amador and Calaveras Counties, CA

Prepared for:
East Bay Municipal Utility District
375 11th Street
MS 610
Oakland, CA 94607

Prepared by:
Lettis Consultants International, Inc.

January 31, 2020

January 31, 2020

Mr. Tom Boardman, P.E., G.E.
East Bay Municipal Utility District
375 11th Street, MS 610
Oakland, CA 94607

SUBJECT: Pardee Dam – Foothills Fault System Study, Amador and Calaveras Counties, CA
LCI Project No. 1772.000

Dear Mr. Boardman,

Lettis Consultants International, Inc. (LCI) is pleased to submit our fault rupture hazard and seismic source characterization report for the East Bay Municipal Utility District's Pardee Dam, located in Amador and Calaveras Counties, California. This report includes the findings from a paleoseismic trenching study of the Waters Peak fault, probabilistic fault displacement hazard analysis (PFDHA), and an updated seismic source characterization for the Foothills fault system in the vicinity of Pardee Dam. Please do not hesitate to contact us with any questions or comments that you may have regarding this report. We can be reached at (925) 482-0360.

Respectfully,
Lettis Consultants International, Inc.

CERTIFIED ENGINEERING GEOLOGIST
JOHN N. BALDWIN
NO. 2167
EXP 4/21
STATE OF CALIFORNIA

John N. Baldwin, C.E.G. 2167, Senior Principal Geologist
baldwin@lettisci.com

Stephen Thompson, C.E.G. 2701, Principal Geologist
thompson@lettisci.com

Brian Gray, C.E.G. 2692, Senior Geologist
bgray@lettisci.com

CERTIFIED ENGINEERING GEOLOGIST
BRIAN GRAY
NO. 2692
EXP 6/20
STATE OF CALIFORNIA

TABLE OF CONTENTS

LIST OF TABLES

LIST OF FIGURES

LIST OF PLATES

APPENDICES

ABBREVIATIONS AND ACRONYMS

CGS	California Geological Survey
DSHA	Deterministic Seismic Hazard Analysis
DSOD	California Division of Safety of Dams
EBMUD	East Bay Municipal Utility District
LCI	Lettis Consultants International, Inc.
Jgo	Gopher Ridge volcanics
Jss	Salt Springs Slate
PFDHA	Probabilistic fault displacement hazard analysis
PSHA	Probabilistic seismic hazard analysis
USACE	United States Army Corps of Engineers
WPF	Waters Peak fault

1.0 PURPOSE AND SCOPE

This report has been prepared by Lettis Consultants International, Inc. (LCI) for East Bay Municipal Utility District (EBMUD) and presents the findings of a seismic hazard investigation of the Foothills Fault System in the vicinity of Pardee Dam in Amador and Calaveras Counties, California (Figure 1-1). The purpose of this project closely follows recommendations developed as part of a recent Five-Year FERC Part 12D Safety Recommendation Report (Rizzo, 2018) that recommended EBMUD evaluate the surface-fault rupture and seismic hazard posed by nearby faults at Pardee Dam. Characterization of the surface fault rupture hazard posed by the Waters Peak fault is a primary focus of this study, as well as re-evaluating seismic source parameters for local faults that comprise the Foothills fault system. These data are then used to update and revise EBMUD's existing Haz45 seismic source model.

Previous studies have mapped the Waters Peak fault about 550 feet (~170 m) downstream of Pardee Dam and 200 feet (61 m) downstream of the South Spillway (ESA, 1992; HCG, 1998). Prior trenching and geologic studies on the Waters Peak fault performed 8 km south of Pardee Dam (Waters Peak South trench site; United States Army Corps of Engineers [USACE], 1995) provide direct evidence of late Cenozoic faulting and displacement of alluvial deposits interpreted as late Pleistocene in age, with a cumulative Quaternary displacement of 1 to 2 m. Based on the findings of the USACE (1995) study, it was concluded that the Waters Peak fault is not capable per USACE criteria, and also meets the criteria for inactivity outlined in the California Department of Safety of Dams (DSOS) document prepared by Fraser (2001). This latest study performed by LCI re-evaluates the previous findings of USACE (1995) as it pertains to the Waters Peak fault, and provides updated and revised fault displacement and seismic source parameters for multiple faults comprising the Foothills fault system.

1.1 SCOPE OF WORK

The scope of work performed by LCI represents a comprehensive earthquake hazard investigation of late Cenozoic faults within the Foothills fault system (FFS) near Pardee Dam and addresses recommendations from the Five-Year FERC Part 12D Safety Recommendation Report (Rizzo, 2018) to:

(1) evaluate the potential for permanent rock surface displacement caused by rupture of nearby faults, including the Waters Peak fault (WPF) mapped directly downstream of Pardee Dam;
(2) perform a probabilistic fault displacement hazard analysis (PFDHA) for Pardee Dam that includes both primary and secondary fault displacement;
(3) develop seismic source model parameters for the Waters Peak and other nearby fault sources—especially the Ione fault—that may be used as input for deterministic and probabilistic seismic hazard analyses (DSHA and PSHA); and
(4) integrate updated seismic ground motions based on the updated seismic source model for planned future seismic slope stability studies at both Pardee Dam and Camanche Dam.

Of the above hazard-related tasks, LCI has completed Tasks (1) through (3). The results of Tasks 1 to 3, as well as a description of the updated seismic source model are included in this technical report for Pardee Dam. EBMUD will complete Task 4 and the updated seismic ground motions at a later date. The seismic hazard analysis of Pardee Dam consisted of the following scope of work:

- Data Review and Work Plan Development
- Field Work and Surface Fault Rupture Study
- Seismic Source Characterization
- Probabilistic Fault Displacement Hazard Analysis
- Areal/Background Seismic Source Zone Model
- Final Technical Report

1.1.1 Data Review and Work Plan Development

LCI collected, compiled and reviewed local and regional published and unpublished geological, geotechnical, and seismological data available from the U.S. Geological Survey (USGS), California Geological Survey (CGS), USACE, EBMUD, Jackson Valley Irrigation District (JVIA), California Division of Safety of Dams (DSOD), and other sources (e.g., Pacific Gas & Electric [PG&E]). The detailed literature search was used to develop a geologic model for Pardee Dam and its vicinity, augmented by pertinent geospatial data, such as satellite imagery, ground-based photographs, historical stereo-paired aerial photography, previous geologic maps, and existing LiDAR-based topographic data (from EBMUD and Calaveras County). LCI also collaborated with CGS geologists, Peter Holland and Janis Hernandez, who are actively mapping and updating the geology of the Valley Springs, Ione, Jackson, and Wallace 7.5-minute quadrangles that comprise much of the Pardee Dam study area (Figures 1-1 and 1-2).

As part of the office-based analysis, LCI prepared and analyzed a longitudinal topographic profile of the Miocene Mehrten and Oligocene Valley Springs Formations to reassess both the rate and magnitude of long-term displacement across faults in the study area (Figure 1-3). The topographic profile was developed near the alignment of an earlier topographic profile (Profile 31) compiled by Page and Sawyer (2001). The surface of a 28.9 Ma tuff within the Valley Springs Formation was mapped and projected across faults comprising, in part, the Foothills fault system using a 1-m-LiDAR-based DEM available for Calaveras County (FEMA, 2013). The profile was used to constrain vertical offsets of the surface of the flow from which to estimate slip rates for faults intersecting the profile.

1.1.2 Local and Site-Specific Geologic Reconnaissance

LCI conducted field reconnaissance of the Waters Peak fault, as well as other regional faults during multiple visits in April 2019. An initial visit was conducted to perform geomorphic and geologic mapping, evaluate the location and width of the Waters Peak fault relative to existing published and unpublished mapping, coordinate regional geologic mapping with CGS geologists

actively working in the area, and locate potential paleoseismic trench sites (e.g., Sites 1 through 6). The field reconnaissance focused on compiling and augmenting data on the Waters Peak and other nearby late Cenozoic faults (including the Ione, Youngs Creek, Haupt Creek, Devils Gate, and Poorman Gulch faults), with the intent purpose to develop information useful for the seismic hazard analysis. From this information, LCI developed fault source parameters for input to DHSA and PSHA (such as evidence for activity, fault location, style of faulting, geometry, slip rate, and magnitude characterization).

Field reconnaissance was performed locally north and south of Pardee Dam along the Waters Peak fault to collect additional subsurface information to aid in selecting a trench site(s) from Sites 1 through 6. Site-specific geologic and geomorphic maps were developed and supplemented with hand-augered borehole information. The geologic reconnaissance was performed by LCI geologists, John Baldwin (CEG), Brian Gray (CEG), and Sarah Smith and is documented in LCI (2019).

1.1.3 Paleoseismic Investigation of the Waters Peak Fault

LCI conducted a paleoseismic fault trenching investigation of the Waters Peak fault during July and August 2019. Three trenches (LCT-T1 to -T3) were excavated across the Waters Peak fault. The primary goal of the trenching study was to develop data on fault activity, displacement per event, recurrence, width of deformation, fault orientation, and sense of slip for input to a subsequent PFDHA. In addition, LCI's paleoseismic investigation also evaluated the results from previous paleoseismic studies performed by the USACE (1995) at their Waters Peak North and South Sites (see Section 3.1 for a summary), and their conclusion that the Waters Peak fault is inactive. Paleoseismic trenching was performed by LCI geologists John Baldwin, Brian Gray, Chris Bloszies, Sarah Smith, and Mark Szymanski, with technical peer review completed by Dr. William Lettis of LCI and Dr. David Schwartz (retired USGS). In addition, a trench review was performed for the larger paleoseismic community and local public agencies (USACE, CGS, Department of Water Resources, and PG&E). The findings of the trenching study are presented in Section 4.

1.1.4 Probabilistic Fault Displacement Hazard Analysis (PFDHA) of the Waters Peak Fault

LCI performed a PFDHA of the Waters Peak, Ione, and Devils Gate faults in the vicinity of Pardee Dam that included data developed from a review of regional and local geologic maps, office-based analysis of existing fault information from Pardee Dam, as well as results developed from the trenching study. The PFDHA included detailed characterization of the Waters Peak fault and selection of fault displacement prediction models consistent with site geologic conditions. The general fault source characterization, which includes the preferred location and geometry of the Waters Peak fault and its magnitude-recurrence relationship, is identical to the characterization developed for the ground motion hazard analysis (PSHA). In addition, the source characterization for the Waters Peak fault for the PFDHA includes a description of the location uncertainty based on detailed mapping of the site area and review of empirical models of aleatory principal fault location uncertainty (e.g., Chen et al., 2013).

Possible locations of secondary (also called “distributed”) faulting were also considered, such as shear and joint discontinuities, prominent foliations, and zones of potential weakness where secondary displacement could be localized. The PFDHA was performed by Dr. Steve Thompson, Dr. Arash Zandieh, and Nora Lewandowski, with support from John Baldwin and Brian Gray. The results of the PFDHA are presented in Section 6.3.

1.1.5 Regional Seismic Source Characterization

Two types of seismic sources were considered in the update of the seismic source model for Pardee Dam: (1) fault sources, and (2) areal source/background source zones. Fault sources represent sources of earthquakes from known, active and conditionally active faults, and are modeled as three-dimensional surfaces. Fault sources are characterized based on their geometry, style of faulting, and earthquake recurrence (magnitude-frequency relationship). Areal (background) source zones account for earthquakes from unknown or unspecified faults, and are modeled as volumes of crust that have similar styles of faulting, maximum earthquake magnitudes, seismogenic thicknesses, and magnitude-frequency relationship. In this source model, the uniformity or non-uniformity of the magnitude-frequency relationship within each areal source zone is a source of uncertainty. The seismic source characterization of local fault sources (within 10 km of Pardee Dam) are described in Section 5.0, and include: Waters Peak – Green Springs Run, Devils Gate, Ione, Youngs Creek – Bowie Flat, Haupt Creek, Poorman Gulch – Rawhide Flat, and Slate Creek. The background source zone model is presented Appendix C. The regional seismic source characterization was completed by Dr. Steve Thompson and Sarah Smith with support from John Baldwin and Brian Gray.

2.0 REGIONAL GEOLOGIC AND TECTONIC SETTING

Pardee Dam is located in the Mokelumne River watershed in the western foothills of the central Sierra Nevada, a broad north-northwest trending mountain range that extends for more than 400 miles in eastern California. Much of the western flank of the Sierra Nevada is composed of Paleozoic and Mesozoic metamorphic rocks that extend westward beneath the Great Valley, and represent the vestiges of island arc terranes that were accreted to the North American continent along ancient subduction zones. Tertiary volcanic flows and volcaniclastic rocks overlie the metamorphic rocks sporadically throughout the western margin of the range front and form broad, accordant divides between the major west-flowing rivers.

The Mokelumne River within the vicinity of Pardee Dam traverses Paleozoic and Mesozoic terranes that are collectively referred to as the western Sierra Nevada Foothills Metamorphic Belt (SNFMB) (Snow and Scherer, 2006)(Figure 1-1). These terranes were originally described by Clark (1964) and form relatively continuous, northwest-trending blocks of late Paleozoic-Mesozoic metamorphic rocks that are typically bounded by east-dipping Mesozoic faults. These terranes represent fragments of subduction zone complexes, oceanic crust (ophiolites), and island arcs. Primary bedding and foliation within the metamorphic rocks generally strike north-northwest, parallel to the trend of the metamorphic belt, and dip steeply to the east. Pardee Dam lies generally along the western margin of the SNFMB. The dam and reservoir are primarily underlain by the SNFMB rocks consisting of the Jurassic Salt Springs Slate and Jurassic Gopher Ridge Volcanics (Wagner et al., 1981; Holland, et al., 2015; Holland and O'Neal, 2019)(Figure 1-1). As these rocks are not wholly in fault contact with adjacent rocks, they are not technically considered to be a distinct lithotectonic terrane (Edelman and Sharp, 1989; Snow and Scherer, 2006). The Jurassic rocks are unconformably overlain by sequences of Tertiary volcanic, volcaniclastic, and sedimentary rocks (Wagner and Saucedo, 1990). In several places, northwest-striking faults offset the Tertiary and younger rocks, indicating reactivation of Mesozoic faults in late Cenozoic time (Bateman and Wahrhaftig, 1966; Woodward Clyde Consultants [WCC], 1977; 1978; Page and Sawyer, 2007).

2.1 FOOTHILLS FAULT SYSTEM

The northwest-striking Mesozoic Foothills fault system is the dominant structural feature of the western Sierra Nevada foothills, and consists of two primary, subparallel fault zones: the Melones (east) and Bear Mountains (west) fault zones (Clark, 1960). Collectively, these faults are referred to as the Foothills fault system, a suite of steeply east-dipping, north- to northwest-striking faults that bound the western flank of the Sierra Nevada (Clark, 1960). Several studies show that portions of these fault zones have been reactivated during the Cenozoic as normal or normal-oblique faults in the current tectonic regime (Woodward-Clyde Consultants, 1978; Bryant, 1983; Page, 1994; USACE, 1995; Page and Sawyer, 2007; Jennings and Bryant, 2010). These faults are thus subject to scrutiny as sources of seismic and fault rupture hazards that need to be evaluated and considered for hazard assessments of critical facilities such as dams (Fraser, 2001).

In the vicinity of Pardee Dam, the Foothills fault system consists of the Melones fault zone (Haupt Creek, Devils Gate, and Poorman Gulch faults to the east) and the Bear Mountain fault zone (Ione, Waters Peak, and Youngs Creek faults to the west) (Clark, 1960). These fault zones are up to 5 km wide and are developed mainly within rocks of ophiolitic origin. Pardee Dam and Reservoir are intersected by, or are in relatively close proximity to, multiple fault traces associated with both the Bear Mountain fault and Melones fault zones (Figure 1-1). Segments of the Foothills fault system have been reactivated since the Late Miocene to Pliocene with onset estimated approximately 3 to 7 Ma, a period of time temporally coincident with interpreted late-stage uplift and westward tilting of the Sierra Nevada (e.g., Unruh, 1991; Zandt et al., 2004; Wakabayashi, 2013; Wakabayashi and Kemp, 2015). The closest reaches of the Mesozoic Melones and Bear Mountain fault zones to Pardee Dam that exhibit clear evidence for late Cenozoic reactivation are based on vertically displaced Miocene to Pliocene volcanic flows and fault trenching (Busby et al., 2008; USACE 1995). Late Cenozoic faults that offset the Miocene-aged Valley Springs and Mehrten Formations in the vicinity of Pardee Dam include the Waters Peak, Youngs Creek, Haupt Creek and Poorman Gulch faults along the Bear Mountains fault zone (WCC, 1978; HCG, 1998) (Figure 1-1). These faults vertically offset the surface of these volcanic flows and deposits, and are interpreted as steeply east-dipping, down-to-the-east normal faults (WCC, 1978) with a possible dextral (right-lateral) slip component (HCG, 1998). Extensive paleoseismic investigation by Woodward-Clyde Consultants (WCC; 1978) and USACE (1995) revealed that a soil horizon, referred to as the “paleo B” horizon, is commonly deformed along some of these fault segments. This soil horizon is estimated to have formed approximately during the mid to late Quaternary (likely prior to 100 ka). If this age determination is correct, then some of these fault segments may have been active in late Quaternary time.

2.2 Bedrock Geology

As noted above, rocks of the SNFMB (Snow and Scherer, 2006) are comprised of fragments of subduction complexes, oceanic crust (ophiolites), and island arcs that in the vicinity of Pardee Dam include primarily the Salt Springs Slate and the Gopher Ridge Volcanics (Holland and O’Neal, 2019; Holland et al., 2015). These rocks are locally overlain by Tertiary volcanics, volcaniclastics, and intervening clastic stratigraphy. In the study area, the Jurassic Salt Springs Slate (Jss) is the predominant unit, comprised of primarily slate with lesser units of sandstone, tuff, and conglomerate. The Salt Springs Slate is best exposed in Pardee Dam spillway (Figure 1-2). Here, the unit is comprised of intensely foliated black to dark gray slate with foliation that dips steeply east. Where freshly scoured, the slate is very hard and resistant to erosion. Along the steep margins of the bedrock spillway, the steep foliation facilitates foliation plane failure where foliation planes project downward and out-of-slope into the spillway (west [left] side of spillway). Flexural toppling mechanisms are also prevalent where foliation dips away from the spillway along the eastern (right) margin. Where in fault contact with Gopher Ridge Volcanics along the WPF, the slate displays apparent ductile deformation/mylonitization, indicating the fault zone now exposed at the surface primarily formed at a depth of several kilometers or more. Local outcrops of the Salt Spring Slate north and south of Pardee dam along Stony Creek Road and at Site 6 expose weakly metamorphosed sandstone and/or tuff interbeds that are whitish in color,

variably resistant to erosion, and have highly variable joint and/or foliation spacing. When partially weathered, the metasandstone and metatuff interbeds can be difficult to distinguish from weathered Gopher Ridge Volcanics (Jgo). Locally, Jss seams are present within the larger Jgo units, as mapped by ESA (1992) in the intervening bedrock between Pardee Dam and the south spillway and noted by Louderback (1928) as part of the dam foundation report. These linear slate bands near the dam and spillway locally termed phyllite by ESA (1992). Louderback (1928; as summarized by ESA, 1992) notes the 15- to 18- ft. thick seam observed in the foundation includes a narrow zone of persistent gouge within the slate, along with bands of quartz and volcanic lenses. Our observations of the phyllite (Jss) between the dam and spillway indicate it is texturally similar to other weathered outcrops of Jss. Based on the lack of associated geomorphology, no special attention or consideration was given to the phyllite during the paleoseismic study or subsequent PFDHA.

As mapped by Holland and O'Neal (2019) and Holland et al. (2015), the Gopher Ridge Volcanics (Jgo) extend both northwest and southeast of Pardee Dam and are locally in fault contact with the Salt Springs Slate along the WPF. The extent of this bedrock fault juxtaposition includes the Pardee Dam tail race and spillway, as well as south to paleoseismic trench Site 5 (Figure 1-2). The Gopher Ridge volcanics are weakly metamorphosed, whitish gray in color, and intensely foliated. Where eroded in the spillway, exposures of fresh rock include conglomerate interbeds comprised of coarse gravel to cobble sized volcanics. Foliation and jointing within the Gopher Ridge volcanics is generally more irregular than that observed in the adjacent slate. Where exposed to soil forming processes, the Gopher Ridge Volcanics produce a distinctive reddish brown soil (as exposed in paleoseismic trench LCI-T1 from this study).

The Oligocene to middle Miocene Valley Springs Formation unconformably overlies the older SNFMB rocks in the southern part of the study area, although not within 3 km of Pardee Dam or near the LCI paleoseismic trench sites (Figure 1-1). The Valley Springs Formation is comprised of tuffaceous sandstone, siltstone, and conglomerate with interbedded tuff. The Valley Springs Formation generally filled paleo topographic lows, such as stream valleys and basins, similar to the Mehrten Formation (described below), and is reflective in the map pattern and regional distribution of the formation. Several of the tuff beds have been radiometrically dated with ages of 28.9, 25.2, and 22.9 Ma for the Campbell Creek (aka Castle Rock), Nine Hill, and Central Hill members, respectively (Holland and O'Neal, 2019; Holland et al., 2015). The tuffs are readily recognizable as ledge-formers and thus are useful strain gauges for topographic profiles utilizing LiDAR-based digital elevation models. Coupled with radiometric dates, tuffs within the Valley Springs Formation are primary targets for assessing both long-term displacement and slip rate.

Locally overlying the Jurassic Salt Springs Slate, Gopher Ridge Volcanics, and Oligocene to Miocene Valleys Springs Formation is the mid Miocene Mehrten Formation comprised of andesite-rich conglomerate, tuff, sandstone, lahars, fan deposits, and interbedded lavas. The type section of the Mehrten Formation is located adjacent to Camanche Reservoir, about 10 km west of Pardee Dam (Figure 1-1). The Mehrten Formation is thought to be the volcanic representation of Pacific-North America plate convergence, prior to the northward passing of the

Mendocino triple junction during the late Miocene. The distribution of the Mehrten deposits in the study area east of the Waters Peak fault is interpreted to mimic the locations of former paleochannels and topographic lows that were filled by the volcanic flows. This "inverted topography" is a function of the Mehrten Formation being generally more resistant to erosion than the adjacent Jurassic bedrock. West of the WPF, near Camanche Reservoir, the Mehrten Formation is broadly distributed (O'Neal et al., 2015) and may be more representative of laterally extensive alluvial fan deposition (i.e. piedmont/bajada).

2.3 PLIO-PLEISTOCENE STRATIGRAPHY AND SOIL CHRONOLOGY

Surficial deposits identified to the north and south of Pardee Dam and in the immediate vicinity of the paleoseismic sites located along the Waters Peak fault (this study; USACE, 1995) are generally alluvial channel, terrace, and fan deposits associated with small ephemeral drainages, and localized slope-derived colluvial deposits. Generally, these localized deposits are associated with deposition within the present geomorphic framework and contain material that is sourced locally from older alluvial deposits, or directly from underlying metamorphic, metavolcanic, and volcanic bedrock. An older sequence of alluvial deposition is reflected by the pre-Quaternary gravels of the Laguna Formation that unconformably overlie the Mehrten Formation. This unconformable relationship is exposed along Sandretto Rd. to the south of Pardee Dam in the vicinity of paleoseismic Site 6 and consists of well-rounded fine to coarse cobbles, gravel and sand (Figure 1-2). The Laguna Formation represents the only instance of widespread (regional) late Cenozoic alluvial deposition in the vicinity of the dam and paleoseismic sites. Although no definitive age is available for the Laguna Formation, the composition of predominantly high-silica clasts (quartzite) sourced from Sierra Nevada granitic and SNFMB rocks in the vicinity of Site 6 is consistent with the descriptions of 3-4 Ma gravel beds within the Laguna Formation exposed along the Merced River (Marchand and Allwardt, 1981). Erosion of Laguna Formation gravel south of Site 6 has remobilized these rounded exotic clasts, many of which are now incorporated within the Pleistocene-Holocene alluvium and colluvium deposited within the linear valley west of Sandretto Road.

Soil-stratigraphic correlations made as part of this and previous studies conducted in the Sierra Nevada foothills and in the vicinity of Pardee Dam (Marchand and Allwardt, 1981; USACE, 1995; WCC, 1978; Page and Sawyer, 2007) were focused on pedogenic development of the alluvial and colluvial deposits represented by the Laguna Formation and younger deposits. In total, these prior studies have characterized multiple distinct periods of depositional quiescence marked by regionally extensive soil formation (paleosols). We summarize the diagnostic pedologic criteria, stratigraphic position, and inferred age of key paleosols relevant to the paleoseismic trenching study in the following subsection.

2.3.1 Summary of Sierra Nevada Foothills Soil Chronology

The age assessment of late Pleistocene soil-bearing deposits encountered in the vicinity of Pardee Dam and LCI trenches relies on a long history of prior work which attempted to (1) identify

and differentiate distinct periods of colluvial and alluvial deposition, and (2) establish a relationship between the degree of soil development and the age and duration of soil formation within alluvial and colluvial deposits (WCC, 1978; Swan and Hanson, 1977; Borchardt et al., 1980; Harden and Marchand, 1979; Harden and Marchand, 1980; Marchand and Allwardt, 1981; Harden and Taylor, 1983; USACE, 1995; PG&E, 2007). These past studies suggest that periods of colluviation and alluviation in the western Sierra Nevada foothills are associated with glacial intervals, whereas subsequent depositional hiatuses and soil formation are linked to interglacial climates (Swan and Hanson, 1977; Harden and Marchand, 1980). Prior studies detail the soil chronosequence for the Sierra Nevada foothills which allows for the correlation of soils observed as part of this study with those of known age, thereby providing a means of assessing the age of faulting. Explicit in this model is the notion that soil formation necessarily, and perhaps significantly, post-dates the deposition of parent materials, thereby complicating both the depositional and pedogenic ages on the basis of soil correlations. As such, soil ages should be considered *minima* for associated deposit ages and should not be applied as a direct proxy of deposit age.

Paleosols in the Sierra Nevada foothills are easily identified by diagnostic stratigraphic, pedologic, paleoecological (palynologic), and geochronologic criteria. In the eastern San Joaquin valley, seven distinct depositional hiatuses and associated periods of soil development in the past ca. (circa) 600 ka are identified in deposits of known age. Figure 2-1 shows a generalized model of the approximated time gaps between unit deposition and soil formation, and lists the unit names of these soil-bearing alluvial deposits.

Because much of the soil-stratigraphic correlations are based on soils developed in coarse arkosic deposits (Riverbank and Modesto Formations) associated with glacial outwash and alluvial deposition by the major fluvial systems draining the western Sierra Nevada, soil correlations in unglaciated colluvial-dominated, non-arkosic, environments like the Pardee Reservoir study area is difficult. To reduce uncertainties associated with linking soil-derived alluvial ages with colluvium, Harden and Marchand (1980) correlate the known periods of soil development in alluvium to colluvial sequences documented in fault trenches across the Sierra Nevada foothills. On the basis of pedogenic properties similar to the well-understood alluvial soil sequence, Harden and Marchand (1980) identified up to six (6) periods of colluvial deposition that are generally coeval (age equivalent) with periods of alluvial deposition (Figure 2-1). The list below summarizes the post-600 ka soil sequence as recognized in alluvial outwash with the interpreted age of soil formation in parentheses, and the corresponding colluvium in brackets. These correlations are also summarized in Figure 2-1, and listed/described below from oldest to youngest.

- Upper Turlock Lake Formation (pre-500 ka) [Auburn colluvium]
- Riverbank Formation
    - lower member (ca. 330 to 400 ka)
    - middle member (ca. 200 to 250 ka) [Bowie Flat colluvium]
    - upper member (80 to 125 ka) [Oroville colluvium]

- Modesto Formation
    - lower member (30 to 50-70 ka) [Wyandotte colluvium]
    - upper member (10 to 30 ka) [Sonora colluvium]
- Post-Modesto Formation surficial deposits (0 to 3 ka) [Keystone colluvium]

In this report, we adopt the convention of naming these paleosols based on the associated depositional unit (i.e. the lower Riverbank soil or upper Modesto soil). Ages cited for these deposits are based on geochronologic samples taken from the uppermost sediments in each profile, as well as stratigraphic relationships, and are thought to closely approximate the cessation of deposition and the initiation of soil formation (Harden and Taylor, 1987; USACE, 1995). We summarize the key properties for each soil developed in alluvium and colluvium as the properties pertain to criteria that facilitate regional correlations with deposits having similar soil development but of an unknown age. Below, we build off of the USACE (1995) summary, a review of regional studies, and our own soil reconnaissance of key previous pedogenic surveys in the Sierra Nevada foothills to summarize the regional soil chronosequence.

2.3.1.1 Upper Turlock Lake soil

The upper member of the Turlock Lake soil is associated with well-developed soil structure, significant accumulation of pedogenic clay and stratification of argillic horizons, and intense rubification (soil reddening from iron oxidation). Evidence of the upper Turlock Lake soil antiquity is the presence of well-developed moderately strong, medium prismatic to angular blocky soil peds (structure), and soil colors that range from 5YR to 2.5YR. The argillic horizon contains many moderately thick clay films coating peds, bridging grains, and filling pores. In a colluvial setting (e.g. Auburn colluvium; Harden and Marchand, 1980), the upper Turlock Lake soil also typically exhibits a $\geq$ 1-m-thick, strong argillic horizon. In type sections as described by Janda (1965, 1966) and Harden (1987), the Friant ash (615 ka) is conformable with, and forms the base of the upper Turlock Lake alluvium, and buries the lower Turlock Lake soil. The lower soil is rarely encountered in colluvial settings due to likely erosional processes, and where the Friant ash is absent, the lower soil is likely overprinted by the upper soil. The lower soil formed between 615 ka and 1 Ma, and the upper soil formed between 500 and 615 ka (Harden, 1987).

2.3.1.2 Riverbank soil

The Riverbank soil is subdivided into three separate soils (lower, middle and upper members) developed within three distinct and separate alluvial terrace deposits. The lower member soil is rare and in most environments is overprinted by the middle member soil (Marchand, 1977). No colluvial deposit is correlated with the lower member of the Riverbank Formation (Marchand and Harden, 1981).

The middle member Riverbank soil is associated with significant clay accumulation with stratified argillic horizons totaling 1 to 2 meters, very well-developed large subangular blocky structure, minor rubification and melanization (darkening by admixture of organics), and clay skins and clay laminae (Harden, 1987). In well-drained arkosic environments, soil colors are typically brown

(7.5YR 4/4) to strong brown (7.5YR 5/6) (Harden, 1987). In colluvial environments (e.g. Bowie Flat colluvium; Harden and Marchand, 1980), the middle Riverbank soil is similar to soils developed in the Auburn colluvium (upper Turlock Lake soil) with slightly lower clay content and less free iron (i.e. less rubified). As with the Turlock Lake soils, Harden and Marchand (1980) speculatively attribute the middle Riverbank soil to the Bowie Flat colluvium. The middle member of the Riverbank soil likely developed during Marine Isotope Stage (MIS) 7, approximately between 200 and 250 ka.

The upper member of the Riverbank soil is relatively common, and thus relatively well characterized throughout the Sierra Nevada, western foothills, and eastern San Joaquin valley (Marchand and Allwardt, 1981, Busacca, 1982; Harden, 1987; Page and Sawyer, 2007). The upper member soil is typically associated with moderate to coarse, subangular blocky to weak prismatic soil structure, significant argillic development with minor stratification, and minor rubification and melanization. Clay skins typically bridge grains and fill pores. The soil is very hard when dry and sticky and plastic when wet. Colors range from brown (7.5YR 4/4) to light brown (7.5YR 6/4). In colluvial environments (e.g. Oroville colluvium), the upper Riverbank soil has a moderate to pronounced clay content, soil slickensides on ped faces, coupled with stress cutans (Harden and Marchand, 1980). Where developed directly above and within bedrock, the soil exhibits minor gleying (colors from 10YR 4/4 to 2.5Y 5/4). The upper Riverbank soil is interpreted to have formed during MIS 5, between 80 and 125 ka.

In the western foothills, Riverbank soils have often been associated with a “paleo-B” soil encountered in multiple trenches throughout the Sierra Nevada foothills (WCC, 1977, 1978; Swan and Hanson, 1977). The “paleo-B” consists of a clay-rich alluvium, colluvium, and saprolite mixture reflective of weathering and bioturbation of bedrock-colluvial-alluvial interface. The paleo-B soil likely reflects several periods of soil formation and overprinting (Harden and Marchand, 1980), possibly spanning the duration of formation for the upper Turlock Lake to upper Riverbank soils. Where observed, the paleo-B is generally interpreted to represent a soil with significant antiquity, but is not linked to any one single period of soil development.

2.3.1.3 Modesto soil

The lower member Modesto soil, developed in alluvial deposits is characterized by minor clay accumulation, low plasticity, minor melanization that lacks noticeable rubification and minor argillic stratification (Marchand and Allwardt, 1981). Soil structure consists of weak to moderate, small subangular blocky peds and colors ranging from brown (10YR 4/3) to yellowish brown (10YR 5/6). The lower Modesto soil, as described by Marchand and Allwardt (1981) is differentiated from underlying Riverbank soil based on a decrease in clay content and soil structural development. It differs from the overlying less well developed upper Modesto soils due to the presence of multiple, weak Bt-horizons. In colluvial environments (e.g. Wyandotte colluvium of Harden and Marchand, 1980), the lower Modesto soil is rarely observed alone and independent of the upper Modesto soil, and thus is commonly overprinted by the upper Modesto soil. Where observed independently, the lower Modesto soil developed in colluvium consists of a single argillic horizon,

with well-developed clay skins and medium to coarse subangular blocky structure. When overprinted by overlying soils, the lower Modesto soil exhibits an increase in clay content, soil structure development, and B-horizon stratification. The lower Modesto soil is estimated to have formed between 30 and 50 ka, and may be as old as 70 ka (Marchand and Allwardt, 1981).

The upper Modesto soil, as developed in alluvium, exhibits little argillic development and lacks evidence for prolonged weathering. Clay films are largely absent, and soil structure ranges from weak, small, subangular blocky to weak, moderate, granular and massive. The upper Modesto soil developed in colluvium (Sonora colluvium of Harden and Marchand, 1980), typically is associated with an increase in clay accumulation with some moderate to thick clay skins, and an increase in soil structural development and presence of a textural B-horizon compared to the equivalent soil developed in alluvium. Structure is weak to moderate, medium to coarse, subangular blocky. Where developed in colluvium, the upper Modesto is about 50 to 70 cm thick. The upper Modesto soil formed between 10 and 30 ka (Marchand and Allwardt, 1981).

Post-Modesto soil - Modern surficial soil

Post-Modesto-age soils are typically observed unburied, associated with the present-day climate and actively forming soils. These soils lack clay skins, and contain little clay in general. Soil structure is typically weak to moderately granular, single-grained to massive. Color is not radically different from the overlying humic layer, typically dark brown to brown (10YR 4/3 to 3/3) with organic detritus imparting darker colors and surface bioturbation and root penetration mixing through the profile. Modern soils are associated with the Keystone colluvium, which is analogous with the ubiquitous surface colluvium (Harden and Marchand, 1980). Modern soils are estimated to have formed less than about 10 ka (Harden, 1987).

3.0 WATERS PEAK FAULT

The Waters Peak fault represents one of the western-most faults comprising the Bear Mountain fault zone. In the vicinity of the study area, the Waters Peak fault (WPF) typically consists of a 50-m wide zone of crushed and sheared rock, and is defined by a prominent northwest-trending lineament that extends from Waters Peak near the north end of Pardee Reservoir, southward through Valley Springs to New Hogan Reservoir, and possibly into Salt Spring Valley as the Green Springs Run fault. The length of the Waters Peak fault is approximately 14 km, excluding the linkage with the Green Springs Run fault (as characterized for the larger WPF seismic source)(Figures 1-1 and 1-2). Section 5.0 explores the length of the fault to the northwest and southeast as possible linkage with lineaments and mapped faults that lie along projection of the WPF. Prior trenching and geologic studies on the Waters Peak fault, performed 8 km south of Pardee Dam (Waters Peak South trench site; USACE, 1995), provide direct evidence of late Cenozoic faulting and displacement of the 100 to 400 ka Riverbank Formation, and a cumulative Quaternary displacement of 1 to 2 m. The style of deformation is expressed primarily as down-to-east normal faulting from mapping and paleoseismic trenching studies. Sparse kinematic data suggests a horizontal to vertical displacement ratio of 1:1 to 2:1 (slickenside orientations on the fault plane)(USACE, 1995).

Regional profiles developed across the Waters Peak fault provide estimates of long-term deformation rates using volcanic flows as strain markers. HCG (1998) and Page and Sawyer (2001, profile 31) both noted east-side down vertical separation of the 28.9 Ma Campbell Creek Tuff member (Henry and John, 2013; Henry, 2014) of the Valley Springs Formation across the Waters Peak fault on the order of 46 to 62 m, and 60 to 120 m, respectively. Reevaluation of offsets of the Campbell Creek Tuff member during this study and using high resolution topography (LiDAR) data provide similar results with an interpreted east-side down vertical separation on the order of 57 to 132 m (this study). Assuming deformation initiated about 5 million years ago, USACE (1995) estimated a vertical slip rate of 0.01 to 0.02 mm/yr using these geologic relations. Our updated seismic source parameters for the Waters Peak fault, coupled with our reevaluation of the topographic profile across the fault zone, yield an average long term net slip rate of about 0.04 mm/yr (with a range of 0.002 to 0.1 mm/yr) assuming that Cenozoic deformation initiated in the vicinity of Mokelumne River about 5 ± 2 Ma. This long-term rate is near the upper limit of the range of late Pleistocene slip rates on the WPF used to calculate fault displacement hazard, as discussed further in Section 5.1.

As part of this study, LCI performed geologic field reconnaissance of the WPF from north of Mokelumne River to Valley Springs in the south. The best exposure of the WPF is found directly downstream of the concrete-section of the Pardee Dam spillway. A list of key observations from the geologic reconnaissance performed by LCI in the spring of 2019 includes the following:

1. The fault is defined by the contact between the Salt Springs Slate (west) and Gopher Ridge metavolcanics (east). This relation is consistent with mapping observations both north and south of the spillway and from paleoseismic exposures.

2. The fault is commonly comprised of multiple fault strands that define a zone of complex shearing and brecciation as much as 15 m (50 ft.) wide. This pattern of deformation is well expressed in the bedrock spillway of Pardee Dam.
3. Fault strands also commonly occur within either the Salt Springs Slate or Gopher Ridge volcanics within the fault zone. Intra-unit fault strands of the WPF were also observed in all three trenches excavated for this study.
4. Both cataclastic (brittle) and mylonitic (ductile) deformation zones are common within and adjacent to the fault zone. Mylonites especially prevalent where fresh Salt Springs Slate is exposed along the fault zone margin.
5. Where exposed to soil-forming process (as observed near the surface along the spillway margins), localized intensely faulted/fractured zones within the larger fault zone weather to clay and are reminiscent of fault gouge. While no gouge was observed in the abraded portion of spillway channel, it is likely that any fine-grained fault material (if present) within the unweathered section of rock in the spillway has been largely removed (eroded) by repeated high-energy flows within the spillway.
6. The fault dips moderately to steeply northeast. Dips measured in the spillway ranged from 64° to 70° NE.
7. Striations in weathered rock near "gouge" zones (in spillway margin exposures) and mineral stretching lineations provide kinematic indicators of fault displacement. Mineral stretching lineations, which are formed at depth and have been subsequently exposed, document rakes of 72° and 76°. These rake values indicate predominantly dip slip displacement at the time of their formation, which could date as far back as the Mesozoic accretion of the rocks to the continental margin. Rake values observed from striations in the two "gouge" zones at the spillway margin were 61° and 64°, both plunging southeast. If these striations represent the most recent (i.e. late Quaternary) deformation, the WPF accommodated down-to-the-southeast displacement with a subordinate oblique dextral (right-lateral) component.

3.1 Previous Studies of the Waters Peak fault (USACE, 1995)

The USACE performed a comprehensive evaluation of Quaternary active faults comprising the Foothills fault system in the vicinity of New Hogan Dam, with an emphasis on evaluating displacement within the last 35,000 years (USACE, 1995). As part of this study, the USACE identified two trench sites: North and South Waters Peak sites, respectively, on the Waters Peak fault (Figures 1-1 and 3-1). The nearest paleoseismic trench site to Pardee Dam is the Waters Peak North site located 2.5 km south of Pardee Dam (Figure 1-2). The "not capable" fault designation by USACE (1995) is based primarily on the findings of the Waters Peak South trench site near the town of Valley Springs (Figures 1-1 and 3-1). A summary of the USACE (1995) findings from the Waters Peak fault studies are provided below, as well as specific review comments from "expert" reviewers.

3.1.1 Waters Peak South Trench Site:

Two northwest-trending lineaments located directly east of Valley Springs were identified through aerial photography analysis and field mapping, and subsequently investigated with 10 exploratory trenches (Figure 3-1). The inferred eastern fault strand was deemed unrelated to faulting based on the trench exposures, whereas the inferred western fault strand coincided with clear bedrock faults exposed in the trenches (Figure 3-1). Multiple trenches provide direct evidence for faulted Riverbank/Turlock Lake terrace deposits, as well as the absence of faulting in the overlying post-Modesto to Holocene-aged deposits (USACE, 1995). A distinct silica-rich pedogenic horizon, located at the boundary between Riverbank and Modesto-aged deposits, and interpreted as early Modesto in age, is used as an additional strain gauge to assess fault activity. The silica horizon is unfaulted across the Waters Peak fault. Based on a combination of the unfaulted younger deposits, and the silica horizon exposed in the trenches, the USACE (1995) interpreted the Waters Peak fault as non-capable (i.e. "inactive"). Similarly, DSOD references the Water Peak South trench site as an example for applying DSOD criteria from which to assess the presence or absence of active or conditionally active faulting (see Figure 1-3 of Fraser, 2001).

3.1.2 Waters Peak North Trench Site:

The Waters Peak North trench site is located 5.5 km northwest of the Waters Peak South site, and 2.5 km southwest of Pardee Dam, and coincides with a prominent linear valley and a topographic saddle mantled by Mehrten Formation (Figures 1-1 and 1-2). Two trenches (T-1 and T-2) were excavated in the topographic saddle underlain by Mehrten Formation, and a third trench (T-3) was located to the northwest of trenches T-1 and T-2 within the linear valley filled with alluvium and colluvium (Figure 1-2). The trenches provided mixed results for the assessment of fault activity because of the pervasively sheared bedrock, difficult excavation conditions within the Mehrten Formation, and the presence of thin alluvial and colluvial deposits, in contrast to the Waters Peak south site. For instance, trenches T-1 and T-2 encountered very hard and cemented Mehrten Formation that limited the length and depth of the explorations. A summary of key findings of trenches T-1 and T-2 are provided below:

- Trench T-1 exposed a steep, northeast (N35°E) striking fault juxtaposing Salt Springs Slate (on the west) and Mehrten Formation (on the east). Although the fault exhibited displacement and juxtaposition of two bedrock types, the strike of the fault is inconsistent with the orientation of the northwest-trending, linear fault-controlled valley and regional strike of the Waters Peak fault.
- In contrast, trench T-2, located 35 m south of USACE trench T-1 exposed an apparent depositional unconformity between the underlying Salt Springs Slate and overlying Mehrten Formation, and the absence of faulting along this contact and within the trench. Based on this relation, the fault location was interpreted to be west of trench T-2.

USACE (1995) trench T-3 provides more valuable information for assessing the presence or absence of faulting in close proximity to Pardee Dam. The trench, located in the broad alluvial

valley north of trenches T-1 and T-2, spans nearly the entire width of the linear valley that constrains the Waters Peak fault. The 209-ft-long trench exposed Salt Springs Slate overlain by multiple packages of alluvium and colluvium ranging from Riverbank to Holocene age. USACE (1995) interpreted the absence of distinct faulting within the trench, and apparently did not identify a clear zone of bedrock faulting coincident with the linear valley (Waters Peak fault). The trench, however, did expose multiple bedrock shears and anomalous wavy contacts that are discussed further below and shown in Figure 3-2.

The trench exposed highly foliated and jointed Jss metasandstone capped by a sandy lean clay (Unit 6) of either alluvial origin or in-place weathered bedrock. Figure 3-2 shows a re-interpreted partial log of USACE trench T-3 where it intersects the central part of the linear valley. The figure also shows the correlation of stratigraphy between the USACE (1995) and LCI trenches. A buried topographic high denoted by Unit 6 lies within the center of the valley and separates older Riverbank alluvial deposits (Units 4, 4a, and 5) on the west from younger Modesto-aged alluvium (Units 3, 3a, and 3b) on the east. The buried topographic high between stations 75 and 95 ft is underlain by highly foliated and sheared Jss metasandstone, however, USACE (1995) did not interpret these features to be a distinct fault associated with the Waters Peak fault (Figure 3-2). The stratigraphic and structural relations exposed in trench T-3 are used to argue for the absence of faulting within the last 35,000 years within the linear valley, and if younger faulting is present, it lies beyond of the footprint of the trench (USACE, 1995).

3.2 Summary of Peer-review Observations of the USACE (1995) Waters Peak Trenches

The USACE (1995) Waters Peak trenches were reviewed by several independent outside technical experts: William R. Lettis, William D. Page, and Roy Shlemon. Summaries of the expert reviews are provided below and reference Figure 3-2.

WLA (1994) – Trenches at the Waters Peak South site provide conclusive evidence of Quaternary activity, as well as the absence of faulting during the last 30 to 70 ka. Cumulative down-to-the-east vertical separation of an unconformity between the Ione and Riverbank Formations is approximately 50 to 80 cm and decreases upsection to 15 cm at the top of the Riverbank deposit. Kinematic indicators (obliquely plunging slickensides) indicate a lateral to vertical ratio of slip of 1:1 to 2:1. The Waters Peak North site provides evidence for the absence of faulting during the past approximately 14,000 years across a bedrock fault that juxtaposes Jurassic Salt Springs Slate and Tertiary Mehrten Formation. Trench T-3 exposed a sequence of Quaternary (Riverbank to Holocene age) colluvial and alluvial deposits and soils overlying Mesozoic bedrock. Bedrock faults and zones of shearing occurred at several locations in the trench but none of the faults appeared to be significant structures. The absence of faulting at this locality can be explained by either: (1) Waters Peak fault consists of a broad zone of minor faults; (2) faulting is defined as a series of en-echelon, discontinuous fault traces; and (3) faulting lies outside of the linear valley. WLA (1994) concludes that the Waters Peak fault lies within the linear stream valley. Evidence for possible Quaternary faulting was interpreted in the valley axis in trench T-3 based on the apparent warping of Quaternary deposits (Unit 6) overlying a bedrock shear zone, as well as

alluvium-filled fractures within Unit 6 (Figure 3-2). Fault shears, however, are not interpreted as extending into the "warped" deposits (Unit 6), nor are the overlying early Modesto age and younger deposits deformed. In summary, the stratigraphic and structural relations in trenches at both the North and South Waters Peak sites provide evidence for the absence of faulting in deposits likely 30 ka or older, and that the "Waters Peak fault is not a capable structure" (WLA, 1994).

Page (1994)

The Waters Peak fault can be traced for up to 500 ft. in multiple trenches at the Waters Peak South site, and exhibits up to 70 cm of vertical separation across the top of the Ione Formation. Vertical separation decreases upsection to about 15 cm across the top of a Riverbank-aged gravel. An overlying silica-rich deposit is unfaulted across this zone of faulting and is estimated to have formed > 30,000 years ago. Page (1994) interprets multiple alluvial and colluvial deposits ranging from pre-Riverbank to Holocene in age. At the Waters Peak North site, Page (1995) describes the central part of trench T-3 as consisting of a pre-Riverbank paleo-B horizon developed directly on bedrock (Unit 6 of USACE, 1995; Figure 3-2). The paleo-B soil horizon forms anomalous, steep, "wave" forms above bedrock faults, and bounds vertical filled fractures. Page (1994) suggests that these features may be indicative of faulting or tectonic squeezing of the ground. The paleo-B horizon is overlain by unfaulted early Modesto age alluvium. Page (1994) concludes that the Waters Peak North site provides evidence of late Quaternary faulting by the offset of the paleo-B horizon (Unit 6), however, the overlying lower Modesto alluvial deposits (Units 3, 3a, and 3b) are unfaulted (Figure 3-2). Page (1995) concludes that the Waters Peak fault "has not had displacement in more than 30,000 years, and probably much more at the south end, and in more than 60,000 years at the north end."

Shlemon (1994)

The Waters Peak South site provides clear evidence for Quaternary displacement and offset of sediments interpreted to be late Riverbank in age (125 to 200 ka). These fault deposits are overlain by unfaulted late Quaternary sediments interpreted to range from early to late Modesto in age. Shlemon (1994) describes the Waters Peak fault at the North site as a diffuse fault zone, unlike the Waters Peak south site, where faulting is clearly expressed. There is no comprehensive discussion of the Waters Peak North trenches. Based on a review of trenches and the USACE trench logs Shlemon (1994) concurs that the early Modesto-age sediments are unfaulted, and that the these deposits are > 30,000 to 40,000 years old.

3.3 Long-Term Vertical Displacement Estimates of the WPF

As part of the office-based analysis, LCI prepared and analyzed a longitudinal topographic profile to reassess vertical displacement of the Miocene Mehrten and Oligocene Valley Springs Formations to better understand both rate and magnitude of long-term displacement across the Foothills fault system (Figure 1-3). The profile was used to re-evaluate the previously estimated

vertical displacements of Tertiary volcanic sequences crossing the Melones and Bear Mountains fault zones (Page and Sawyer, 2001).

This re-evaluation focused on estimating vertical offsets of the Campbell Creek member (stratigraphic equivalent to the Castle Rock Tuff) of the Oligocene Valley Springs Formation across the Waters Peak fault. While the Miocene Mehrten Formation was considered for this analysis, we determined that it is was inappropriate for assessing potential vertical offsets for the following reasons: (1) the base of the Mehrten represents an erosional boundary and is not a planar projectable contact; thus the elevations along the basal contact can only be used to define a range of constraints on the basal gradient; and (2) there are a lack of Mehrten Formation outcrops west of the Waters Peak fault with which to correlate outcrops on the east (south of LCI Site 6) (Figure 1-3).

While the Campbell Creek member represents a more uniform marker bed, there are few outcrops in the vicinity of the Waters Peak fault, and most are less than 0.2 km in extent. The lack of regional continuity of the unit suggests that any calculation of basal gradients across a single outcrop are likely to be unrepresentative of the unit as a whole. For this reason, we chose to assume a range of gradients across the basal contact based off of gradients calculated from the top of Mehrten Formation at Table Mountain to the south (Page and Sawyer 2001). Gradients for the Mehrten ranged from 20-25 m/km. However, because the Mehrten Formation underwent a differential depositional history than the Valley Springs tuff, we conservatively use a wider range of gradients spanning 15 to 30 m/km. To calculate the vertical offset, four point locations were chosen along the basal Campbell Creek tuff using publically available 1-m LiDAR. Points were selected to represent minimum and maximum elevation constraints for the tuff (Figure 1-3). Three of these points were located west of the fault and one was located east of the fault at Castle Rock. Projecting each of these points to the Waters Peak fault yielded estimated minimum and maximum vertical offsets across the fault ranging from 57-132 m (Figure 1-3). In summary, these vertical displacement estimates are similar to the 60 to 120 m estimates estimated by Page and Sawyer (2001)

4.0 WATERS PEAK FAULT PALEOSEISMIC INVESTIGATION

During the spring of 2019, and as part of the geologic field reconnaissance, LCI identified two paleoseismic trench sites (Sites 5 and 6) within the linear valley of the Waters Peak fault and south of Pardee Dam (Figures 1-2 and 4-1). Three trenches (LCI-T1 to -T3) were excavated across the Waters Peak fault directly north of the former USACE (1995) Waters Peak North trench site. Approximately 285 total lineal feet (87 m) of trench were excavated for primary trenches (LCI-T1 and –T2) at Sites 5 and 6, with an additional 33 lineal feet (10 m) of trench (LCI-T3) excavated at Site 6 for a supplementary exposure of the fault zone (Figures 4-1 and 4-2).

As described in the Waters Peak Fault Trenching Work Plan (LCI, 2019), six potential trench locations were sited to expose the fault zone where Quaternary deposits were interpreted to overlie the fault, thus providing a means of evaluating Quaternary displacement history. Four of the six sites evaluated as part of the reconnaissance mapping and trench siting study were deemed poor candidates for one or more reasons that included limited or no Quaternary stratigraphic cover, anthropogenic modification, and limited or no site access for equipment. Sites 5 and 6 were chosen due to favorable tectonic-related geomorphology, bedrock mapping, Quaternary deposition based on hand-augered borehole data, and efficient site access and permitting. Furthermore, LCI chose to conduct investigations at these two separate sites in slightly different geomorphic settings to maximize the potential for exposing fault deformation (if present) at various temporal scales and at locations with differing depositional and erosional rates. Detailed descriptions of Sites 5 and 6 are presented in the following Subsections 4.5 and 4.6.

4.1 METHODS

Prior to conducting the subsurface study, LCI directed public (811 Underground Service Alert) utility clearance of the trench locations in addition to consultation with EBMUD maintenance personnel familiar with the site, and independent utility location subcontracted through a professional utility locator. Additionally, LCI worked with EBMUD to ensure the proposed trench sites were cleared for cultural resources and sensitive flora/fauna prior to excavation. Public site access during the trenching program was restricted using the locked entrance gate along Sandretto Road along with temporary construction fencing erected around individual trenches and spoils piles.

The trenches were excavated using a Caterpillar 320 track-mounted hydraulic excavator with a 3-foot-wide bucket. Trenches were excavated to refusal or near refusal into weathered bedrock to allow for clear identification of rock type, faults, bedding and/or foliation, and joints. Across both sites, the depth of refusal ranged from approximately 1 to 2.8 m (3.3 to 9.2 ft.). Where trench depth exceeded 1.5 m, hydraulic shores were installed. Upon completion of the paleoseismic study trench spoils were used for backfilling. Spoils were wetted and compacted with a sheep's foot roller in lifts to reduce possible future long-term settlement.

Upon excavation and stabilization with hydraulic shoring, trench walls were cleaned to provide a fresh exposure. Following cleaning, colored flagging and nails were placed in the trench walls to

delineate soil and stratigraphic contacts, faults, and other structural features. A level line and markers were used to establish a metric survey grid for subsequent trench photography and logging. After completion of the survey grid and initial flagging, trenches were photographed and photomosaic trench logs were generated using Agisoft photogrammetry software and LCI's well-established photomosaic methodology (Gray et al., 2016). Trenches were logged at a scale of 1 inch = 0.5 meter to show lithology, lithologic contacts between units, and geologic structure. Where necessary, fault zones were logged in greater detail (1 inch = 0.25 m) to show key structural and stratigraphic relations and to provide a means of logging and testing multiple depositional/fault models. Faults were logged as red (primary) and faults/shears (secondary) as blue. Secondary faults were typically associated with limited evidence of shearing and/or lacked lateral continuity because they could not be tracked with confidence between trench walls. Trench logs of the south walls for trenches LCI-T1 to -T3 are provided as Plates 1 to 3. All other (undrafted) trench logs of the north walls are provided in Appendix A (A-1 to A-3).

4.1.1 Geochronology

Due to the absence of detrital charcoal in the deposits exposed in the trenches, LCI relied heavily on regionally developed soil chronosequences for the Sierra Nevada foothills (described in Section 2.3.1), combined with the previous soil ages defined by USACE (1995) at the Waters Peak North trench site to assess the age of the deposits in trenches LCI-T1 to -T3. Using these soil ages as a minimum age for the deposit (because the soil formed subsequent to deposition), we used the soil stratigraphy as strain gauges to document the presence or absence of active faulting. Section 4.3 provides descriptions of the soil correlations.

To test for radiocarbon samples, bulk soil samples were collected from the three trenches for sifting of fine charcoal, seeds, sticks and organic matter, since the trenches lacked charcoal fragments observable with the naked eye. Four bulk soil samples collected from Unit 600 were submitted for screening by Beta Analytical, Inc. in Florida. The analysis failed to identify organic matter (seeds, sticks) and larger charcoal in the sediment, nor were the small organic contributions significant enough for a meaningful bulk soil age. As a test-case only, a single screened bulk sample of combined organic matter from Unit 600 was analyzed and yielded an anomalous young age of about 5,500 yr BP (Appendix B), compared to the regional soil age of 30 to 70 ka (Table 4-1). The test confirmed that the samples contain abundant younger organic contributions and root matter, and thus provide unreliable ages and are not considered further in the analysis of deposit ages.

LCI also collected multiple sediment samples in metal tubes for possible future optically stimulated luminescence (OSL) analysis. These samples were not submitted for analysis because laboratory return times far exceeded the schedule for completing this technical report to EBMUD. These samples have been retained by LCI for possible future dating.

4.1.2 Peer Review

As a critical component of the paleoseismic investigation, LCI enlisted the expertise of internal and external peer reviewers to provide feedback on interpretations, logging, and models associated with stratigraphy and faulting. Trenches were reviewed by Dr. William Lettis of LCI and Dr. David Schwartz (formerly with U.S. Geological Survey). Dr. Lettis worked previously at the Waters Peak North site and reviewed and interpreted the USACE trenches, and provided guidance on the pedologic (soil) analysis of the trenches (USACE, 1995). Dr. Schwartz is considered an expert on the FFS and worked extensively on evaluating the activity of the FFS for the Auburn Dam project, as well as the proposed Stanislaus nuclear facility while an employee with Woodward-Clyde Consultants. Additional peer review was provided by Dr. Chris Madugo of PG&E and Bryan Dussel of DSOD. LCI also conducted a trench review party with local, state and federal agencies, including CGS, U.C. Berkeley, DWR, and USACE experts and interested parties. The trench review provided an opportunity for LCI to present preliminary findings of the Waters Peak fault trenching study and solicit feedback. Dr. William Page of PG&E, and former technical reviewer of the USACE (1995) trenches, provided technical review of the trench logs and soil profile descriptions through a conference call with LCI geologists Brian Gray and Chris Bloszies.

4.1.3 Qualitative Uncertainty

As part of our assessment of paleoearthquakes interpreted from the collected paleoseismic data, we use the terms outlined in Table 4-2 to reflect our qualitative degree of certainty for an event, scenario, or fault relation, as supported by the pertinent and available paleoseismic, stratigraphic, and geochronologic data encountered within the trench. The procedure for assigning a term from Table 4-2 involves a careful assessment of the center, body, and range of available data collected. LCI has employed this methodology (and derivations thereof) to characterize qualitative event probabilities for numerous paleoseismic studies of varying scales throughout the western US and abroad. Where used explicitly in the text, the qualitative terms presented in Table 4-2 will be italicized for clarity.

Table 4-2. Terms Used to Qualitatively Assess Degree of Certainty for Events and Interpretations

Likely
Probable
Possible
Unlikely

4.2 GEOMORPHOLOGY

In preparation for the paleoseismic study, LCI conducted field reconnaissance along a 4-km-long section of the of the WPF to perform geomorphic and geologic mapping, evaluate the location and width of the WPF relative to existing published and unpublished mapping, coordinate regional geologic mapping with CGS geologists, and locate potential paleoseismic trench sites. The

following list provides a summary of geomorphic observations along the length of the fault north of Pardee Dam to the saddle at the southern end of the fault-parallel valley coincident with USACE (1995) Waters Peak North Site.

- Geomorphology along the fault is largely controlled by the location of bedrock units (slate, metasandstone, metavolcanics, volcanics) and associated topographic highs that crop out along or near the fault as a result of differential weathering and/or long-term fault displacement.
- Quaternary deposits and soils along the WPF are typically thin where exposed in roadcuts, fluvial cuts, hand augers, and trenches. Tectonic geomorphic features commonly targeted for paleoseismic studies, such as Quaternary alluvium and colluvium along scarps or depressions (i.e., slope-derived and ponded deposits) are limited in extent. Areas where Quaternary deposits are thickest along the fault appear to be associated with differential (i.e. increased) weathering of rocks in the fault zone. In trenches, this weathering is coincident with topographic lows and associated localized deposition and/or soil development.
- Other than localized areas of fluvial deposition adjacent to drainages, surficial Quaternary deposits are generally limited to laterally extensive but shallow/thin colluvial and alluvial deposits.
- From approximately 500 feet (150 m) north of the chemical plant to the south along the linear valley, the location of the WPF is generally well defined by the presence of partially weathered outcrops protruding through shallow colluvium along both sides of the fault (Figure 1-2).

4.3 Paleoseismic Soil Chronology

Critical to the evaluation of activity for the Waters Peak fault is the estimation of the relative age of the faulted and unfaulted deposits exposed in trenches LCI-T1, -T2, and -T3. Previous paleoseismic studies to assess the activity of faults within the Foothills faults System (WCC, 1978; USACE, 1995; PG&E, 2007) have relied on the robust soil chronology extensively studied in the Sierran foothills to correlate exposed soil-bearing deposits to those of known age based on similarities in soil structure, clay development, plasticity, and other pedogenic properties (Harden and Marchand, 1980; Marchand and Allwardt, 1981; Harden and Taylor, 1983; Harden, 1987). Soils and diagnostic properties relevant to this and previous paleoseismic fault evaluations are summarized in Section 2.3.1.

In addition to preparing detailed unit descriptions for each stratigraphic unit, pedologic (soil) profiles were described at several key locations in trenches LCI-T1 to -T3. Soil descriptions are summarized in Table 4-1, and the location of each profile is shown on the trench logs (Plates 1 to 3). Soil morphology was described according to standard methods and nomenclature (Birkeland, 1999), with careful consideration for soil properties described by Marchand (1978), Harden and Marchand (1980), Marchand and Allwardt (1981), and Harden (1987) as diagnostic to Sierra

Nevada foothills soils. The soil descriptions reflect pedologic morphology encountered within approximately 25 cm on either side of the vertical soil profile datum.

In the LCI trenches, discrete soils are confined to stratigraphic layers with little obvious soil overprinting (except local instances where fine-grained deposits are in contact; such as with Unit 600 where it occasionally overlies silt- and clay-rich deposits), consistent with observations made elsewhere in erosional environments in the Sierra Nevada foothills (Marchand and Harden, 1980; USACE, 1995; PG&E, 2007). The lower contacts of most deposits exposed in the LCI trenches are interpreted to be erosional, thus the underlying deposits typically contain only B-horizons, with most of the overlying organic material removed (i.e. buried A-horizons are absent). This interpretation is supported by elevated clay content and prominent soil structure developed in buried units and the lack of obvious cumulic soils or significant organic soil fractions. Therefore, soil correlations are made easier because, for the most part, each stratigraphic unit contains a single, unique soil with little to no soil overprinting (as noted previously, the exception being Unit 600 overprinting older underlying units). Table 4-1 summarizes the soils encountered by stratigraphic unit number for the LCI trenches and correlation with USACE (1995) trench T-3.

As part of this study, LCI compared the soils observed in trenches LCI-T1, -T2, and -T3 with:

- the descriptions of soils previously documented through a similar analysis in USACE trench T-3 (USACE, 1995; and WLA, 1994); see also Figure 3-2;
- with type descriptions of Sierra Nevada foothills colluvial soils made by Harden and Marchand (1980); and
- with descriptions of soil parameters input into a foothills soils chronosequence by Marchand and Allwardt (1981), Harden and Taylor (1983), and Harden (1987).

Relative age estimates for deposits in the LCI trenches were developed, in part, by comparing the soil profiles described in LCI trenches with the soil chronosequences referenced above in the USACE (1995) trenches. For example, deposits exposed in LCI trenches were correlated directly to similar deposits in USACE (1995) trench T-3 based on stratigraphic position, sediment characteristics, and structural relationships, thus, the soil ages estimated by the USACE (1995) were applied to the deposits in the LCI trenches. Table 4-1 summarizes the estimated soil ages assigned by this method, which are briefly discussed below.

In addition to directly correlating stratigraphic deposits and soils between USACE and LCI trenches, we also used published descriptions of regional Sierra Nevada foothills soils to compare the relative degree of soil formation within the LCI trenches to the published regional soil chronosequence. The underlying assumption is that soils of similar age that have formed on similar parent material under similar topographic and climatic regimes will have comparable pedogenic development. In this manner, a soil of unknown age can be correlated to a soil of known age within an established chronology using characteristic pedogenic properties. Care needs to be taken with soils developed in the foothills, however, due to the variability in the colluvial parent material, rock types (metamorphic, plutonic and volcanic), and reworking and

deposition of older eroded soils. For example, soils formed on volcanic or metavolcanic parent material appear to form more rapidly than soils of the same age on arkosic parent materials (Harden and Marchand, 1981). Thus, our comparison of soils is based on soil properties considered to be the least influenced by parent material composition: soil structure, B-horizonation and stratification, argillic accumulation, and clay skin development, and to a lesser degree soil color and plasticity. Table 4-1 summarizes the results of these correlations, which are briefly discussed below.

Ultimately, the soil age for the deposits in trenches LCI-T1 to -T3 is estimated through both comparison with the USACE (1995) soil ages and published descriptions of Sierra Nevada foothills chronosequences of Marchand and Harden (1980) and Harden (1987). Table 4-1 provides the preferred soil age for each stratigraphic unit. The soils/deposits observed in trenches LCI-T1, -T2, and -T3, correlate moderately well with the deposits and soils described in the USACE (1995) trench T-3, located approximately 220 ft. (67 m) southeast of trench LCI-T2. The soil profile descriptions from the LCI trenches also correlate with the well described, established Sierra Nevada foothills soil chronosequence. We acknowledge a direct correlation of deposits between USACE trench T-3 and LCI trenches is interpretative and uncertain in some instances; however, where stratigraphy is correlative, the age estimates of USACE (1995) have been adopted. Some clarity is gained through comparison of soils exposed in LCI trenches with those described in greater detail elsewhere in the Sierra Nevada foothills. Both soil correlations form the basis for the depositional ages assigned to deposits exposed in LCI trenches (Table 4-1).

4.4 Bedrock Geology at Sites 5 and 6

Bedrock at the WPF trench sites is comprised of the Jurassic Salt Springs Slate (Jss) and Gopher Ridge metavolcanics (Jgo) rocks (Figure 4-1). In the study area, Jss consists of two principal facies: (1) a primary slate facies, as exposed in the Pardee Dam spillway, and (2), a lesser facies of metasandstone that may or may not have a volcanic component. Foliation in Jss is typically well-developed, strikes northwest (parallel to the WPF), and dips steeply east. Salt Springs slate and metasandstone typically weather to light gray (slate) or very light gray to greenish gray (metasandstone) colors, whereas soils developed in colluvium generated from Jss parent material are typically associated with 10 YR to 7.5 YR colors for the slate, and 7.5 YR to 5YR (more reddish) colors in the metasandstone.

The Gopher Ridge Metavolcanics comprise the other bedrock unit exposed in the paleoseismic study area. Foliation in these rocks is oriented similarly to the Jss rocks (striking northwest and dipping steeply east). Gopher ridge rocks typically weather to a gray to greenish gray color and can be difficult to distinguish from metasandstones of the Salt Springs Slate. Additionally, foliation thickness and joint spacing for the Jss metasandstone facies and Jgo are similar. Soil colors in Jgo-derived colluvium are typically in the 5YR range; more red than those in Jss slate-derived colluvium. This color contrast is readily apparent in trench LCI-T1 and provides a means of determining parent material provenance when clasts are intensely weathered. As shown on Figure 4-1, Jss occurs both east and west of the mapped trace of the WPF whereas Jgo rock are

only observed east of the WPF (at least in vicinity of Pardee Dam and the paleoseismic sites). As is discussed in subsequent sections, at some unknown distance south of Site 5, the Jgo unit either pinches out or is faulted out to the east; however, existing data cannot be used to determine the geometry of the southward Jgo termination.

4.5 Age of Deposits at Sites 5 and 6

The stratigraphically oldest depositional units exposed in LCI trenches are represented by a sequence of coarse and fine alluvium and/or saprolite (Units 200, 300, and 400 from oldest to youngest). All units are correlative with a similar sequence exposed in USACE Trench 3 thought to be Riverbank-age or older by USACE (1995). Clearly Unit 200 has experienced significant pedogenic alteration based on the intense clay development, well developed medium prismatic structure, continuous clay films prominently slickensided, and high plasticity. These features are consistent with descriptions of the regional paleo-B soil (WCC, 1977, 1978; Swan and Hanson, 1977) previously determined to represent many episodes of soil development (Harden and Marchand, 1980). The overlying deposits (Unit 300 and 400) contain soils of two distinct ages, with the younger, overprinting soil consistent with late Riverbank age development in fine-grained, well-drained alluvium (Marchand and Allwardt, 1980; Harden, 1987). It is therefore likely that the late Riverbank period of soil formation was the most recent for all three deposits, and it is possible, therefore, to establish a minimum age of soil formation of 80 ka (Harden and Taylor, 1983; Harden, 1987), but difficult to establish a maximum age given the multiple soils developed in each unit. Therefore an age of 80 ka or older is preferred for Units 200, 300, and 400 (Table 4-1).

The coarse alluvial deposit represented by Unit 500 is correlated to Units 3a and 3b of USACE (1995) trench T-3 determined to have a Modesto-age soil by USACE (1995). The soil developed into Unit 500, however, is more closely correlated regionally to a soil of late Riverbank age, based on moderate clay development, weak to moderate subangular to angular blocky structure, and common moderately thick clay films. In contrast to the soil developed in the overlying Unit 600, the soil in Unit 500 is stratified, with two distinct Bt horizons reflective of relative antiquity. The preferred age range of 50 to 125 ka shown in Table 4-1 captures this uncertainty in age estimates.

The fine-grained alluvium of Unit 600 is stratigraphically consistent with Unit 3 in Waters Peak North trench T-3, determined by USACE (1995) to be Modesto in age. The regional soil chronosequence of Harden (1987) subdivides the Modesto age deposits into an upper and lower units on the basis of greater differences in argillic development in the lower member. The soil exposed in LCI trenches is consistent with the increased clay accumulation and melanization diagnostic of the early Modesto age soils. The preferred age estimate for the soil developed into Unit 600, therefore, is between 30 and 70 ka (Table 4-1).

Directly below the surficial colluvium, Unit 700 is consistent with colluvium exposed in a similar stratigraphic position in Waters Peak North trench T-3, determined to be Holocene in age (USACE, 1995). The pedogenic properties of the soil developed into Unit 700, however, is more consistent with an interpretation of late Modesto age, based on the increased clay content relative

to Holocene age (post-Modesto) soils described by Marchand and Allwardt (1980) and Harden and Marchand (1981), and may be correlative with regional "Sonoran Colluvium" of Harden and Marchand (1980). The Unit 700 soil is slightly plastic, with weak, fine, subangular blocky structure, but clay films are absent and the deposit is broadly nonplastic. Unit 700a is interpreted as a channel deposit incised into Unit 700 in trench LCI-T2, and thus is considered of contemporaneous age to, or closely post-dating deposition of Unit 700. In Unit 700a, argillic soil development exceeds that of Unit 700, with weak prismatic structure and very few thin clay films. On balance, descriptions more closely match Modesto age soils rather than those determined to be post-Modesto, as described by Harden (1987). Conservatively, the preferred age estimate of 5 to 30 ka for Units 700 and 700a includes both interpretations.

The youngest unit exposed in trenches LCI-T1, -T2, and -T3 is the overlying surficial colluvium (Unit 800; Plates 1, 2, and 3), estimated to be late Holocene in age by both USACE (1995) and based on soil properties. No significant surficial geomorphic features exist between USACE Trench 3 and the LCI trenches to suggest surficial deposits of different age. Further, the descriptions of surficial post-Modesto soils developed in arkosic alluvium (Marchand and Allwardt, 1981) and in the Keystone colluvium (Harden and Marchand, 1980) are consistent with the soil properties of Unit 800, specifically exhibiting a lack of significant soil structure, few to no clay films, and no plasticity, indicative of a lack of pedogenic clay overall. The preferred estimated of age for this soil is between 0 and 10 ka (Table 4-1).

4.6 PALEOSEISMIC SITE 5 (TRENCH LCI-T1)

Site 5 is located approximately 1,000 feet (300 m) south-southeast of EBMUD's chemical plant at the northern end of the linear valley occupied by the WPF (Figure 1-2). The site lies at the base of a broad and gently west-sloping colluvial surface that extends from an area east of Sandretto Road to near small (unnamed) ephemeral drainage located 35 m west of trench LCI-T1 (Figure 4-1). Slate (north and south) and metavolcanic (northeast) outcrops delineate the fault zone. Site 5 was interpreted to represent a potential fault bounded basin where colluvial and slope wash deposits accumulate at or near the base of an east-facing bedrock escarpment and east of a small drainage ("wind gap?"). Soil cuttings from hand-augers conducted during the field reconnaissance indicated the potential for different (albeit shallow) Quaternary deposits on either side of the projected trace of the WPF, based on color and textural differences (LCI, 2019). Because of the potential for ponded sediment and a relatively well constrained fault zone, Site 5 was chosen as one of two paleoseismic trench sites. Trench LCI-T1 was 31 m (102 ft.) long and ranged between 1.4 and 2.6 m (4.6 and 8.5 ft.) in depth, and intersected the mapped fault zone of the WPF.

4.6.1 Trench LCI-T1 Stratigraphy

Paleoseismic trench LCI-T1 exposed moderately to intensely weathered bedrock comprised of Jss slate (west of the WPF) and Jgo metavolcanics (east of the WPF) that unconformably are overlain by multiple colluvial deposits interpreted as late Pleistocene (Riverbank) to late Holocene in age (Plate 1). West of the fault, Jss slate is moderately weathered and maintains a prominent,

uniform east-dipping foliation, except where it approaches or lies within the fault zone between stations 9.5 m and 14 m, and bedrock shears disrupt the foliation. East of the WPF, Jgo metavolcanics are moderately to intensely weathered. Intense weathering coincides with zones of increased fracture density (joints, localized shears, and through-going faults). A series of locally-sourced late Pleistocene colluvia overlie the Jss and Jgo bedrock and intervening WPF. The oldest colluvium (Unit 500) extends from station 18 m to the west end of the trench, and is primarily comprised of sandy silt with gravel (Plate 1). The basal contact is irregular, abrupt, and locally associated with a stone line interpreted to represent incipient incorporation of underlying bedrock clasts into the colluvial mass. The basal contact steps vertically across multiple foliation boundaries in the Jss bedrock and forms a saw-tooth-like pattern. Across the fault zone between stations 9.5 and 14 m, Unit 500 is discontinuous and present only in localized areas where the top of rock is low relative to the base of Unit 500 (Plate 1; Appendix A, Figure A-1). These isolated pockets of Unit 500 suggest that the overlying contact with Unit 600 represents an erosional surface. Based on soil development characteristics and stratigraphic position relative to overlying deposits and their associated soils, Unit 500 is interpreted as likely Riverbank in age (50 to 125 ka; Table 4-1).

Unit 600 overlies Unit 500, and is differentiated from other colluvial deposits due to an increase in fines content and the presence of a moderately well-developed soil with a distinct Bt horizon. Unit 600 is a dark grayish brown, silty clay and can be traced laterally continuously from station 25 m to 1 m at the west end of the trench. The deposit gradually increases in thickness from east to west (Plate 1). The fines content suggests Unit 600 has a significant eolian component. At the fault zone, clast content (predominantly Jss slate clasts) gradually increases westerly, coincident with a decrease in clay content and soil structure. The increase in clast content may be related a westerly colluvial transport and associated erosion of the underlying bedrock surface. Alternatively, as the trench approaches the east-facing topographic escarpment at the end of the trench, relatively rock-rich colluvium is likely being shed from the topographic high and incorporated into Unit 600 (Plate 1). From Station 4.5 m to the west, Unit 600 displays weak stratification, and the basal contact with Unit 500 becomes diffuse (Plate 1). Based on the degree of soil development interpreted from soil profile LCI-SPI and SP2, and stratigraphic position below younger colluvia, Unit 600 is interpreted as an early Modesto age (30-70 ka) deposit (Table 4-1).

Unit 600 is capped by two younger colluvial deposits: a laterally extensive colluvium with weakly developed soil structure (Unit 700), and a surficial colluvium with a weakly developed soil structure and modern plow (Ap) zone (Unit 800). The laterally extensive nature and relatively weak soil development associated with Unit 700 suggests it may be correlative with the Sonora colluvium, and interpreted to represent a major colluvial pulse coincident with ecological succession following the last glacial maximum (Figure 2-1). Based largely on the soil development represented in Unit 600 and limited soil development in Unit 700, we believe there is a significant age difference (possibly several tens of thousands of years) between the two colluvial deposits. Unit 700 is estimated to be of late-Modesto to post-Modesto in soil age (5 to 30 ka) and Unit 800 is post-Modesto in age (0 to 10 ka; Table 4-1).

4.6.2 Trench LCI-T1 Structural Observations

Faulting and localized shearing associated with the WPF are well exposed in trench LCI-T1 (Plate 1). The fault zone is commonly associated with zones of variably crushed rock, gouge, and crushed/disarticulated quartz veins. In particular, between stations 9.5 and 14 m, the WPF is approximately 4.5 m wide and is bounded by bedrock faults dipping steeply east and west along the western and eastern margins, respectively (Plate 1; Figure A-1). The majority of the fault zone occurs within Jss slate with the eastern fault defining the contact between Jss slate and Jgo metavolcanic rocks.

The western fault strand strikes northwest (320° to 358°), dips east between 51° and 65°, and generally aligns with the overall northwest (338°) strike of the WPF along the linear valley (Plate 1, Table 4-3). The western fault strand is associated with a 60-to 75-cm-wide zone of pulverized rock and incipient gouge that becomes progressively weathered to clay near the top of rock. Individual shears comprising the western fault strand are readily defined along the margins between intact rock and crushed rock, but are difficult to differentiate within the zones of intensely crushed rock. The oldest colluvium (Unit 500) fills a structural or erosional low that overlies the western strand (Plate 1; Figure A-1). The western margin of this colluvial low is coincident with the upward projection of the western margin of the fault zone, and a small (5 to 7 cm) bedrock step at the transition from relatively undeformed Jss slate (west) to crushed bedrock (east). Additionally, the overlying colluvial Unit 600 displays a slight easterly dip over the western fault zone.

The eastern strand of the WPF is defined by the juxtaposition of Jss (west) and Jgo (east), and is expressed as a narrow zone of crushed rock and localized clay. The eastern fault strand strikes northwest between 332° and 348°, and dips about 70° east (Plate 1, Table 4-3), or subparallel to foliation at depth (Plate 1). The fault “flowers” and branches upsection across multiple shears with variable dips near the bedrock/colluvium interface. Pockets and linear bands of clay are common along the shears and define the margins of disarticulated blocks of Jss and Jgo bedrock. Units 500 and 600 overlie the eastern fault strand.

As shown in Plate 1 (depicted as blue lines on the log), secondary faults/shears are common within both the slate and metavolcanic units west and east of the WPF, respectively. These secondary faults/shears are often parallel to foliation and delineated as planar zones of weathered/crushed rock, sand/silt sized weathered rock, clay, and localized quartz. These features typically display limited evidence for shearing or large (long-term) displacements, and do not disrupt the overlying colluvial units.

4.6.3 Evidence for Paleoearthquakes in Trench LCI-T1

One of the primary goals of the paleoseismic study is to evaluate and document the presence or absence of evidence for late Pleistocene fault deformation on the Waters Peak fault. Trench LCI-T1 exposed two primary fault strands in bedrock – a western fault strand at station 9 m, and an eastern fault strand at station 14.5 m (Plate 1).

For the eastern fault strand, only a small bedrock step (4 to 5 cm) and associated thickening of Unit 500 at station 14 could represent post-Riverbank faulting. Careful observations of Unit 500 and the underlying bedrock, however, indicate the absence of shearing or other deformation in Unit 500 across the bedrock step. Therefore, this feature likely represents differential weathering across the fault (non-tectonic) or an earlier (pre-Riverbank) offset of the top of rock subsequently filled with the deposits of Unit 500. The upward projection of the fault within bedrock does not appear to displace Unit 500 or the overlying basal contact of Unit 600. Thus, surface faulting event(s) that post-date Unit 500 (50 to 125 ka) are considered *unlikely*.

For the western fault strand of the fault, colluvial Units 500 and 600 exhibit similar vertical changes in elevation across the fault zone, and Unit 500 exhibits localized stratification within the topographic low. Both Units 500 and 600 show an absence of shearing or displacement along their basal contacts, and no shearing is observed at the small step in bedrock that occurs up-section of the mapped bedrock fault. The origin of the colluvial-filled low and subsequent deposition of overlying Unit 600 can be interpreted as either tectonic or non-tectonic in origin. These two end-member scenarios for the origin of the topographic low are presented below:

Scenario One (non-tectonic origin): The colluvium of Unit 500 is unfaulted. In this model, the bedrock low forms as a result of differential erosion and long term weathering of the western fault zone and subsequently is filled by Unit 500 colluvium. Clear observations of foliated slate blocks toppling into the topographic low require the presence of a pre-existing swale to facilitate downslope creep of foliated bedrock prior to, or during, deposition of Unit 500. Colluvial infilling by Unit 500 then results in the observed stratification with basal tabular slate clasts overlain by massive clast-rich and clast poor zones of colluvium. Based on the observation of stratigraphic infilling and stratification, we consider it to be *likely* that Unit 500 is undeformed, and thus the most recent fault activity pre-dates 50 to 125 ka.

Scenario Two (tectonic origin): In this scenario, Unit 500 is faulted at the western fault zone, resulting in localized down-to-the-east displacement of 5 to 20 cm. We believe this model is unlikely because: 1.) Unit 500 lacks evidence of shearing, 2.) there is no apparent net vertical displacement across the fault, and 3.) observations indicate Unit 500 was deposited in a pre-existing low either through colluvial or fluvial processes, or a combination of both. Based on the absence of fault deformation features and lack of net vertical displacement of the bedrock surface, we consider it *unlikely* that Unit 500 is deformed.

Similar to Unit 500, the base of Unit 600 appears to broadly step vertically across the western fault zone (Plate 1). However, projections of the base of Unit 600 across the entire western fault zone show no indication of net vertical displacement (Plate 1). Any potential fault deformation, therefore, would require predominantly lateral displacement (also valid for Unit 500). This model is inconsistent with the oblique normal displacement inferred from spillway kinematic measurements, Tertiary volcanic flows used as strain gauges across the Foothills fault system, and USACE (1995) trenches, but may be consistent with evidence for lateral displacement in trenches LCI-T2 and -T3 described below. Based on our review of regional trenching studies in

the Sierra Nevada foothills (WCC, 1978; Page and Sawyer, 2007) the apparent downward warping observed in trench LCI-T1 is also a common occurrence above both active and inactive fault strands. This especially occurs above localized zones of intensely weathered and sheared bedrock. Based on these observations, and the lack of net vertical displacement across the fault zone, we consider tectonic deformation that post-dates Unit 600 (30 to 70 ka) to be *unlikely*.

Our analysis of potential late Quaternary faulting in trench LCT-T1 indicates that fault-related minor deformation of the Riverbank (Unit 500) and lower Modesto (Unit 600) colluvial deposits is *unlikely*. Assuming that our preferred interpretation is incorrect, and that Unit 500 is faulted, the displacement of Riverbank-age Unit 500 and an unfaulted, overlying Modesto age Unit 600 indicates that the most recent activity on the western fault strand is constrained to be between 50 to 125 ka (Unit 500) and 30 to 70 ka (Unit 600), and thus falls outside of the DSOD criteria for an active fault. Lastly, there is no clear reason to favor the faulting model over a simple downwarp associated with differential weathering and erosion of materials along the western fault zone (Plate 1).

4.7 Paleoseismic Site 6 (Trenches LCI -T2 and -T3)

Site 6 is located about 365 m (1,200 ft.) south of Site 5 within the linear fault-controlled valley of the WPF (Figure 4-1). At Site 6, trenches LCI-T2 and -T3 were excavated about 67 m (220 ft.) north of previous trench USACE T-3 (1995) where previous trenching documented reasonably thick Quaternary deposition (Figure 4-1). At this site, the linear valley is bounded on the west by a steep east-facing topographic escarpment and on the east by a broad gentle west-facing slope. Late Quaternary alluvium and colluvium of moderate thickness (compared to Site 5) unconformably overlie Jss metasandstone. Trench LCI-T2 spans a large part of the linear valley and shadows much of previous trench USACE T-3; whereas trench LCI-T3 intersects a 3.5-to 4-m-wide zone of faulting exposed in trench LCI-T2. The trenches are located south of an unnamed ephemeral drainage that flows north through the linear valley and is incised along much of its length (Figure 4-1).

4.7.1 Site Geology

Based on published geologic mapping (CGS, 2014) and previous trenching (USACE, 1995), coupled with exposures from trenches LCI-T2 and -T3, the WPF coincides with the axis of the linear valley and juxtaposes similar metasandstone facies of Jurassic Salt Springs Slate (Jss) both west and east of the fault. Bedrock exposures are limited to the ridge top to the west of the trench site and southeast along Sandretto Road. The Jss metasandstone ranges from fine-to coarse-grained and due to metamorphism and a strong foliation can appear similar to the Jurassic Gopher Ridge volcanics mapped to the north of the site (Figure 4-1). The Jss bedrock is unconformably overlain by late Quaternary alluvial and colluvial deposits with different degrees of soil development.

4.7.2 Trench LCI-T2 Stratigraphy

The stratigraphy at Site 6 includes the Jss metasandstone, pedogenic clay accumulation at the top of rock, and a 0.8 to 1.1 m-thick sequence of fluvial, eolian and colluvial deposits (Plate 2; Appendix A). In general, the larger number of units and increased depositional complexity at Site 6 relative to Site 5 affords a higher level of paleoseismic resolution for evaluating late Pleistocene faulting. Site 6 was chosen primarily for this reason, as well as its proximity to previous trench USACE-T3.

Bedrock exposed in trenches LCI-T2 and LCI-T3 is comprised of Jss metasandstone that is partially or wholly volcanically derived. The foliation is fault-parallel, weak to strong, and has a consistent strike to the northwest and moderate to steep (55° to 65°) dip (Plate 2). The variability in the distribution of foliation results in heterogeneous bedrock blocks of different sizes and changes in the degree of weathering. Individual grains within the metasandstone are elongated parallel to foliation dip, indicating a previous phase of ductile deformation. Within the valley axis bedrock is capped by a zone of pedogenic clay (Unit 200, Plate 2) derived from both in-situ saprolite development as well as accumulation of translocated clays. The presence of Unit 200 is limited to the valley floor, which suggests the clay formed as a function of the topographic low and shallow groundwater flow. It is unclear if the clay formed higher on the valley margins, but if so, it has been subsequently eroded. Additional bedrock saprolite zones are observed throughout trench LCI-T2, but generally lack the uniform clay composition, continuity, and prominent yellow brown color that is used to delineate Unit 200. Unit 200 is estimated to be of Riverbank age or older (Table 4-1) and correlative with Unit 6 in trench USACE T-3 (Figure 3-2).

Bedrock and Unit 200 are overlain by a series of locally sourced alluvial deposits (Units 300, 400, and 500) containing clasts of metasandstone, andesite, quartzite, and angular quartz. Well-rounded andesite and quartzite clasts are interpreted to be sourced from the nearby Mehrten and Laguna Formations to the south-southeast, respectively. The angular quartz is interpreted to be sourced from quartz veins localized within the foliated and sheared Jss bedrock. The random distribution of quartz and quartzite pebbles and cobbles in the alluvium is similar to the heterogeneous bed load of the present-day channel between Sites 5 and 6 (Figure 4-1). Mehrten clasts encountered in the trench are moderately to completely weathered, whereas the silica-rich clasts are largely unweathered. Units 300 and 400 are mapped between stations 22 and 24.5 m, and represent the oldest alluvium encountered in the paleoseismic trenches. Soil profile LCI-T2-SP1 indicates a single soil is developed in Units 300 and 400 suggesting that these deposits are close in age (Table 4-1). Unit 300 is a coarse-grained sand and gravelly alluvium overlain by fine-grained overbank deposits (Unit 400). The western margins of Units 300 and 400 onlap onto bedrock. To the east, Unit 300 is truncated by fault F1, and Unit 400 pinches out west of fault F1 (Plate 2; Appendix A, Figure A-2). Units 300 and 400 are estimated to be of Riverbank age (Table 4-1) and equivalent to Units 4a and 4, respectively, in trench USACE T-3 (Figure 3-2).

Unit 500 represents the next youngest phase of alluvial deposition. This deposit is generally laterally continuous between stations 21 and 33 m (Plate 2). Relative to both the underlying

alluvial and overlying colluvial deposits, Unit 500 is enriched in angular quartz and is coarser-grained than the underlying Unit 400. Based on weak stratification and geometric relations at station 25.3 m, along with soil profile LCI-T2-SP2, Unit 500 likely represents multiple, similarly aged, alluvial deposits of Riverbank age (Table 4-1; Plate 2). Unit 500 pinches out to the west on the bedrock slope at station 22 m, and also pinches out to the east at station 27.75 m on a buried topographic high comprised of Unit 200 and underlying bedrock. Unit 500 reappears east of fault F2 between stations 28 and 33 m (Plate 2). This apparent gap in the lateral continuity of Unit 500 may represent erosion prior to deposition of Unit 600, possibly as a result of faulting and uplift, or alternatively it may be a function of non-tectonic depositional onlap onto or around the buried topographic high coincident with fault F2 (Plate 2; Figure A-2). Unit 500 is correlative with Unit 3a and 3b of trench USACE T-3 (Figure 3-2).

Overlying Unit 500 is an eolian/alluvial deposit (Unit 600) with a distinct soil that is relatively laterally continuous in trench LCI-T2 between stations 21 and 36 m, and with an additional localized zone between stations 42 and 44 m (Plate 2). Similar to Unit 600 encountered in trench LCI-T1, this fine-grained deposit is differentiated from other units in the trench due to the concentration of fines and presence of a moderately well-developed soil with a pronounced Bt horizon. Unit 600 is characterized by well-developed subangular blocky peds, and a distinct dark grayish brown color indicative of early Modesto age (Table 4-1). Unit 600 is interpreted to be largely eolian sourced, combined with a lesser alluvial component, as evidenced by few Mehrten and Laguna Formation clasts of andesite and quartzite, respectively, that range in size from coarse sand to cobbles. Large concentrations of subangular to subrounded quartzite cobbles and pebbles suggests Unit 600 may have been channelized, or infilled an earlier erosional channel near the eastern fault zone. The depositional character and erosional channel base of Unit 600 are similar to the present-day bedload and localized incision of the ephemeral creek north of the trenches. Unit 600 represents a key temporal marker horizon for stratigraphic correlation between the LCI trenches and USACE (1995) trench T-3, where it is correlated to Unit 3 in trench USACE T-3 (Figure 3-2). Unit 600 is undeformed across fault F1, but displays both thickness and elevation variability across fault F2 at station 28 m (Plate 2).

Overlying Unit 600 are two younger colluvial deposits (Units 700 and 800), and an alluvial channel deposit (Unit 700a). Unit 700 is a laterally extensive colluvium with weakly developed soil structure. Unit 700a represents an inset channel that is texturally similar to Unit 700 but contains clasts of quartzite. Unit 800 represents modern surficial colluvium and the Ap horizon, and has a weakly developed soil structure. The laterally extensive nature and relatively weak soil development of Unit 700 indicates it is likely correlative with the late Pleistocene to Holocene Sonora colluvium of late Modesto age (Table 4-1) and is correlative with Unit 2 of trench USACE T-3 (Figure 3-2). The channel of Unit 700a is inset into Units 700, 600, and 500 (Plate 2) and is distinguished from the other units based on texture, color, pedogenic variations, as well as an unconformable basal contact. Based largely on the soil development represented in Unit 600, and limited soil development in Unit 700, we interpret a significant age difference (possibly several tens of thousands of years) between Units 600 and 700. Units 700 and 700a are estimated to be

associated with the upper Modesto soil series or younger (Table 4-1). Unit 800 is estimated to be associated with post-Modesto soils (0 to 10 ka), and is correlative with Units 1a and 1 of trench USACE T-3 (Figure 3-2).

The stratigraphy exposed in trench LCI-T2 is present as a function of bedrock elevation, alluvial channel deposition, and colluviation associated with bedrock stripping on the upper slopes and deposition within the valley axis. In both trenches LCI-T2 and LCI-T3, as well as USACE-T3, the oldest alluvial deposits are typically found near or directly west of the western margin of faulting, while the youngest alluvial units are located farther east. In all three trenches, deposition spanning Riverbank to late Modesto age has migrated eastward. This eastward migration is consistent with late Pleistocene west-side-up/east-side-down displacement along the WPF and the overall late Cenozoic east-side-down sense of slip.

4.7.3 Trench LCI-T2 Structure

Faulting and localized shearing of the bedrock and younger deposits are preserved in trench LCI-T2 (Plate 2). Bedrock features indicative of faulting consist of zones of variably crushed rock, gouge and linear bands of saprolitic clay, and crushed/disarticulated quartz veins. Localized faults with evidence of discreet shearing are present but less commonly observed. Two main faults are present in the trench: F1 (western strand) and F2 (eastern strand) (Plate 2; Figure A-1).

Fault F1 (western strand) is located at station 24.5 m, and is expressed as a near-vertical plane within Jss metasandstone. The fault strikes northwest (344°) and branches upsection as a near-vertical fault into several east-vergent fault strands near the bedrock and saprolite (Unit 200) interface. Fault F1 clearly displaces the top of rock, pedogenic clay (Unit 200), and the oldest alluvium (Unit 300) in a down-to-the-west vertical sense. Because this strand is oriented parallel to the overall strike of the WPF, sense of slip on the fault should be a good proxy for the overall contemporary sense of slip on the WPF. However, the vertical displacement is opposite of the interpreted down-to-the-east oblique normal late Cenozoic sense of slip seen elsewhere along the fault and other adjacent faults comprising the Foothills fault system. Kinematic indicators along fault F1 were not observed in trench LCI-T2. One possible explanation for west-side-down displacement along F1 is that the most recent event accommodated predominantly lateral (strike slip) displacement.

Fault F2 (eastern strand) represents the eastern margin of the primary WPF zone in trench LCI-T2. The fault strikes west-northwesterly at 129° (rotated approximately 30° west of the regional orientation of the WPF) and dips 69° southwest. This orientation is oblique to the overall strike of the fault (Figure 4-2) and has a dip that is inconsistent with the regional northeast dip of the WPF. Fault F2 vertically displaces Jss bedrock and Unit 200 in a down-to-the-west. This sense of slip is consistent with two high quality kinematic measurements from striae in bedrock fault gouge that indicate oblique reverse faulting with rakes of 64° and 67° (Table 4-3). Based on a projection of the top of rock across fault F2, cumulative dip-slip displacement is estimated to be 32 to 38 cm, with net displacement ranging from 35 to 42 cm using a rake of 66°.

Due to the lack of lateral continuity of Unit 500 across fault F2, it is permissible to also interpret faulting extending up into Units 500 and possibly into Unit 600. Alternatively, the apparent truncation of Unit 500 may be due to depositional onlapping of Unit 500 onto the topographic high of Unit 200 (Plate 2). These relations are also present in trench USACE T-3 where alluvial units are shown as onlapping a buried topographic high (Figure 3-2). We interpret that Unit 500 either onlaps Unit 200 in the hanging wall of fault F2, or Unit 500 is paraconformable with Unit 200, and subsequently has been uplifted (faulted) and then eroded. Directly above fault F2, Unit 600 thickens across the fault zone, and exhibits a concentration of quartzite gravel that is suggestive of channelization. Clarification of these stratigraphic and structural relations indicative of possible faulting along fault F2 were the primary focus of supplemental trench LCI-T3.

4.7.4 Summary of Findings from Supplemental Trench LCI-T3

Trench LCI-T3 is located about 7 m north of trench LCI-T2 (Figure 4-1). The trench was excavated to shadow the along-strike projection of faults F1 and F2 in trench LCI-T2 to provide a second exposure of the fault zone and stratigraphic relationships of Quaternary deposits across the fault. The trench provides additional clarification on the complex fault relations exposed in trench LCI-T2 and the related possible offset of Units 500 and 600 across fault F2 (Figure 4-2 and 4-8). Trench LCI-T3 crosses the northern projection of faults F1 and F2 as observed in trench LCI-T2. Specifically, trench LCI-T3 provides additional exposures to assess the presence or absence of faulting of Units 500 and 600.

4.7.4.1 Stratigraphic Relations of Trench LCI-T3

Trench LCI-T3 exposed stratigraphy similar to trench LCI-T2, thus providing additional stratigraphic context and permitted a re-evaluation of stratigraphic/structural relations observed trench LCI-T2. The trench encountered similar alluvial and colluvial stratigraphy directly overlying bedrock (Unit 100) and Unit 200 (Plate 3). Similar to trench LCI-T2, Unit 200 overlies weathered, fractured and sheared Jss bedrock, and appears to have been eroded and removed by younger alluvial deposits (Units 310 and 500) between stations 5 and 7 m (Plate 3). Unit 310, a discontinuous alluvial deposit, is inset into Unit 200 near station 7 m. This deposit contains rounded clasts and may be correlative with Unit 300 in trench LCI-T2. Unit 320, a prominent fine-grained clay-rich alluvial deposit, is inset into Unit 310 near station 7 m. These alluvial deposits are overlain by relatively laterally continuous Units 500, 600, 700 and 800, with the exception of a discontinuous alluvial deposit (Unit 410) near the center of the trench (Plate 3). Similar to trench LCI-T2, melanization observed in Unit 600 tends to overprint the colors of the underlying clay-rich units when in close proximity. This masking of colors makes distinguishing the basal contact of Unit 600 and/or the upper contacts of underlying clay rich deposits difficult where they are in contact.

Units 500 and 600 are key to assessing the recency of activity across the WPF. Unit 500 is laterally continuous across the fault zone that includes the northern projection of faults F1 and F2 from trench LCI-T2. The base of Unit 500 is irregular and reflects the variability in the bedrock surface and Unit 200 Plate 3). In addition, Unit 600 is laterally continuous across the fault zone

and provides a distinct strain gauge to assess recency of activity. Thickness is locally variable but generally thickens slightly where the deposit is infilling apparent paleo-channels in Unit 500 and older deposits.

4.7.4.2 Structural Relations of Trench LCI-T3

Structural and stratigraphic relations observed in trench LCI-T3 provide key constraints on the timing of the most recent displacement on the western (F1) and eastern (F2) fault strands of the WPF at Site 6.

Fault F1: Fault F1 strikes northwest at 332°, and dips 82° southwest, generally similar to fault F1 in trench LCI-T2 and the overall strike of the WPF (Plate 3; Appendix A, Figure A-3). Fault F1 on the south wall does not appear to extend to the top of rock, nor does it deform Unit 200. However, along an upward projection of fault F1, Unit 200 makes an apparent down-to-the-east step at about station 6.5 (Plate 3). Shearing in the bedrock below this vertical step appears to be absent or is modified, in part, by a discontinuous deeper zone of saprolitic weathering directly west of the upward projection of faulting. It is permissible that Unit 200 is faulted and overprinted by saprolitic process, but it is unclear given the existing stratigraphic relationships. Unit 500, which overlies Unit 200, is clearly unfaulted indicating that any faulting pre-dates 50 to 125 ka, and thus exceeds the DSOD criteria of 35,000 years for an active fault.

Fault F2: Fault F2 strikes west-northwest at 133° and dips 84° northeast, similar to fault F2 in trench LCI-T2 (Plate 3; Figure A-3). Fault F2 is clearly expressed in Jss bedrock at about Station 4.5 m and extends upsection to a west-dipping contact where bedrock (on the west) overlies Unit 200 (on the east). This relation is observed on both the north and south walls of trench LCI-T3. The apparent juxtaposition of these two units is suggestive of a reverse sense of slip along fault F2. Similar to trench LCI-T2, the apparent displacement of Unit 200 provides evidence for probable late Quaternary faulting along the WPF. The faulting, however, does not extend upward into Units 405 and 500. If the apparent juxtaposition of the bedrock and Unit 200 saprolite is representative of fault displacement, then the sense of slip on F2 is reverse. If this contact is faulted, then the observed vertical displacement is approximately 23 to 34 cm. It is important to note that the overlying Unit 500 and younger deposits are unfaulted and provide evidence for the absence of younger faulting that is permissible along a similar fault F2 strand in trench LCI-T2. This observation indicates fault F2 is inactive per DSOD criteria. Lastly, the overall similar up-to-the-west reverse faulting on strands striking westerly across the more northerly oriented WPF is consistent with shortening along a fault with significant right-lateral (strike-slip) displacement.

4.7.5 Evidence for Paleoearthquakes at Site 6

Based on detailed analysis of stratigraphic and structural relations observed in trenches LCI-T2 and -T3, the WPF displays clear evidence of likely late Quaternary displacement. The timing and number of events recorded in trench LCI-T2 are more equivocal, as are the event relationships between faults F1 and F2 (i.e. contemporaneous or independent rupture). The following section details evidence for paleo-slip events in trench LCI-T2 with additional context from trench LCI-T3.

Evidence for paleoearthquakes is subdivided by faults F1 and F2 for ease of discussion. Faults F1 and F2 for both trenches should be considered the same fault (i.e. F1 in LCI-T2 = F1 in LCI-T3) for simplicity but may or may not be the same fault strands. Fault F1 is the western strand oriented parallel to the overall strike of the WPF, and fault F2 is a more westerly striking fault accommodating shortening. The age of faulting is estimated from soil development parameters established for the site by USACE (1995), regional soil models (Table 4-1, Figure 2-1), and multiple soil profiles in trenches LCI-T2 and -T3.

4.7.5.1 Fault F1

In trench LCI-T2, fault F1 displaces the base of Unit 200 vertically about 15 to 23 cm, as measured on the north and south walls, respectively (Plate 2, Appendix A, Figure A-2). The base of Unit 300 is displaced vertically about 19 cm on the north wall, and at least 16 cm on the south wall. On the south wall Unit 300 lacks an offset equivalent across the fault, therefore the vertical displacement is considered a minimum. The similarity in vertical displacements of Units 200 and 300 across fault F1 in both trench walls is likely due to displacement during a single event. Unit 300 is estimated to be of Riverbank age, and thus demonstrates that fault F1 is Quaternary active. Fault F1, however, does not offset overlying Unit 500 that has an estimated soil age of early Modesto to late Riverbank (50 to 125 ka)(Table 4-1). Thus, the age of the most recent fault displacement is > 50 ka and falls outside the range of DSOD criteria (<35,000 yrs) for an active fault. We note that the down-to-the-west sense of slip is inconsistent with the late Cenozoic down-to-the-east sense of displacement. This sense of displacement cannot be readily explained by an anomalous fault orientation that favors oblique displacement. It is possible that the apparent vertical separations observed across fault F1 are the result of primarily strike slip faulting. Fault F1 in trench LCI-T3 does not appear to extend to the top of rock or deform Unit 200 (Plate 3), although saprolitization may obscure this potential relation. The overlying Unit 500 deposit is not deformed above fault F1 in LCI-T3, consistent with the absence of Unit 500 deformation above fault F1 in LCI-T2. Based on the estimated 50 to 125 ka for the Unit 500, the age of faulting on F1 falls outside of the DSOD criteria (<35,000 ka) for an active fault.

4.7.5.2 Fault F2

Stratigraphic and structural relations observed along and above fault F2 in trench LCI-T2 display greater complexity than those observed across fault F1 (Plate 1). Similar to fault F1, fault F2 exhibits clear evidence of late Quaternary faulting. To account for the additional complexity, multiple event models are presented to explore the range of uncertainty in the interpretations of event stratigraphy. Three primary models (models 1 to 3) are considered and all recognize a late Quaternary event on fault F2 that displaces Jss bedrock (Unit 100) and Unit 200 similar to fault F1. The three models are shown in Figure 4-3. Clear displacement of Unit 200, a Riverbank to Turlock Lake-aged paleosol and clay, indicates fault F2 is a Quaternary active fault, similar to fault F1.

Model 1: This model represents a single-event scenario where only Jss metasandstone and Unit 200 are faulted. Model 1 considers the geometric complexity observed in overlying Units 500 and

600 as related to non-tectonic processes, such as deposition and erosion over the fault zone (Figure 4-3; Plate 2). In this model, unfaulted Unit 500 is partially eroded by channelization that is coincident with Unit 600 deposition. This model is supported by an increase in subangular quartzite clasts located within an inferred paleochannel thalweg that aligns with the fault, not unlike what is observed in the present-day ephemeral channel north of Site 6.

The net displacement of the top of bedrock for this event is estimated to be 35 to 42 cm, with the majority of the slip occurring as dip-slip displacement. The age of this postulated event, therefore, predates the interpreted 50 to 125 ka age of the soil developed into Unit 500 that is undeformed across fault F2 (Figure 4-3). Lastly, due to the proximity of faults F1 and F2 (separated by less than 4 m), together with evidence indicating both fault strands are Quaternary active, it is probable that both faults ruptured in the same event. In this scenario, faults F1 and F2 displace the bedrock and Unit 200, but not the overlying Unit 500. It is inferred that if Unit 300 were present across Fault F2 during this event, Unit 300 also would be faulted; therefore, the combined net displacement is at least 49 to 65 cm. This value is considered a minimum since no kinematic measurements were available from F1 to allow for conversion of the vertical displacement values to net displacement. Model one is less complex than the other two models and doesn't invoke more complicated scenarios to explain different fault histories between faults F1 and F2, and the absence of the same features in the adjacent trench LCI-T3 (Section 4.6.5). The model 1 event is considered *probable*.

Model 2: This model recognizes an apparent single event on fault F2 that displaces bedrock, Unit 200, and Unit 500 in trench LCI-T2. Unit 600 is unfaulted across fault F2 (Figure 4-3; Plate 2). Fault model 2 is similar to model 1, but the earthquake event occurs post-deposition of Unit 500 and results in a younger faulting event than model 1 (Figure 4-3). Unit 600 is undeformed in model 2 and provides a minimum age for the absence of faulting. The age of this event would post-date the 50-125 ka soil age for Unit 500 and predate the 30 to 70 ka soil age for Unit 600. The age of faulting, therefore, falls outside of the DSOD criteria for an active fault. Note that this postulated earthquake displaces Unit 500 on fault F2, but Unit 500 is unfaulted across fault F1; the scenario earthquake only ruptured fault F2. Net displacement for this hypothetical event on fault F2 is 35 to 42 cm.

In trench LCI-T3, Units 405 and 500 are not displaced by fault F1 in the south wall exposure but display a small warp across the bedrock saprolite fault contact (F2; Plate 2). Unit 600 is not deformed across fault F2. We believe the warp of Units 405 and 500 is most likely related to differential weathering of the bedrock and saprolite rather than faulting. This is because the vertical deformation necessary to generate the warp is considerably smaller than the displacement required to juxtapose Jss over the Unit 200 saprolite. A second earthquake could be invoked to warp these units, but stratigraphic relations of Unit 500 in LCI-T3 make this unlikely. Based on the observed relations in trench LCI-T3, we consider it *likely* that an event displaced bedrock and Unit 200, but did not displace overlying younger strata.

Model 2 is partly supported by the apparent juxtaposition of Unit 500 against Unit 200 near the upward termination of F2 in trench LCI-T2 (Figure 4-3). Importantly, shearing was not observed at the contact, yet the juxtaposition of these units is suggestive of faulting. We note that a channel inset of Unit 500 could also explain the geometry of this contact (see model 1). In summary, the model 2 event would be considered *possible* given the observations from trench LCI-T2 alone, but the stratigraphic and structural relations in trench LCI-T3 (Section 4.6.5) make this event *unlikely*.

Model 3: This model, interpreted from relations observed in trench LCI-T2, invokes a two-event scenario where all deposits below Unit 700 are faulted, with the net displacement of Unit 600 being much less than Units 200 through 500 (Figure 4-3). The first event is consistent with a model 2 earthquake where Unit 500 and older deposits are faulted, and then is followed by a younger event that displaces Unit 600. The hypothesized second event accounts for the geometric changes of Unit 600 across fault F2. For instance, the apparent vertical separation of 10 to 14 cm of the base of Unit 600 is less than the net displacement across Unit 200. We note that there is no evidence for discrete faulting (i.e. shearing) within Unit 600. If the apparent vertical warp in Unit 600 is associated with fault deformation, it was most likely was accommodated through folding during a relatively small hypothetical most recent event. If the event did occur, then it must post-date the 30 to 70 ka soil age, suggesting that fault F2 may be active within the DSOD criteria (<35 ka). As described above, exposures of Unit 600 in trench LCI-T3, above fault F2, indicate Unit 600 is unfaulted and likely undeformed. While the interpretation that Unit 600 is deformed by F2 in trench LCI-T2 is equivocal, trench LCI-T3 provides clear evidence for the absence of faulting along fault F2. Therefore, we consider model 3 *unlikely* based largely on stratigraphic relations encountered in trench LCI-T3.

4.8 Summary of Results from the Waters Peak Fault Paleoseismic Study

Paleoseismic trenches excavated as part of the fault rupture hazard investigation of the WPF exposed stratigraphic and structural relations useful for evaluating the mid to late Quaternary paleoseismic rupture history of the fault. These studies provide valuable information on the timing of the most recent event (MRE), possible sense of slip, and width of deformation. LCI's analysis of the 2019 trench exposures, together with a detailed review of the earlier USACE (1995) T-3 results, indicate the WPF is *likely* inactive per DSOD criteria (<35 ka; Fraser, 2001) for active faults in California. These findings are consistent with previous results from USACE (1995) studies at the Waters Peak North and South sites.

Collectively, the trenches expose alluvial and colluvial deposits and multiple buried paleosols that range in age from late Holocene (surficial soil) to potentially as old as mid Pleistocene (Unit 200; Riverbank; Table 4-1). These deposits provide a record of deposition that likely spans one hundred to possibly several hundred thousand years, and thus provide key strain gauges to assess fault activity. This investigation ultimately focused on the widely distributed Unit 600 (eolian deposit with alluvial and colluvial components) as the primary strain gauge for the presence or absence of recent activity. The soil developed in associated Unit 600 is interpreted

as early Modesto age (30 to 70 ka; Table 4-1). This soil age provides a minimum age for Unit 600, because the deposit age must be older than the soil age. Therefore, Unit 600 largely predates the <35 ka age distinction for active faults according to DSOD criteria (Fraser, 2001). Similar to the findings of USACE (1995), we recognize clear evidence for late Pleistocene faulting on the WPF with the displacement of Units 200 and 300 of Riverbank age, but find evidence for an absence of <35 ka (post-Unit 600 and younger) surface rupturing earthquakes. Observations from trench LCI-T2 provide conclusive evidence for one or two surface rupturing earthquakes that displace the Unit 200 saprolite (Turlock Lake to Riverbank age) and Unit 300 alluvium (late/middle Riverbank age). Evidence supporting a more recent event that displaces the lower Modesto Unit 600 in trench LCI-T1 is generally poor and thus *unlikely*; in trench LCI-T2 is equivocal, but also *unlikely*. The exposure in trench LCI T-3 indicates Units 500 and 600 are unfaulted. We thus conclude that the youngest fault displacement (MRE) on the Waters Peak fault is older than 50-120 ka (Unit 500), and therefore the fault is inactive per DSOD criteria. These findings are consistent with findings from USACE (1995) and associated conclusions by the expert peer reviewers for the previous Waters Peak fault investigation (Page, 1994, Shlemon, 1994; WLA, 1994).

Because the sense of slip on the WPF is an important parameter for evaluating fault displacement hazard and seismic source modeling, resolving the late Pleistocene slip direction of the WPF was a primary objective of the paleoseismic study. Kinematic observations from the spillway mapping and data compilation support dextral oblique normal faulting (Table 4-3). These findings are consistent with the long term Cenozoic east-side-down sense of slip of the WPF developed from geologic mapping and topographic profiles of the Campbell Creek tuff member of Valley Springs and Mehrten Formations. However, kinematic observations of reverse faulting on westerly-oriented (restraining geometry) faults in trenches LCI-T2 and -T3, coupled with clear west-side-down displacement on faults in the trenches support a potentially greater contribution of lateral slip on the WPF in the late Quaternary than would be expected from spillway observations and regional studies. Because the WPF is oriented subparallel to the overall northwest direction of macroscopic dextral shear, paleoseismic evidence of a dextral slip component is anticipated.

5.0 SEISMIC SOURCE MODEL

Current geological and seismological evaluations of seismic hazards for critical facilities in the western foothills of the Sierra Nevada are built on information and concepts introduced by projects that began in the 1970s. Major seismic hazard studies in the subject region included those in support of PG&E's proposed Stanislaus nuclear power plant (Woodward-Clyde Consultants (WCC), 1978), the proposed Auburn Dam by the US Bureau of Reclamation (Schwartz et al., 1977), EBMUD's Pardee Dam (ESA, 1992; HCG, 1998), and the US Army Corps of Engineers' New Melones Dam (Biggar et al., 1978) and New Hogan Dam (Dames and Moore, 1993; USACE, 1995). During the initial years of these studies, particularly the alternative siting studies conducted for PG&E for a nuclear power plant site along the western Sierra Nevada foothills (WCC, 1978), the August 1, 1975, local magnitude (M_L) 5.7 Oroville earthquake stuck near Oroville Dam (Morrison et al., 1976; California Department of Water Resources, 1979). This earthquake occurred on the Cleveland Hill fault, a pre-existing Mesozoic fault that had been identified prior to the earthquake as part of the Swain Ravine *lineament*, with evidence suggestive of prior Quaternary activity (Schwartz et al., 1977). This earthquake and the concurrent and following geologic investigations led to the recognition that Mesozoic reverse faults of the Foothills fault system have been locally reactivated as normal and normal-strike-slip-oblique faults during the late Cenozoic (approximately the past 10 million years or so), and that these reactivated faults should be considered in seismic hazard analyses for critical facilities despite the very low rates of historical seismicity within the geodetically "rigid" Sierra Nevada microplate.

Since the 1975 Oroville earthquake, seismic hazard studies have generally followed a standard methodology designed to identify "active" faults in the western Sierra Nevada foothills (focusing on the Foothills fault system) that should be considered for seismic hazard assessment (e.g., WCC, 1978). The methodology consists of mapping lineaments suggestive of active faulting (such as scarps, linear valleys, aligned benches or saddles, aligned springs or ponds), evaluating the association of bedrock faults or shear zones with the lineaments, evaluating locations where these lineaments intersect or cross late Cenozoic geologic units for signs of faulting within the Cenozoic units, and, if possible, examining the late Quaternary activity of these faults through paleoseismic trenching (e.g., Page and Sawyer, 2007). The challenges of these studies include the low rates of historical seismicity in the foothills, the low rates of movement on the faults (and the resulting long recurrence intervals of earthquakes large enough to produce surface-fault rupture) compared to rates of landscape erosion, and the relative lack of geologic units useful for evaluating fault slip rate or recency of activity.

Recognizing these challenges, regulators have provided guidance regarding criteria to use in determining whether a fault should be included in a seismic hazard assessment. Because the seismic safety of Pardee Dam falls under the regulatory jurisdictions of the California Department of Water Resources, Division of Safety of Dams and the Federal Energy Regulatory Commission (FERC), we focus on the definitions and criteria for identifying active faults developed by these agencies. Current DSOD guidelines define an *active fault* as having ruptured within the last 35,000 years, and a *conditionally active fault* as having ruptured in the Quaternary, but its

displacement history during the last 35,000 years is unknown (Fraser, 2001). In addition, pre-Quaternary faults that can be "reasonably shown to have attributes consistent with the current tectonic regime" are also considered by DSOD to be conditionally active, and the guidelines specifically provide the example that Mesozoic faults in the foothills of the Sierra Nevada geomorphic province are considered conditionally active unless proven otherwise (Fraser, 2001).

DSOD guidelines state that active and conditionally active faults are used to develop deterministic design ground motions, but faults judged to be inactive may be eliminated from further consideration. An *inactive fault* is "demonstrated by a confidently located fault trace that is overlain by unbroken geologic materials older than 35,000 years" (Fraser, 2001). Faults that have no indication of Quaternary activity are presumed to be inactive as well.

Current FERC guidelines for the evaluation of earthquake ground motions are presented in Idriss et al. (2018). These guidelines summarize the recency of fault displacement criteria used by various federal regulatory agencies to distinguish potentially active faults from inactive faults, including the US Bureau of Reclamation (100,000 years), and the US Army Corps of Engineers (35,000 years). The FERC guidelines, however, do not use fixed criteria based on recency of last displacement, and instead highlight key fault parameters such as fault slip rate, amount of displacement per event, earthquake fault rupture dimensions, earthquake size, and earthquake recurrence interval. The FERC guidelines for deterministic seismic hazard analysis require that ground motions (a target spectrum) be developed for "each source" that is, "significant to the site" based on a geologic and seismologic evaluation, with the statistical level (percentile) of ground motion based on the slip rate of the fault source (Idriss et al., 2018, their Section 6.3). Elsewhere, the FERC guidelines specify that, "Special studies are required if a fault traverses or is suspected to traverse the dam or a critical appurtenant structure." (Idriss et al., 2018, their Section 6.1).

The scope of this current study included consideration of previously recognized fault sources within approximately 10 km of Pardee Dam. Our review focused on developing parameters useful for probabilistic seismic hazard analysis (PSHA), but these data may be considered for deterministic seismic hazard analysis (DSHA) as well. Our approach consisted of reviewing previously published data and conducting desk-top evaluations of digital topographic data and imagery. State-wide fault databases we reviewed include the Fault Activity Map of California (Jennings and Bryant, 2010) and the national Quaternary fault database (USGS and CGS, 2006; updated 2018). Previous geological and engineering reports on fault sources in the Pardee Dam vicinity we reviewed included WCC (1978), ESA (1992), Dames and Moore (1993), USACE (1995), HCG (1998), and Page and Sawyer (2001; 2007). We also reviewed several other geotechnical reports that included seismic hazard evaluations for Pardee Dam, but these reports did not contain additional new data or analysis regarding the characterization of local fault sources. Recent geologic maps reviewed for the assessment included 7.5-minute quadrangle maps of the Ione, Jackson, Valley Springs, and Wallace quadrangles (Gutierrez et al., 2015; Holland and O'Neal, 2019; Holland et al., 2015; and O'Neal et al., 2015, respectively). Digital topographic data reviewed included LiDAR data for Calaveras County and 10 m NED digital

elevation data for the remainder of the Pardee Dam region. Imagery from Google Earth and ESRI were also reviewed.

Based on our evaluation, we recognize seven fault sources within 10 km of Pardee Dam that should be considered for inclusion in PSHA and may be reviewed and considered for DSHA. The fault sources, listed in order of proximity to Pardee Dam, are the following:

Waters Peak – Green Springs Run	(0.2 km)
Devils Gate	(1.0 km)
Ione	(1.2 km)
Youngs Creek – Bowie Flat	(3.8 km)
Haupt Creek	(5.9 km)
Poorman Gulch – Rawhide Flat	(9.7 km)
Slate Creek	(10.2 km)

Below we describe each of the seven fault sources, including their geologic and geomorphic basis for inclusion, geometry, evidence for late Cenozoic activity, evidence for recency of activity, style of faulting, and basis for slip rate in the current tectonic regime. Figure 5-1 shows the fault sources, and Table 5-1 provides a summary of activity information for each fault along with simplified fault source parameters that may be considered for DSHA. Activity information includes a listing of the youngest age of activity documented for the fault, and the oldest age of inactivity documented for the fault. These ages are associated with qualitative confidence rankings using the scheme shown in Table 4-2. The activity information is listed to help explain the DSOD fault activity categories in Table 5-1.

Fault source parameters needed for PSHA include source location and geometry (length, dip, and depth), style of faulting, and a description of the magnitude-recurrence relationship. The magnitude-recurrence relationship requires definition of a functional form of the relationship (called the magnitude probability density function or magnitude PDF), an evaluation of characteristic or maximum rupture lengths and/or estimation of the largest earthquake magnitudes that can occur on the fault source, and a means to calculate earthquake rates. Figure 5-2 contains a logic tree for the fault source characterization that presents these parameters, epistemic alternative parameter values, and logic-tree branch weights for the alternative values based on our evaluation. The simplified source parameters listed in Table 5-1 are drawn from the fault parameters in Figure 5-2. In the subsections below, we summarize the basis for the logic-tree values and weights for each fault source as well as the summary information for Table 5-1.

In addition to the local fault sources, LCI also prepared a background source model for inclusion in a PSHA. The background model represents the source contribution from background earthquakes (earthquakes of engineering significance on faults that are unknown or not recognized as being active). A description of the background source model and a hazard input document (HID) describing how to implement it is in Appendix C. A full PSHA for Pardee Dam

should consider contributions from local fault sources, regional fault sources (e.g., San Andreas and Great Valley fault sources to the west; fault sources representing the eastern margin of the Sierra Nevada microplate (Walker Lane) to the east), and the background source.

5.1 WATERS PEAK – GREEN SPRINGS RUN FAULT SOURCE

The Waters Peak fault (WPF) is the primary subject of this report and is discussed in Sections 3 and 4, including details from previous trenching and mapping studies, as well as LCI's recent evaluation of WPF. The following section provides an overview of these previous and current results, and details the basis for the source characterization of the WPF.

The WPF was recognized as a potentially active fault by ESA (1992) and Dames and Moore (1993) on the basis of a strong northwest-trending geomorphic lineament coinciding with a mapped fault in Mesozoic metamorphic bedrock west of Pardee Dam. Located 200 m west of Pardee Dam at closest approach, the WPF is well expressed in the Mokelumne River gorge and Pardee Dam spillway where it dips steeply to the east at 64° to 70° (ESA, 1992; HCG, 1998; this study, Section 3.0). Late Cenozoic offsets have been noted by many previous authors (e.g. ESA, 1992; USACE, 1995; HCG, 1998; Page and Sawyer, 2001; 2007). HCG (1998) and Page and Sawyer (2001, their profile 31) both noted east-side down vertical separation of the Castle Rock Tuff (Oligocene Valley Springs Formation) across the WPF on the order of 46 to 62 m, and 60 to 120 m, respectively. Reevaluation of offsets of the Campbell Creek Tuff (stratigraphic equivalent to the Castle Rock Tuff) show east-down vertical separations on the order of 57 to 132 m (this study, Section 3.). Trenches across the WPF at multiple locations between Pardee Dam and New Hogan Reservoir document offset of Miocene Mehrten Formation and offset of younger alluvium/colluvium interpreted to be middle to late Quaternary age (USACE, 1995; this study). The summary fault activity and parameter table (Table 5-1) and Section 4.8 list the youngest activity documented for the WPF to be Riverbank to early Modesto in age; estimated to have occurred between 50 to 120 ka. Based on the data and analysis presented in Sections 4.6 to 4.8, the most recent event and associated age are given a qualitative confidence ranking of *Likely* (Table 4-2). The "oldest inactivity documented" for the WPF is early Modesto age (30 to 70 ka; Table 5-1), with a confidence of *Likely*, based on the documented absence of offset of unit 600. Based on this inactivity constraint, the Waters Peak fault is inactive under DSOD criteria (Table 5-1).

The style of faulting across the WPF in the current tectonic regime is east-down, strike-slip-normal oblique based on structural and stratigraphic evidence in trenches (WLA, 1994; this study), south-plunging slickensides on faults exposed below Pardee Dam (this study), and possible dextral offsets of Mehrten Formation north of Pardee Dam (HCG, 1998). The WPF is classified as Quaternary age in the Fault Activity Map of California (Jennings and Bryant, 2010) and in the national Quaternary Fault and Fold database (CGS and USGS, 2006; updated 2018).

For seismic source characterization, we consider a 62-km-long, north-northwest-striking fault source that combines the east-side down WPF with the east-side down Green Springs Run fault

(part of the east-facing O'Byrne Ferry Monocline) mapped along strike to the southeast across the Miocene Table Mountain Latite near the Stanislaus River (WCC, 1978; Page and Sawyer, 2007) (Figure 5-1). Pardee Dam lies at the northern end of the Waters Peak – Green Springs Run seismic source. ESA (1992) and Dames and Moore (1993) both recognized the continuity of the trend of lineaments and bedrock structures connecting the WPF with the Green Springs Run fault to the southeast. The Green Springs Run fault is mapped near the western-most boundary of the Bear Mountains fault zone, and juxtaposes Jurassic Salt Springs Slate to the west with Copper Hill volcanics to the east (WCC 1978). Along much of the length of Green Springs Run fault it is defined by a strong geomorphic lineament and east-facing scarps. The east-facing O'Bryne Ferry Monocline (which includes the Green Springs Run fault at its eastern synclinal hinge) shows approximately 50-70 m of east-side down vertical separation of the Miocene Table Mountain Latite (WCC, 1978; Page and Sawyer, 2001, their profile 32; PG&E, 2017). This vertical separation is on the same order as the east-down separations of the Valley Springs Formation marker horizons measured across the WPF south of Pardee Dam (Page and Sawyer, 2001, their profile 31; this study). The north end of the Waters Peak – Green Springs Run fault source is located at the northern end of Pardee Reservoir by Stoney Creek Road and is modified from Jennings and Bryant (2010) based on updated geologic mapping of the WPF in the Ione 7.5-minute Quadrangle (Gutierrez et al., 2015). This location coincides with a loss of a clear geomorphic expression of the WPF farther north. The south end of the fault source extends to the southern reaches of the Green Springs Run fault, located where the structure intersects the Keystone structure, as defined in WCC (1978).

Our fault source characterization for the Waters Peak – Green Springs Run fault source is shown graphically in Figure 5-2. The probability of activity of the source is [1.0] based on clear evidence for offset late Cenozoic and Quaternary strata. We note that this probability of activity is intended for PSHA input, and is separate from the activity classification of DSOD based on recency of displacement (Fraser, 2001; Table 5-1). The source length of 62 km is derived from north of Pardee Reservoir to approximately 5 km south of Table Mountain (Figure 5-1). This source length is longer than those previously considered by ESA (1992) or HCG (1998), but those studies did not document a technical basis for terminating the fault source to the south, and our review suggests a connection with a similarly active late Cenozoic structure along strike to the southeast without significant steps, bends, or structural complexities is a compelling basis for considering the fault source to be at least 62 km long. The average dip of the fault source through the seismogenic crust is modeled to range from 50°NE to 80°NE (logic-tree branch weights of 0.3 each to the low and high values), with a preferred value of 65°NE (logic-tree branch weight of 0.4) based on the near-surface fault dip observed in trench exposures and the spillway of Pardee Dam. The 0.3, 0.4, 0.3 weighting scheme for the three epistemic alternative values reflects an approximation of the 10th, 50th, and 90th percentile values of a continuous uncertainty distribution (Keefer and Bodily, 1983). The middle, preferred value is listed in the summary table (Table 5-1) and is suggested for use in DSHA. The maximum rupture depth of the fault source has a three-point uncertainty distribution in the source characterization, with values of 20 km, 15 km, and 10 km with weights of 0.3, 0.4, and 0.3, respectively. These alternative maximum thickness values

reflect uncertainty in both the seismogenic thickness of the crust under the western Sierra Nevada foothills (evaluated based on microseismicity depths) and uncertainty in the geometry of the reactivated faults (i.e., depth to a gently-dipping detachment at the base of the Foothills fault system that would represent the bottom of the fault source). As with fault dip, the middle, preferred value is listed in the summary table (Table 5-1) and is suggested for use in DSHA.

The magnitude-recurrence relationship for the Waters Peak – Green Springs Run fault source is based on two alternative magnitude PDFs, three alternative "characteristic" magnitudes (Mchar), and three alternative slip rates representing the average rate of seismogenic slip in the current tectonic regime. The "maximum magnitude" magnitude PDF model (Wesnousky et al., 1983) is weighted 0.8 and the truncated exponential model (Cornell and Vanmarcke, 1969) is weighted 0.2. The notes in Figure 5-2 explain how we recommend parameterization of the two magnitude PDF models, including the recommendation to set the maximum magnitude of the fault source in the truncated exponential model to a value that is 0.5 magnitude units greater than the Mchar values. Our suggested use of a combination of these two functional forms of the magnitude-recurrence relationship is intended more to represent aleatory variability in the magnitude-frequency distribution rather than epistemic alternatives. In this more aleatory concept, fault sources are estimated to rupture most commonly in earthquakes of a size proportional to some characteristic rupture dimension (Klinger, 2010), but also, less frequently, may rupture in smaller patches up to large, complex ruptures that exceed the characteristic rupture dimensions (e.g., Biasi and Wesnousky, 2016). For this Pardee Dam seismic source update, values of Mchar for the Waters Peak – Green Springs Run fault source are **M** 7.0, **M** 6.4, and **M** 6.0 with weights of 0.3, 0.4, and 0.3, respectively. These weights are based on characteristic rupture lengths of about 40 km, 20 km, and 12 km, respectively, and estimated rupture areas from these rupture lengths that take into account maximum fault source widths (a function of source dip and maximum depth), and earthquake rupture aspect ratios (ratio of rupture length to rupture width; see Leonard, 2010). The resulting Mchar values are mainly based on the empirical magnitude-area relation of Hanks and Bakun (2014) developed mostly from a dataset of strike-slip earthquake ruptures. The three-point distribution of Mchar values plus the magnitude variability from the alternative magnitude PDFs capture both natural variability in earthquake size and epistemic uncertainty in empirical magnitude scaling models, rupture aspect ratios, and rupture geometries considered in the analysis. We note that the middle value of Mchar, **M** 6.4, is similar to the MCE magnitude estimates for DSHA used by HCG (1998) and AMEC (2012), and the low value of Mchar, **M** 6.0, was considered by ESA (1992). The high Mchar value of **M** 7.0 is close to an estimate of maximum magnitude for the combined Waters Peak and Green Springs Run faults of **M** 6.8 proposed by USACE (1995). These magnitudes are generally consistent with the finding from paleoseismic trench data on the Waters Peak fault and elsewhere in the western Sierra Nevada foothills for single-event displacements less than 1 m, and possibly on the order of a few decimeters (WCC, 1978; WLA, 1994; USACE, 1995; Page and Sawyer, 2007; this study) when considering empirical scaling between average displacement and moment magnitude (Wells and Coppersmith, 1994).

We note that an earthquake rupture of the entire, 62-km long source would be approximately **M** 6.8-7.3 depending on the values used for fault dip and rupture thickness and using the Hanks and Bakun (2014) magnitude-area relation. This "full source length" rupture scenario is captured in the PSHA through the combinations of Mchar values and the magnitude variability in the magnitude PDFs between Mchar and Mmax. For example, the preferred Mchar value of **M** 6.4 is associated with an Mmax value of **M** 6.9 using the truncated exponential magnitude PDF model (following our rule to set Mmax = Mchar +0.5; Figure 5-2). The largest magnitude considered for the fault source in the PSHA is **M** 7.5, which is represented by the high branch Mchar value of **M** 7.0 plus the 0.5 magnitude offset for Mmax; this event would represent a higher than average stress drop event on the entire, 62-km-long fault source. Although these higher, full-source length ruptures are included in the PSHA, we consider them to represent very unlikely magnitudes given the observations of fault displacement in trenches, and thus consider the range of Mchar values in the logic tree to be more likely estimates of a "maximum" earthquake size consistent with past practice in DSHA. We suggest use of the middle, preferred Mchar value of **M** 6.4 in the summary fault parameters (Table 5-1).

The recommended method to calculate earthquake recurrence for the Waters Peak – Green Springs Run fault source is using fault slip rate and performing moment balancing of the fault source (Figure 5-2). For slip rate we consider the long-term slip rate using Cenozoic age volcanic strain gauges and shorter-term rates constrained by middle-late Quaternary deformation collected from trenches. Using the east-down vertical separation of the tuff in Valley Springs Formation (57 to 132 m), an estimated fault dip of about 65° (range 80° to 50°), and an estimated horizontal to vertical displacement ratio of 1.5:1 (range 0.5:1 to 3:1) results in late Cenozoic net offset of approximately 190 m (range about 54 to 504 m). This net displacement estimate considers a greater range of horizontal to vertical displacement ratios than previous studies; particularly than the ESA (1992) study that did not recognize possible significant lateral components of slip. Estimating an onset of late Cenozoic deformation in the Mokelumne River vicinity of approximately 5 million years ago (MA), with an uncertainty range of 7 to 3 MA (Wakabayashi, 2013; Wakabayashi and Kemp, 2015; and PG&E, 2017), results in a long-term average net slip rate of about 0.04 mm/yr, with a range of 0.002 to 0.1 mm/yr. The preferred rate is about twice the slip rate of 0.02 mm/yr estimated by HCG (1998), although they did not explore slip rate uncertainty in their analysis.

The preferred and maximum long-term average rates of slip estimated from offset Cenozoic strata do not appear to be consistent with middle to late Quaternary fault activity as suggested by trench data collected south of Pardee Dam. Accordingly, we use trench observations from USACE (1995) and this study to modify the fault slip rate distribution for the logic tree (Figure 5-2). The trench data suggest, approximately, a record of zero earthquakes in the past approximately 60,000 years and likely one (possibly two) event in the past approximately 130,000 yrs (resulting in about 0.5 m vertical displacement of the older saprolitic and alluvial Units 200 and 300. In order to explore what constraint these data may have on fault slip rate, we considered a range of *vertical* fault slip rates, implied accumulated fault slip over the 130,000 yr observational period from the

trenches, and a broad range of estimated single-event earthquake slips to see what combinations of slip rate and per-event slip were inconsistent with the trench data.

We estimated the accumulated vertical slip on the fault assuming a range of *vertical* slip rates from 0.002 to 0.03 mm/yr (the range derived from our late Cenozoic slip rate analysis) over the past 130,000 years (a "young" estimated age of the deformed deposit). This results in 0.26 m to 3.9 m of accumulated slip, from which 0.5 m of slip was subtracted representing the vertical offset noted in the 2019 LCI trenches. Using the remaining accumulated slip (values range from -0.24 m to 3.4 m), and estimated average vertical slips per event, we can estimate the number of "expected" slip events that are missing from the trench record. Based on trench data from the Waters Peak fault (USACE, 1995; this study) and other faults in the western Sierra Nevada foothills (WCC, 1978), we evaluated a range of estimated average vertical slips per event of 0.2 m, 0.5 m, and 1 m. The combination of "slip deficit" and average slip per event estimates results in a range of "expected" numbers of events that are missing from the trench data. A low number of "expected" events is considered a satisfactory result and consistent with the estimated slip rate used to estimate the slip deficit; if the earthquake cycle for large, surface-rupturing events is periodic, for example, values would range between -1 and 1. In our evaluation, we consider a number of "expected" slips of about 4 to be the limit of a slip deficit allowable given that earthquake recurrence is not a periodic process. If values are greater than 4 we consider the combination to be extremely unlikely. This approach suggests that vertical slip rates less than 0.02 mm/yr are consistent with the trench data, and vertical rates 0.03 or higher are highly inconsistent with the trench data.

Using the paleoseismic constraints but also considering the long-term slip rate data, we derive a preferred net slip rate of 0.01 mm/yr with an uncertainty range of 0.004 to 0.045 mm/yr (Figure 5-2). These slip rates are consistent with vertical displacements of 0.5 to 2 m in 130,000 years, and a range of rake values implying horizontal to vertical ratios of about 1.5 with a range of 0.5 to 3. These values are given weights of 0.4 for the preferred slip rate and 0.3 each for the lower and upper slip rate values. The final logic-tree values for Waters Peak slip rate span a broad range of uncertainty that are within the uncertainty bounds of the longer-term geologic slip rate estimated using the Valley Springs Formation. The preferred slip rate value of 0.01 mm/yr is listed in the summary table (Table 5-1) and is suggested for implementing the FERC approach to calculate a deterministic ground motion percentile (Idriss et al., 2018).

5.2 Devils Gate Fault Source

The Devils Gate fault was proposed as a late Cenozoic fault by ESA (1992), Dames and Moore (1993), and HCG (1998) on the basis of topographic steps in Tertiary volcanic strata at two locations northwest and southeast of Pardee Dam. Located approximately 1 km east of Pardee Dam at closest approach (Figure 5-1), WCC (1978), ESA (1992), USACE (1995), and HCG (1998) all recognized the Devils Gate as a strong topographic lineament on the eastern side of Pardee Reservoir, coinciding with the western margin of the Bear Mountains fault zone, though WCC (1978) noted it as part of the Spring Valley structure. Structural offsets were documented by WCC

(1978), ESA (1992), and Dames and Moore (1993), who interpreted a west-facing topographic step in late Tertiary volcanic rocks east of Pardee Reservoir, an east-facing topographic step in Miocene Mehrten Formation south of Pardee Reservoir, and a 12 m west-side down vertical stratigraphic offset in Mehrten Formation north of Lake Amador, respectively. A west-side down offset in the Castle Rock Tuff (Valley Springs Formation) was later suggested by Page and Sawyer (2001) from a geomorphic profile in the Comanche Reservoir-Mokelumne Hill area (profile 31; Figure 5-1). Dextral strike-slip displacements were proposed by HCG (1998) from an exposure of a secondary fault trace in the Jackson Creek Spillway channel that locally juxtaposed Jurassic Salt Springs Slate with Late Jurassic Copper Hill volcanics, as well as from a palinspastic reconstruction of Mehrten-age channels across Highway 88 that suggested 150-450 m of displacement. Based on its location 1-2 km east of the Waters Peak fault, and west-dipping nature, WCC (1978) interpreted the Devils Gate fault as the eastern margin of a Cenozoic graben. On the basis of the west-dip and proximity to the Waters Peak and Green Springs Run faults, we agree with the WCC (1978) assessment that it is likely an antithetic fault to the longer, east-dipping faults.

The age of most recent faulting on the Devils Gate fault is highly uncertain in the absence of detailed geologic and geomorphic mapping or subsurface investigations. The fault is not included as a Quaternary fault in the Fault Activity Map of California (Jennings and Bryant, 2010), or in the national Quaternary fault database (CGS and USGS, 2006; updated 2018). No paleoseismic trenching studies have been completed on the Devils Gate fault; USACE (1995) attempted to trench the fault but were denied right of entry. Our office-based interpretation of LiDAR data and ortho-imagery suggests that the fault *may* displace Quaternary landforms east of Salt Spring Valley Reservoir (Figures 5-1 and 5-3). Here, the fault is geomorphically expressed as two northwest-trending, 0.6- and 2-km-long topographic escarpments across a gently southwest-inclined set of geomorphic surfaces. Multiple southwest flowing streams cross or head at the escarpment. The fault appears to be expressed as a nearly-continuous west-facing scarp with vertical displacements (if present) that range between 0.3 and 5 m (Figure 5-3) with local linear depressions and numerous aligned springs. Apparent vertical separation across the scarp is typically 0.3 to 1.5 m. Smaller scarps are generally observed closer to modern stream channels (in younger deposits or surfaces), with larger scarp heights observed across apparently older geomorphic surfaces and faulted bedrock (Figure 5-3). The geomorphic surfaces adjacent to the streams are either Quaternary alluvial surfaces (alluvial fan deposits), strath surfaces (planated bedrock), or bedrock surfaces with thin mantles of alluvium and colluvium, that appear to preserve the northwest-trending, west-facing topographic escarpment and springs aligned along the lineament. If these interpretations are correct, then the surfaces east of Salt Springs Reservoir may record multiple episodes of surface faulting along the Devils Gate fault. Because this site has not been mapped and evaluated in detail, however, we consider the youngest activity documented for the Devils Gate fault to be Late Cenozoic (with a confidence ranking of *Probable*). The oldest age of inactivity has not been documented for the Devils Gate fault (Table 5-1), which indicates that there is no detailed information to provide a useful constraint. Because the fault is subparallel to other conditionally active or active faults per DSOD criteria, and it is a Mesozoic fault in the

foothills with probable late Cenozoic activity, we classify the Devils Gate as a conditionally active fault per DSOD criteria in Table 5-1.

For the seismic source characterization, we consider a 39-km-long fault source, similar to that recommended by ESA (1992) and Dames and Moore (1993) (Figure 5-1). The north end of the fault source is located directly southeast of Ione and directly north of the Mehrten Formation outcrops along geomorphic profile 30 (Page and Sawyer, 2001) that were interpreted to indicate minor vertical and dextral offset (HCG, 1998). We end the fault source due to the absence of a clear topographic lineament farther north. The south end of the fault source extends southeast of the location shown in Figure 5-3 where the strong geomorphic expression of the fault ends. This southern end is approximately 9 km northwest of Copperopolis and about 20 km northwest of the Stanislaus River and Table Mountain. We do not extend the fault farther south due in part to the interpretation of faulting of the Table Mountain Latite (WCC, 1978; Page and Sawyer, 2001, their profile 32). The primary zones of faulting across Table Mountain extending along strike to the northwest to coincide with the Waters Peak (Section 5.1) and Youngs Creek (Section 5.4) fault sources; if the Devils Gate fault extends farther south, it would likely be a secondary structure to the Green Springs Run fault and would likely intersect it at shallow depths such as not to be a separate source. Long-term geologic slip rates of the Devils Gate fault of hundredths of millimeters per year or less have been estimated based on interpreted west-down vertical separation of approximately 12 m on the Miocene Mehrten Formation (Dames and Moore 1993) east of Ione, and dextral strike-slip displacements of approximately 150-450 m (HCG 1998) at a similar location.

Our fault source characterization for the Devils Gate fault source is shown graphically in Figure 5-2. The probability of activity of the source is [0.5] based on suspected, but unconfirmed Late Cenozoic and late Quaternary activity suggested by interpreted offsets in the Miocene Mehrten Formation and clear geomorphic expression across young geomorphic surfaces (Figure 5-3). The average dip of the fault source is modeled to range from 60°SW to 90° (with logic-tree branch weights of 0.3 each to the low and high values), with a preferred value of 75°SW (with a logic-tree branch weight of 0.4), similar to dips suggested by WCC (1978), HCG (1998), ESA (1992), and USACE (1995). This range of values are appropriate for antithetic splays in the seismogenic crust. The 0.3, 0.4, 0.3 weighting scheme for the three epistemic alternative values reflects an approximation of the 10th, 50th, and 90th percentile values of a continuous uncertainty distribution (Keefer and Bodily, 1983). The maximum rupture depth of the fault source has a three-point uncertainty distribution in the source characterization, with values of 15 km, 10 km, and 6 km with weights of 0.3, 0.4, and 0.3, respectively. These alternative maximum thickness values represent a range of estimated depths to intersection with the east-dipping Waters Peak – Green Springs Run fault source whereby the Devils Gate fault could host moderate to large earthquakes independent of the adjacent, connecting fault. The preferred dip of 75° SW and preferred depth to bottom of faulting of 10 km are listed in Table 5-1.

The magnitude-recurrence relationship for the Devils Gate fault source is modeled in a similar manner to the Waters Peak – Green Springs Run fault source described in Section 5.1 above.

Values of Mchar for the Devils Gate fault source are **M** 6.5, **M** 6.0, and **M** 5.8 with weights of 0.3, 0.4, and 0.3, respectively. These weights are based on characteristic rupture lengths of about 20 km, 10 km, and 10 km, respectively, and resulting rupture areas from these rupture lengths when taking into account fault dip, maximum fault depth, and earthquake rupture aspect ratios (ratio of rupture length to rupture width; see Leonard, 2010). The resulting Mchar values are mainly based on the empirical magnitude-area relation of Hanks and Bakun (2014) developed mostly from a dataset of strike-slip earthquake ruptures. The three-point distribution of Mchar values plus the magnitude variability from the alternative magnitude PDFs capture both natural variability in earthquake size and epistemic uncertainty in the correct empirical magnitude scaling models, rupture aspect ratios, and rupture geometries considered in the analysis. Similar to the Waters Peak – Green Springs Run fault source, rupture of the entire 39 km length of the fault source would be equivalent to an earthquake of **M** 6.6-7.0, and this earthquake size is represented in the PSHA with a very low probability (i.e., with the high Mchar branch value of **M** 6.5 and the Mmax = Mchar + 0.5 = **M** 7.0 rule). We note that the middle value of Mchar, **M** 6.0, is lower than the MCE magnitude estimate for DSHA used in HCG (1998) (**M** 6.4), which is closer to our high Mchar value. One difference between the two studies is our interpretation that the source is likely antithetic to the longer Waters Peak – Green Springs Run fault source, and the narrower width of the west-dipping Devils Gate fault likely would impact a “characteristic” rupture length (Leonard, 2010) and earthquake magnitude. The preferred Mchar value of **M** 6.0 is listed in Table 5-1 and is recommended for consideration in a DSHA.

The available method to calculate earthquake recurrence for the Devils Gate fault source is using estimates of fault slip rate and moment balancing (Figure 5-2). The slip rate for the fault source is estimated by averaging two analyses: (1) vertical offset of the Castle Rock Tuff member of the Valley Springs Formation, and (2) lateral offset of Mehrten-age channels. The lateral separation of 150 to 450 m of Mehrten age channels interpreted by HCG (1998) was assumed to represent one estimate of net displacement; we selected a preferred value of 200 m based on the evidence presented in HCG (1998) for purposes of the slip rate calculations. The estimate based on vertical separation of the Castle Rock Tuff calculated net fault slip based on an estimated vertical separation of 9 to 18 m (preferred value 12 m; Page and Sawyer, 2001), a near-surface dip of 70° to 85° (preferred value 80°), and rakes corresponding to horizontal to vertical ratios between 0.5 and 3 (preferred value 1.5). The alternative net offset values from both approaches are assumed to have started between approximately 3 and 7 MA, with a preferred value of 5 MA, coincident with the approximate start of the current tectonic regime in the central Sierra Nevada (Wakabayashi, 2013; Wakabayashi and Kemp, 2015; and PG&E, 2017). The averaged net offsets and offset ages yield a preferred slip rate of 0.02 mm/yr, with an uncertainty range of 0.002 to 0.05 (values rounded to one significant digit). These values are given weights of 0.4 for the preferred slip rate and 0.3 each for the lower and upper slip rate values reflecting an approximation of the 50th, 10th, and 90th percentile values of a continuous uncertainty distribution, respectively (Keefer and Bodily, 1983). The preferred slip rate value of 0.02 mm/yr is listed in the summary table (Table 5-1) and is suggested for implementing the FERC approach to calculate a deterministic ground motion percentile (Idriss et al., 2018).

We note that the preferred slip rate of the Devils Gate fault source (0.02 mm/yr) is a factor of 2 greater than the preferred slip rate of the Waters Peak – Green Springs Run fault source (0.01 mm/yr) despite the assessment that the probability of activity of the Devils Gate fault [P(a)=0.5] is less than that of the Waters Peak [P(a)=1.0] (Figure 5-2). This apparent inconsistency is explained by the different types (and quality) of data available to estimate fault slip rate. For the Waters Peak fault, paleoseismic observations from trench studies are considered and used to refine a preferred slip rate that is based on late Quaternary activity information. On the other hand, the information available for estimating slip rate of the Devils Gate fault is limited to interpreted offsets of Late Cenozoic strata, estimates of the timing of displacement of those strata, and estimates that a late Cenozoic average slip rate is a reasonable assumption for a present-day (i.e., late Pleistocene) average slip rate. The different calculated values for preferred slip rate, therefore, are based on different data types and data quality, and as such the slip rate values are not quantitatively related to the assessments of probability of activity. Qualitatively, it can be stated that better geologic data allow for a more refined (and confident) preferred slip rate value, and better data should result in reduced slip-rate uncertainties compared to uncertainties estimated from poorer quality data. The better geologic data collected for the Waters Peak fault also allow for a more confident assessment of the probability of activity of that fault in a PSHA compared to the Devils Gate fault.

5.3 Ione Fault Source

The Ione fault was proposed as a late Cenozoic fault by ESA (1992), Dames and Moore (1993), and USACE (1995) on the basis of offset Eocene Ione Formation northwest of Pardee Dam to the town of Ione (Figure 5-1). Located approximately 1 km west of Pardee Dam at closest approach, the Ione fault is recognized by its strong geomorphic expression as a southwest-facing scarp mainly north of the Mokelumne River. HCG (1998) observed faulting across a 200 m wide zone within the Salt Springs Formation in the Lake Amador Spillway channel that was oriented parallel to foliation, with an average strike and dip of N15°W, 80°E. Vertical offsets of the Eocene Ione Formation were noted by Dames and Moore (1993), USACE (1995), and HCG (1998), and these offsets were suggested to have occurred either continually since the Eocene or to have started later (i.e., in late Cenozoic time coincident with onset of westward tilting of the Sierra Nevada block; Unruh, 1991; Wakabayashi, 2013). Estimates of southwest-side down vertical separation of the Ione Formation across the fault vary from about 150 to 250 m (Dames and Moore, 1993) to 40 to 120 m (this study using mapping by Gutierrez et al., 2015; also 76 m from HCG, 1998).

USACE (1995) trenched the Ione fault northwest of the Lake Amador spillway channel (Figure 5-1). Their Trench-1 exposed a steeply dipping bedrock fault zone with multiple Holocene-aged debris flows overlying bedrock. An “injected” clay fault gouge was observed in one of the trench walls and interpreted as interfingering with the lower debris flow units. Overlying debris flow deposits were logged as overlying the clay unit. The USACE (1995) presented an interpretation of this relationship as evidence for a faulting event that post-dates the lower debris flow deposits and pre-dates the upper deposits. The USACE (1995) documented that this stratigraphic and/or

structural relationship was not observed in the other trench wall, and thus the evidence of late Quaternary (Holocene) activity of the Ione fault could not be confirmed. Based on the alternative interpretation from the single trench wall that faulting post-dated Holocene debris flow deposits, the Fault Activity Map of California (Jennings and Bryant, 2010) and national Quaternary fault database (CGS and USGS, 2006; updated 2018) classify the Ione fault as late Quaternary active. In our summary table (Table 5-1), we list two alternative interpretations for the youngest activity documented on the Ione fault: either Cenozoic (with a confidence ranking of *Likely*) to represent the confident interpretation of offset Ione Formation, or latest Pleistocene to Holocene (with a confidence ranking of *Possible*) to represent the interpretation of the trench wall as recording a Holocene rupture (Page 1994; USACE, 1995; WLA, 1994). Table 5-1 shows two alternatives for the oldest inactivity documented for the Ione fault. Either the oldest activity is latest Pleistocene to early Holocene (with a confidence ranking of *Possible*), or it is late Holocene based on the trench data showing unfaulted overlying late Holocene debris flow deposits (Page, 1994; WLA, 1994; confidence ranking of *Likely*). These constraints result in a DSOD activity category of active or conditionally active.

For the seismic source characterization, we consider a 17-km-long fault source extending from north of Dry Creek near Ione to a point directly north of the Mokelumne River. The north end of our source follows CGS mapping (Gutierrez et al., 2015), and follows a prominent southwest facing escarpment directly east of the Jurassic Salt Springs Slate and Ione Formation depositional contact. Our north end coincides with the termination of the prominent lineament. The south end of our source is located directly north of the Mokelumne River, modified from Jennings and Bryant (2010) to follow the bedrock contact between the Jurassic Salt Springs Slate to the northeast and the Jurassic Gopher Ridge volcanics to the southwest; this southern termination is similar to that selected by HCG (1998) and CGS (2019). We note that ESA (1992) continued their trace of the Ione fault south of Valley Springs to Valley Springs Peak; we reject this extension on the basis of the disappearance of a strong geomorphic escarpment south of the Mokelumne River, and a change from a west-facing escarpment to an east-facing topographic step.

Our fault source characterization for the Ione fault source is shown graphically in Figure 5-2. The probability of activity of the source is [0.5] based on clear evidence for offset Cenozoic strata, and possible but unconfirmed late Quaternary activity (possibly faulted Holocene debris flow deposits). The average dip of the fault source through the seismogenic crust is modeled to range from 50°SW to 90° (with logic-tree branch weights of 0.3 each to the low and high values), with a preferred value of 70°SW (with a logic-tree branch weight of 0.4). The 0.3, 0.4, 0.3 weighting scheme for the three epistemic alternative values reflects an approximation of the 10th, 50th, and 90th percentile values of a continuous uncertainty distribution (Keefer and Bodily, 1983). The maximum rupture depth of the fault source is similar to that of the Waters Peak – Green Springs Run fault source (Section 5.1) with values of 20 km, 15 km, and 10 km and weights of 0.3, 0.4, and 0.3, respectively. The preferred dip value of 70°SW and preferred depth to bottom of faulting of 15 km are listed in Table 5-1.

The magnitude-recurrence relationship for the Ione fault source is modeled in a similar manner to the Waters Peak – Green Springs Run fault source described in Section 5.1 above. Values of Mchar for the Ione fault source are **M** 6.5, **M** 6.2, and **M** 6.0 with weights of 0.3, 0.4, and 0.3, respectively. These weights are based on characteristic rupture lengths of about 20 km, 15 km, and 12 km, respectively, and resulting rupture areas from these rupture lengths when taking into account fault dip, maximum fault depth, and earthquake rupture aspect ratios (ratio of rupture length to rupture width; see Leonard, 2010). The resulting Mchar values are mainly based on the empirical magnitude-area relation of Hanks and Bakun (2014) developed mostly from a dataset of strike-slip earthquake ruptures. The three-point distribution of Mchar values plus the magnitude variability from the alternative magnitude PDFs capture both natural variability in earthquake size and epistemic uncertainty in the correct empirical magnitude scaling models, rupture aspect ratios, and rupture geometries considered in the analysis. We note that the high value of Mchar, **M** 6.5, is similar to MCE magnitude estimates for DSHA used in previous studies (e.g., **M** 6.4 by HCG, 1998; **M** 6.5 by TERRA/GeoPentech, 2010; **M** 6.4 by AMEC, 2012). The middle Mchar value of **M** 6.2 is listed in Table 5-1 and is recommended for consideration in DSHA.

The available method to calculate earthquake recurrence for the Ione fault source is using estimates of fault slip rate and moment balancing (Figure 5-2). The slip rate is estimated using 40 to 120 m (preferred value 75 m) vertical separation of the Eocene Ione Formation, estimated near-surface dips of 55° to 85°SW (preferred value 70°), and estimated rakes between 20° and 65° (preferred 34°), corresponding to lateral to vertical displacement ratios of 0.5 to 3 (preferred 1.5). The resulting high, low, and preferred net displacement estimates are combined with alternative estimates of the timing of onset of deformation that represent the start of the current tectonic regime between approximately 3 and 7 MA, with a preferred value of 5 MA, coincident with the approximate start of the current tectonic regime in the central Sierra Nevada (Wakabayashi, 2013; Wakabayashi and Kemp, 2015; and PG&E, 2017). The averaged net offsets and offset ages yield a preferred slip rate of 0.03 mm/yr, with an uncertainty range of 0.002 to 0.1 mm/yr (values rounded to one significant digit). These values are given weights of 0.4 for the preferred slip rate and 0.3 each for the lower and upper slip rate values reflecting an approximation of the 50th, 10th, and 90th percentile values of a continuous uncertainty distribution, respectively (Keefer and Bodily, 1983). The preferred slip rate of 0.03 mm/yr is listed in Table 5-1 for use in DSHA applying the FERC methodology of Idriss et al. (2018).

5.4 YOUNGS CREEK – BOWIE FLAT FAULT SOURCE

The Youngs Creek fault was proposed as a late Cenozoic fault by WCC (1978), Dames and Moore (1993), and USACE (1995), on the basis of offset Miocene Mehrten Formation in trenches (WCC, 1978). Located approximately 4 km east of Pardee Dam at closest approach (Figure 5-1), the Youngs Creek fault is identified by a strong geomorphic lineament within the highly sheared Mélange belt of the Bear Mountains fault zone. WCC (1978) first observed east-side down faulting in the Miocene Mehrten Formation in their Trenches 1, 2, and 3 (Figure 5-1), and report a fault strike of N27°W, with dips ranging from 60°E to vertical, in their Trench 1. Geomorphic profiles across the Youngs Creek fault show approximately 5 m of vertical displacement of the Mehrten

Formation and Chili Hill Tuff (Valley Springs Formation) (WCC, 1978; Page and Sawyer, 2001, their profile 31; Figure 5-1).

The fault is classified as Quaternary active fault in both the Fault Activity Map of California (Jennings and Bryant, 2010), and the national Quaternary fault database (CGS and USGS, 2006; updated 2018). The basis for a Quaternary activity assessment is trench exposures documented by WCC (1978) and USACE (1995), though the interpretations are variable. In the WCC trench 1, the "paleo B" horizon is potentially unfaulted over the western strand of the Youngs Creek fault zone, and WCC (1978) concludes that there are insufficient late Quaternary units exposed in the trench to evaluate the capability of the fault. USACE (1995) came to a similar conclusion based on their trench which exposed an unfaulted Sonora-age (late Modesto) colluvium. WLA (1994) interpret the age of the unfaulted material as Sonora or younger with an associated age of <8 to 14 ka and indicate the lack of older unfaulted deposits means the presence or absence of activity cannot be assessed. Page (1994) states that the USACE (1995) trench shows sufficient cover to strongly indicate no offset in the last 14,000 to 60,000 yrs. Based on these geologic constraints, we list the youngest activity documented for the Youngs Creek fault to be late Cenozoic age (with a confidence ranking of *Likely*) and the oldest inactivity documented is late to early Modesto (8 to 14 ka) age (with a confidence ranking of *Probable*). These constraints suggest the Youngs Creek fault is conditionally active per DSOD criteria.

For the seismic source characterization, we consider a 64-km-long fault source that combines the east-side down Youngs Creek fault with the east-side down Bowie Flat fault mapped along strike to the southeast across the Miocene Table Mountain Latite near the Stanislaus River (WCC, 1978; Page and Sawyer, 2007) (Figure 5-1). Similar to the Youngs Creek fault, the Bowie Flat fault is located within the Bear Mountains fault zone, shows 6 to 15 m of east-down vertical offset of the Miocene Table Mountain Latite on a steeply east-dipping fault, and truncates a "paleo B" horizon in trenches (WCC, 1978; Biggar et al., 1978). WCC (1978) report fault orientations from their trenches 1, 2, and 4b with strikes ranging from N30°W to N50°W, and dipping 70° to 85° E, similar to orientations for the Youngs Creek fault. The north end of our source is located 5 km west of Ione, and follows mapped lineaments. Previous authors have suggested combining the Youngs Creek fault with the Sunnybrook East fault to the northwest (e.g. PG&E, 2017), however we determined that a continuation to the south along the Bowie Flat fault is preferable based on lateral continuity of bedrock structure, comparable geomorphic expression, and comparable evidence for activity. The south end of the fault source extends 5 km southeast past the Table Mountain Latite based on mapping by WCC (1978). Long-term geologic slip rates of the Youngs Creek fault of hundredths of millimeters per year or less have been estimated based on interpreted east-down vertical separation of approximately 5 m of the Miocene Mehrten Formation and 5 m of the Chili Hill Tuff (WCC, 1978; PG&E, 2017).

Our fault source characterization for the Youngs Creek – Bowie Flat fault source is shown graphically in Figure 5-2. The probability of activity of the source is [1.0] based on the clear evidence for offset late Cenozoic strata and potential offset of late Quaternary deposits (including the paleo B soil). The average dip of the fault source through the seismogenic crust is modeled

to range from 55°NE to 85°NE (with logic-tree branch weights of 0.3 each to the low and high values), with a preferred value of 70°NE (with a logic-tree branch weight of 0.4). The 0.3, 0.4, 0.3 weighting scheme for the three epistemic alternative values reflects an approximation of the 10th, 50th, and 90th percentile values of a continuous uncertainty distribution (Keefer and Bodily, 1983). The maximum rupture depth of the fault source is identical to the nearby Waters Peak – Green Springs Run fault source (Section 5.1) with alternative logic-tree branch values of 20 km, 15 km, and 10 km with weights of 0.3, 0.4, and 0.3, respectively. The preferred dip value of 70°SW and preferred depth to bottom of faulting of 15 km are listed in Table 5-1.

The magnitude-recurrence relationship for the Youngs Creek – Bowie Flat fault source is modeled in a similar manner to the Waters Peak – Green Springs Run fault source described in Section 5.1 above. Values of Mchar for the Youngs Creek – Bowie Flat fault source are **M** 7.0, **M** 6.4, and **M** 6.0 with weights of 0.3, 0.4, and 0.3, respectively. These weights are based on characteristic rupture lengths of about 40 km, 20 km, and 12 km, respectively, and resulting rupture areas from these rupture lengths when taking into account fault dip, maximum fault depth, and earthquake rupture aspect ratios (ratio of rupture length to rupture width; see Leonard, 2010). The resulting Mchar values are mainly based on the empirical magnitude-area relation of Hanks and Bakun (2014) developed mostly from a dataset of strike-slip earthquake ruptures. The three-point distribution of Mchar values plus the magnitude variability from the alternative magnitude PDFs capture both natural variability in earthquake size and epistemic uncertainty in the correct empirical magnitude scaling models, rupture aspect ratios, and rupture geometries considered in the analysis. We note that the middle value of Mchar, **M** 6.4, is comparable to MCE magnitude estimates for DSHA used in previous studies (e.g., **M** 6.5 by ESA, 1992; **M** 6.5 by Dames and Moore, 1992; **M** 6.4 by HCG, 1998). The middle Mchar value of **M** 6.4 is listed in Table 5-1 and is recommended for consideration in DSHA.

The available method to calculate earthquake recurrence for the Youngs Creek – Bowie Flat fault source is using estimates of fault slip rate and moment balancing (Figure 5-2). The slip rate for the fault source is estimated using the vertical offset of the Miocene Mehrten Formation, estimates of net slip on the underlying fault considering fault dip and rake, and estimates of the timing of onset of deformation that represent the start of the current tectonic regime. We estimate a range of net offsets using a vertical separation of 3.75 to 7.5 m of the Mehrten Formation (WCC, 1978; PG&E, 2001), a near-surface fault dip of 70° to 85°NE, and a rake of between 20° and 65°. The alternative net offset values from both approaches are assumed to have started between approximately 3 and 7 MA, with a preferred value of 5 MA, coincident with the approximate start of the current tectonic regime in the central Sierra Nevada (Wakabayashi, 2013; Wakabayashi and Kemp, 2015; and PG&E, 2017). The averaged net offsets and offset ages yield a preferred slip rate of 0.002 mm/yr, with an uncertainty range of 0.001 to 0.008 (values rounded to one significant digit). These values are given weights of 0.4 for the preferred slip rate and 0.3 each for the lower and upper slip rate values reflecting an approximation of the 50th, 10th, and 90th percentile values of a continuous uncertainty distribution, respectively (Keefer and Bodily, 1983). We note that the Bowie Flat fault to the south has a vertical separation of 20 m of the Table

Mountain Latite, suggesting a possible higher slip rate to the south. The preferred slip rate value of 0.002 mm/yr is listed in the summary table (Table 5-1) and is suggested for implementing the FERC approach to calculate a deterministic ground motion percentile (Idriss et al., 2018).

5.5 HAUPT CREEK FAULT SOURCE

The Haupt Creek fault was evaluated as a late Cenozoic fault by WCC (1978), Dames and Moore (1993), and USACE (1995) on the basis of a prominent vegetation change and spring line, and weak to moderate geomorphic lineament. The Haupt Creek fault is located on the eastern limit of the Bear Mountain fault zone, and juxtaposes the Rabbit Flat volcanic breccia (Logtown Ridge Formation) to the west with the mélange zone to the east. Located approximately 6 km east of Pardee Dam at closest approach (Figure 5-1), it was first investigated for potential Late Cenozoic activity by Biggar et al. (1978) and WCC (1978) at four trench sites located 6 km east of Valley Springs. Trenches exposed a Mesozoic bedrock contact, inferred to be a fault within the Bear Mountain fault zone, however the overlying Miocene Mehrten Formation was undisturbed at all four trench sites (WCC, 1978). Page and Sawyer (2001) similarly do not interpret any offset of the Miocene Mehrten Formation across the Haupt Creek fault in their profile located near Comanche Reservoir and Mokelumne Hill (profile 31), however we note that the data constraints are poor. Page and Sawyer (2007) conclude that the Haupt Creek fault is not late Cenozoic active (and therefore pre-Quaternary) based on evidence for the absence of displacement of Cenozoic strata. However, the Haupt Creek fault is classified as a Quaternary fault in the Fault Activity Map of California (Jennings and Bryant, 2010) with a citation of Page and Sawyer (2007). Based on the trench data, we list in Table 5-1 the youngest age of activity documented as Mesozoic (with a confidence ranking of *Likely*), and the oldest age of inactivity documented as late Cenozoic (with a confidence ranking of *Probable*). These constraints suggest the Haupt Creek fault should be classified as inactive per DSOD criteria (Table 5-1).

For the seismic source characterization, we consider the 17-km-long fault source as characterized by Jennings and Bryant (2010). This source extends from directly northeast of the southern margin of Pardee Reservoir at its north end to a location east of New Hogan Reservoir (Figure 5-1).

Our fault source characterization for the Haupt Creek fault source is shown graphically in Figure 5-2. The probability of activity of the source is [0.2] based on clear evidence of no offset in Miocene Mehrten Formation in four trenches, but a possibility that an active strand exists but was missed by the trench study. The average dip of the fault source through the seismogenic crust is modeled to range from 55°NE to 85°NE (with logic-tree branch weights of 0.3 each to the low and high values), with a preferred value of 70°NE (with a logic-tree branch weight of 0.4). The 0.3, 0.4, 0.3 weighting scheme for the three epistemic alternative values reflects an approximation of the 10th, 50th, and 90th percentile values of a continuous uncertainty distribution (Keefer and Bodily, 1983). The maximum rupture depth of the fault source has a three-point uncertainty distribution in the source characterization, with values of 20 km, 15 km, and 10 km with weights of 0.3, 0.4, and 0.3, respectively. These alternative maximum thickness values reflect uncertainty in both the

seismogenic thickness of the crust under the western Sierra Nevada foothills and uncertainty in the geometry of the reactivated faults (i.e., depth to a gently-dipping detachment at the base of the Foothills fault system that would represent the bottom of the fault source). The preferred dip value of 70°SW and preferred depth to bottom of faulting of 15 km are listed in Table 5-1.

The magnitude-recurrence relationship for the Haupt Creek fault source is modeled in a similar manner to the Waters Peak – Green Springs Run fault source described in Section 5.1 above. Values of Mchar for the Haupt Creek fault source are **M** 6.4, **M** 6.2, and **M** 6.0 with weights of 0.3, 0.4, and 0.3, respectively. These weights are based on characteristic rupture lengths of about 17.3 km, 15 km, and 12 km, respectively, and resulting rupture areas from these rupture lengths when taking into account fault dip, maximum fault depth, and earthquake rupture aspect ratios (ratio of rupture length to rupture width; see Leonard, 2010). The resulting Mchar values are mainly based on the empirical magnitude-area relation of Hanks and Bakun (2014) developed mostly from a dataset of strike-slip earthquake ruptures. The three-point distribution of Mchar values plus the magnitude variability from the alternative magnitude PDFs capture both natural variability in earthquake size and epistemic uncertainty in the correct empirical magnitude scaling models, rupture aspect ratios, and rupture geometries considered in the analysis. We note that prior studies reviewed have not included the Haupt Creek fault in DSHA assessments and thus there are no MCE magnitude estimates for comparison to our Mchar values. The middle Mchar value of **M** 6.2 is listed in Table 5-1 and is recommended for consideration in DSHA.

The recommended method to calculate earthquake recurrence for the Haupt Creek fault source is using estimates of fault slip rate, estimates of net slip on the underlying fault considering fault dip and rake, and estimates of the timing of onset of deformation that represent the start of the current tectonic regime (Figure 5-2). As no offsets have been recorded on the Haupt Creek fault, we assign a range of 0.2 to 5 m of vertical separation (about the resolution threshold of detection), a fault dip of 70° to 80°NE, and a rake between 20° and 65°. The alternative net offset values are assumed to have started between approximately 3 and 7 million years ago, similar to the values used for other sources in this study. The resulting net offsets and offset ages yield a preferred slip rate of 0.0006 mm/yr, with an uncertainty range of 0.00003 to 0.005 (values rounded to one significant digit). These values are given weights of 0.4 for the preferred slip rate and 0.3 each for the lower and upper slip rate values. The preferred slip rate value of 0.0006 mm/yr is listed in the summary table (Table 5-1) and is suggested for implementing the FERC approach to calculate a deterministic ground motion percentile (Idriss et al., 2018).

5.6 Poorman Gulch – Rawhide Flat Fault Source

The north-south to northwest-southeast-striking Poorman Gulch fault was named and recognized as a late Cenozoic fault by WCC (1978) on the basis of offset Miocene Mehrten Formation strata capping a ridge southwest of Mokelumne Hill south of the Mokelumne River (Figure 5-1). Also named the Motherlode fault by previous authors, the Poorman Gulch fault juxtaposes rocks from the Late Jurassic Mariposa Formation to the west with the Calaveras Complex to the east and is within the regional Melones fault zone. Located approximately 9.7 km east of Pardee Dam at

closest approach (Figure 5-1), WCC (1978), ESA (1992), and Dames and Moore (1993) all recognized topographic lineaments associated with the Poorman Gulch fault north and southeast of the offset in Mehrten Formation, although the studies interpreted different linear features believed to comprise the fault source. WCC (1978) observed east-side down faulting in Mehrten Formation in cut and trench exposures coincident with underlying faults in Jurassic bedrock, and report a fault strike, dip, and rake of N34°W, 78°E, and 64°S, respectively, consistent with normal-dextral oblique slip. Other rakes of 74°S are reported that are also consistent with normal-dextral oblique slip. The Poorman Gulch fault is classified as Late Quaternary active in both the Fault Activity Map of California (Jennings and Bryant, 2010), and the national Quaternary fault database (CGS and USGS, 2006; updated 2018) with an identical location and length of approximately 15 km. The basis for a late Quaternary activity assessment is trench exposures documented by WCC (1978). In their Trench 1, a “paleo B” horizon present east of a primary fault is truncated at the primary fault plane, with no continuation of the paleo B soil west of the fault. Nearby trenches (their No. 2 and 3) show shears truncating silty colluvium deposits that are undated but interpreted to be younger than the paleo B soil and possibly early Modesto in age (~30 to 70 ka) by Page and Sawyer (2007). The uppermost horizons in the trenches, which are interpreted to be Sonora in age (8 to 14 ka; Page and Sawyer, 2007), are not offset by faulting. From these data, we list in Table 5-1 the youngest age of activity documented on the Poorman Gulch fault to be early Modesto (with a confidence ranking of *Probable*) and the oldest age of inactivity to be latest Pleistocene to early Holocene (also with a confidence ranking of *Probable*). On this basis, the Poorman Gulch fault is classified as active under DSOD criteria.

For the seismic source characterization, we consider a 62-km-long fault source that combines the east-side down Poorman Gulch fault with the east-side down Rawhide Flat fault zone mapped along strike to the southeast across the Miocene Table Mountain Latite near the Stanislaus River (WCC, 1978; Page and Sawyer, 2007) (Figure 5-1). These two faults are within the Melones fault zone, have an identical east-down offset of late Cenozoic strata on steeply east-dipping faults, and topographic lineaments are recognizable between the two (e.g., Dames and Moore, 1993). The source length is longer than proposed previously, but we consider it defensible based on the along-strike continuity in the absence of major bends, steps, or structural complexities that may be persistent barriers to rupture. The north end of our source is located directly south of Jackson and coincides with a change in strike of the Melones fault zone from almost north-south to northwest-southeast; we select a location similar to the one mapped by ESA (1992). We note that PG&E (2017) decided to combine the Poorman Gulch fault with the Gopher Gulch fault farther to the north; we consider this combination permissible but less preferred than our combination of the fault with others to the south based on the clearer along-strike relationship to Mesozoic faulting. The south end of the fault source is drawn through the middle of the Rawhide Flat fault zone where it crosses Table Mountain (WCC, 1978; Page and Sawyer, 2001, profile 32; Page and Sawyer, 2007) to a location approximately 14 km south of the Stanislaus River directly east of the community of Chinese Camp (Figure 5-1). Long-term geologic slip rates of the Poorman Gulch fault of hundredths of millimeters per year or less have been estimated based on interpreted east-down vertical separation of approximately 30 m on the top of Miocene Mehrten Formation

(Page and Sawyer, 2001, profile 31), which is comparable to the ~45 m east-down vertical separation of Miocene Table Mountain Latite estimated across the Rawhide Flat fault zone (Page and Sawyer, 2001, profile 32).

Our fault source characterization for the Poorman Gulch – Rawhide Flat fault source is shown graphically in Figure 5-2. The probability of activity of the source is [1.0] based on the clear evidence for offset late Cenozoic strata and late Quaternary deposits (including the paleo B soil and younger colluvium). As described above, our source length is 62 km from near Jackson in the north to Chinese Camp in the south. The average dip of the fault source through the seismogenic crust is modeled to range from 55°NE to 85°NE (with logic-tree branch weights of 0.3 each to the low and high values), with a preferred value of 70°NE (with a logic-tree branch weight of 0.4). We note the preferred value is slightly less than the measured value at the surface based on the reasoning that the fault likely shallows at depth. The 0.3, 0.4, 0.3 weighting scheme for the three epistemic alternative values reflects an approximation of the 10th, 50th, and 90th percentile values of a continuous uncertainty distribution (Keefer and Bodily, 1983). The maximum rupture depth of the fault source has a three-point uncertainty distribution in the source characterization, with values of 20 km, 15 km, and 10 km with weights of 0.3, 0.4, and 0.3, respectively. These alternative maximum thickness values reflect uncertainty in both the seismogenic thickness of the crust under the western Sierra Nevada foothills and uncertainty in the geometry of the reactivated faults (i.e., depth to a gently-dipping detachment at the base of the Foothills fault system that would represent the bottom of the fault source). The preferred dip value of 70°SW and preferred depth to bottom of faulting of 15 km are listed in Table 5-1.

The magnitude-recurrence relationship for the Poorman Gulch – Rawhide Flat fault source is modeled in a similar manner to the Waters Peak – Green Springs Run fault source described in Section 5.1 above. Values of Mchar for the Poorman Gulch-Rawhide Flat fault source are **M** 7.0, **M** 6.4, and **M** 6.0 with weights of 0.3, 0.4, and 0.3, respectively. These weights are based on characteristic rupture lengths of about 40 km, 20 km, and 12 km, respectively, and resulting rupture areas from these rupture lengths when taking into account fault dip, maximum fault depth, and earthquake rupture aspect ratios (ratio of rupture length to rupture width; see Leonard, 2010). The resulting Mchar values are mainly based on the empirical magnitude-area relation of Hanks and Bakun (2014) developed mostly from a dataset of strike-slip earthquake ruptures. The three-point distribution of Mchar values plus the magnitude variability from the alternative magnitude PDFs capture both natural variability in earthquake size and epistemic uncertainty in the correct empirical magnitude scaling models, rupture aspect ratios, and rupture geometries considered in the analysis. We note that the middle value of Mchar, **M** 6.4, is generally comparable to MCE magnitude estimates for DSHA used in previous studies (e.g., **M** 6.25 by ESA, 1983; **M** 6.5 by ESA, 1992; **M** 6.4 by HCG, 1998). The middle Mchar value of **M** 6.4 is listed in Table 5-1 and is recommended for consideration in DSHA.

The available method to calculate earthquake recurrence for the Poorman Gulch – Rawhide Flat fault source is using estimates of fault slip rate and moment balancing (Figure 5-2). The slip rate for the fault source is estimated using the vertical offset of the Miocene Mehrten Formation,

estimates of net slip on the underlying fault considering fault dip and rake, and estimates of the timing of onset of deformation that represent the start of the current tectonic regime. We estimate a range of net offsets using a vertical separation of 30 ± 15 m of the Mehrten Formation (Page and Sawyer, 2001), a near-surface fault dip of 70° to 80°NE, and a rake of between 20° and 65°. The alternative net displacements are assumed to have initiated between approximately 3 and 7 MA, with a preferred value of 5 MA, coincident with the approximate start of the current tectonic regime in the central Sierra Nevada (see Wakabayashi, 2013; Wakabayashi and Kemp, 2015; and PG&E, 2017). The resulting net offsets and offset ages yield a preferred slip rate of 0.009 mm/yr, with an uncertainty range of 0.002 to 0.05 (values rounded to one significant digit). These values are given weights of 0.4 for the preferred slip rate and 0.3 each for the lower and upper slip rate values reflecting an approximation of the 50th, 10th, and 90th percentile values of a continuous uncertainty distribution, respectively (Keefer and Bodily, 1983). The preferred slip rate value of 0.009 mm/yr is listed in the summary table (Table 5-1) and is suggested for implementing the FERC approach to calculate a deterministic ground motion percentile (Idriss et al., 2018).

5.7 Slate Creek Fault Source

The Slate Creek fault was evaluated as a late Cenozoic fault by Dames and Moore (1993) and USACE (1995). Located approximately 10 km west of Pardee Dam at closest approach (Figure 5-1), the Slate Creek fault was identified based on a strong geomorphic lineament directly downstream of New Hogan Reservoir, and defines the contact between the Jurassic Salt Springs Slate to the east and the Gopher Ridge volcanics to the west. In addition to the strong lineament, USACE (1995) cited incised drainages, faceted ridges, and spring lines as suggestive of late Cenozoic activity. The prominent lineament is restricted to an area between outcrops of late Cenozoic deposits, however, so there are no direct evaluations for late Cenozoic activity other than the observation that late Cenozoic faulting does not continue south along strike to the Stanislaus River or across the Table Mountain Latite (Figure 5-1; Page and Sawyer, 2001, profile 32).

The USACE (1995) excavated two trenches across the Spring Creek lineament northwest of Salt Spring Valley Reservoir (Figure 5-1). The trenches exposed a near-vertical, east-side down bedrock fault within the Salt Springs Slate, overlain by undisturbed Riverbank and Modesto Formations, which they interpreted as evidence for inactivity of the fault (USACE, 1995). However, we question the confidence in that findings based on the observation that the trenching did not cross the entire width of the scarp, and based on the USACE (1995) trenching studies of the Waters Peak fault where it was recognized that multiple trenches in different locations were required to establish clear evidence of Quaternary faulting. The Slate Creek fault is not included as a Quaternary fault in the Fault Activity Map of California (Jennings and Bryant, 2010) or in the national Quaternary fault database (CGS and USGS, 2006; updated 2018). In Table 5-1, we list the youngest activity documented for the Slate Creek fault to be Mesozoic (with a confidence ranking of *Likely*) or Late Cenozoic (with a confidence ranking of *Possible*) based on the initial assessment of USACE. The oldest age of inactivity documented for the fault is listed as Riverbank (30 to >100k ka) with a confidence ranking of *Possible* based on our interpretation that the entire

scarp was not assessed and that the fault was only evaluated in one study location. Based on these age constraints, the Slate Creek fault may be classified as either inactive or perhaps conditionally active following DSOD criteria (Table 5-1).

For the seismic source characterization, we consider a 34-km-long fault source extending from west of New Hogan Reservoir to 7 km south of State Highway 4. The north end of our source is located where the prominent lineation begins to die out directly north of the Calaveras River, as described by USACE (1995). The south end of our source is constrained by the lack of vertical offsets along strike to the south on the Table Mountain Latite (Page and Sawyer, 2001). We choose to terminate our Slate Creek fault source 4 km north of the Stanislaus River where the prominent northwest trending geomorphic expression reaches a bend, and begins to trend more west-northwest.

Our fault source characterization for the Slate Creek fault source is shown graphically in Figure 5-2. The probability of activity of the source is [0.2]. We assign a low probability based on the USACE (1995) trenching results that demonstrated, at least locally, the absence of late Quaternary faulting. The non-zero probability of activity reflects the clear geomorphic expression (comparable to other late Cenozoic and late Quaternary faults, favorable orientation, and the argument that the paleoseismic studies were insufficient to conclusively demonstrate inactivity for purposes of a PSHA. As described above, our source length is 34 km from near the New Hogan Reservoir in the north to just south of highway 4 in the south. The average dip of the fault source through the seismogenic crust is modeled to range from 55°NE to 85°NE (with logic-tree branch weights of 0.3 each to the low and high values), with a preferred value of 70°NE (with a logic-tree branch weight of 0.4). The 0.3, 0.4, 0.3 weighting scheme for the three epistemic alternative values reflects an approximation of the 10th, 50th, and 90th percentile values of a continuous uncertainty distribution (Keefer and Bodily, 1983). The maximum rupture depth of the fault source has a three-point uncertainty distribution in the source characterization, with values of 20 km, 15 km, and 10 km with weights of 0.3, 0.4, and 0.3, respectively. These alternative maximum thickness values reflect uncertainty in both the seismogenic thickness of the crust under the western Sierra Nevada foothills and uncertainty in the geometry of the reactivated faults (i.e., depth to a gently-dipping detachment at the base of the Foothills fault system that would represent the bottom of the fault source). The preferred dip value of 70°NE and preferred depth to bottom of faulting of 15 km are listed in Table 5-1.

The magnitude-recurrence relationship for the Slate Creek fault source is modeled in a similar manner to the Waters Peak – Green Springs Run fault source described in Section 5.1 above. Values of Mchar for the Slate Creek fault source are **M** 6.6, **M** 6.2, and **M** 6.0 with weights of 0.3, 0.4, and 0.3, respectively. These weights are based on characteristic rupture lengths of about 23 km, 15 km, and 12 km, respectively, and resulting rupture areas from these rupture lengths when taking into account fault dip, maximum fault depth, and earthquake rupture aspect ratios (ratio of rupture length to rupture width; see Leonard, 2010). The resulting Mchar values are mainly based on the empirical magnitude-area relation of Hanks and Bakun (2014) developed mostly from a dataset of strike-slip earthquake ruptures. The three-point distribution of Mchar values plus the

magnitude variability from the alternative magnitude PDFs capture both natural variability in earthquake size and epistemic uncertainty in the correct empirical magnitude scaling models, rupture aspect ratios, and rupture geometries considered in the analysis. We note that the middle value of Mchar, **M** 6.2, is comparable to the MCE magnitude estimate of **M** 6.3 from USACE (1995). The middle Mchar value of **M** 6.2 is listed in Table 5-1 and is recommended for consideration in DSHA.

The available method to calculate earthquake recurrence for the Slate Creek fault source is using fault slip rate and moment balancing (Figure 5-2). As there are no recorded offsets on the Slate Creek fault, we assume a slip rate approximately comparable to that of the Waters Peak – Green Springs Run fault source based on comparable geomorphic expression and orientation. This results in a preferred slip rate of 0.01 mm/yr, with an uncertainty range of 0.0005 to 0.05 (values rounded to one significant digit). The low slip rate value is less than the low slip rate value of all other local fault sources (with the exception of the Haupt Creek fault) in order to expand uncertainty where there are few or no data constraints. These values are given weights of 0.4 for the preferred slip rate and 0.3 each for the lower and upper slip rate values. The preferred slip rate value of 0.01 mm/yr is listed in the summary table (Table 5-1) and is suggested for implementing the FERC approach to calculate a deterministic ground motion percentile (Idriss et al., 2018).

6.0 PROBABILISTIC FAULT DISPLACEMENT HAZARD ANALYSIS

A probabilistic fault displacement hazard analysis (PFDHA) was conducted for Pardee Dam in order to provide EBMUD with a general understanding of the hazard posed by a discrete earthquake-induced displacement beneath the dam that may accompany strong ground shaking. We note that PFDHA is a relatively new field and currently available fault displacement prediction models are few (Petersen and Chen, 2018) and remain fairly crude. In consultation with EBMUD, the PFDHA consisted of the generation of hazard curves (annual frequency of exceedance versus net fault displacement amplitude) for Pardee Dam and its powerhouse. As the Waters Peak, Ione, and Devils Gate faults are all within 2 km of the dam, the PFDHA calculated the total hazard as the sum contributed from these three nearby fault sources (Section 5). Within location uncertainties, none of the surface traces of these three primary faults underlie Pardee Dam, so the type of displacement hazard posed to the facility is one of secondary or distributed displacement, as explained below.

6.1 FAULT DISPLACEMENT HAZARD ANALYSIS METHODOLOGY

The PFDHA methodology implemented in this study follows Youngs et al. (2003) and Petersen et al. (2011), which are based on the more common probabilistic seismic hazard analysis (PSHA) of Cornell (1968). Instead of estimating the annual rate of exceeding a specified earthquake ground motion at a site, PFDHA estimates the annual rate of earthquake-induced displacement D exceeding a specified level, d, at a site x,y of site dimension z (geographic and geometric definitions are shown in Figure 6-1). The time-independent rate of exceedance, $\lambda_{xyz}(D > d)$, is computed as:

$$\lambda_{xyz}(D > d) = \alpha(M_{min}) \int_M f_M(m) \int_S f_{S|M}(s|m) \times \int_R f_R(r)\, P_{xy}[D > d|m,s,r,z]\, dr\, ds\, dm \quad (6\text{-}1)$$

where $\alpha(M_{min})$ is the rate of all earthquakes on the fault of interest above a minimum magnitude M_{min}, $f_M(m)$ is the probability density function (PDF) of earthquake magnitudes M (from M_{min}, to a maximum earthquake the fault can produce), and $f_{S|M}(s|m)$ is a PDF of (magnitude-dependent) earthquake rupture locations on the fault source, as measured by the distance S from the end of the fault source to the end of the rupture. These initial terms in (6-1) are exactly comparable to fault source characterization that is required for a PSHA, whereby the location and rate of earthquakes are defined for each seismic source. Additional terms in (6-1) that are specific to PFDHA include a PDF describing the across strike rupture location uncertainty, $f_R(r)$, where R refers to the closest distance from the site to the principal fault rupture, and a conditional probability of displacement exceedance term (a fault displacement attenuation relation), $P_{xy}[D > d|m,s,r,z]$. This displacement attenuation relation itself may consist of three separate terms, as follows:

$$P_{xy}[D > d|m,s,r,z] = P[sr \neq 0|m]P_{xy}[d \neq 0|s,z,r,sr \neq 0]$$
$$\times P_{xy}[D \geq d|m,s,r,d \neq 0]. \quad (6\text{-}2)$$

The first term, $P[sr \neq 0|m]$, is the conditional probability that some amount of surface rupture occurs as a result of an earthquake of magnitude m. Whereas in PSHA all earthquakes are presumed to cause some amplitude of vibratory ground motion, in PFDHA not all earthquakes rupture to the surface (or near-surface). Examples of this include the 1994 moment magnitude (**M**) 6.7 Northridge, California earthquake on the Northridge blind thrust (Yeats and Huftile, 1995), and the 2010 **M** 7.0 Haiti earthquake adjacent to the strike-slip Enriquillo fault zone (Prentice et al., 2010). The second term, $P_{xy}[d \neq 0|s,z,r,sr \neq 0]$, is the conditional probability that some amount of surface rupture occurs at the site x,y, given the location of the principal rupture relative to the site (s, z, r) and an earthquake that produces some surface rupture. The third and final term in (6-2) is the conditional probability of displacement exceedance at the site of interest, where displacement is expressed as a PDF that is dependent on m, s (represented in Petersen et al. (2011) by the ratio l/L as show in Figure 6-1), and r.

The functional forms and/or parameter values of the PDFs and conditional probabilities change based on the style of faulting (strike-slip, normal, or reverse), and the location and size of the site xyz relative to the principal fault trace. If the site straddles the principal fault (and $r \sim 0$), the site is subjected to a principal displacement hazard as well as distributed deformation adjacent to the principal rupture. If the site of interest is away from the principal fault ($r > z$), the hazard is from secondary (also called "distributed") fault displacement only. In rare cases, typically associated with reverse faulting environments, the permanent ground deformation hazard is not discrete surface-fault rupture but rather abrupt tilting or warping, such as in the production of fold scarps (Streig et al., 2007; ANSI/ANS 2.30-2015). Figures 6-2 and 6-3 show examples of historic strike-slip surface-fault ruptures from Petersen et al. (2011), and the separate hazards of principal, secondary, and distributed deformation.

For this study, Pardee Dam is located within an area of potential secondary or distributed deformation hazard, at a distance of approximately 220 m from the Waters Peak – Green Springs Run fault source which represents the closest principal rupture source (Figure 6-4). The dam is also located approximately 1.0 km from the Devils Gate fault source and 1.2 km from the Ione fault source (Figure 6-5), so the hazard posed by more distant distributed displacement from those principal rupture sources is considered as well. The hazard is calculated using a single site coordinate (with location x,y) that represents the approximate center point of the dam footprint (Table 6-1 and yellow star in Figures 6-4 and 6-5). The selected cell dimension (z) is a single 200 m × 200 m cell, which underestimates the approximately 300 m length of the dam but greatly overestimates the < 100 m width of the dam at its widest point (Figure 6-4). The use of a cell footprint that represents a larger area than the site footprint is justifiable as the historical earthquake rupture data used to derive the distributed displacement relationships (e.g., Figures 6-2 and 6-3) likely underestimate of the true extent of distributed deformation (Youngs et al., 2003).

Table 6-1 lists the longitude and latitude (x and y), cell dimension (z), and distances to the principal fault sources from the cell center point (r). We did not evaluate the contribution to fault displacement hazard from fault sources at greater distances than 2 km due to the diminishing conditional probability that earthquakes on these more distant faults would produce secondary displacements at the site (Petersen et al., 2011).

Table 6-1. PFDHA Center Point Locations and Closest Distance to Fault Sources

Facility	Longitude (x), NAD83	Latitude (y), NAD83	Cell Dimension (z)	Distance to Fault Source (r)		
				Waters Peak – Green Springs Run	Devils Gate	Ione
Pardee Dam	-120.850384	38.257068	200 m	220 m	1040 m	1180 m

The PFDHA hazard formulation in (6-1) and (6-2) was calculated for the three fault sources at the site using LCI's software code TDISE. Alternative fault source and fault displacement prediction equation parameter values are captured in logic trees as presented in Section 6.2. The results are shown graphically in hazard curves of annual probability (or rate or frequency) of exceedance versus net displacement amplitude in Section 6.3. We note that additional information about fault orientation, displacement direction, and displacement width is typically required for evaluating facility performance or safety given a displacement event. This additional information is beyond the scope of this study, as we focus here on presenting the general hazard condition in a probabilistic framework and not a specific hazard assessment that would be used for engineering analysis.

6.2 PFDHA Logic Tree

The PFDHA logic trees are presented in Figures 5-2 (for fault source characterization) and 6-6 (for fault displacement prediction models). As stated above, the analysis considered hazard contributions from secondary or distributed displacements generated by earthquakes on the Waters Peak – Green Springs Run, Devils Gate, and Ione fault sources only. Sources more distant from the dam were not considered to contribute significantly to displacement hazard based on their distance from the dam and their dip direction away from the dam.

The logic trees consist of nodes and branches that collectively provide the information needed to calculate hazard and capture hazard uncertainty. Nodes are organized in columns in Figures 5-2 and 6-6. Each node represents a model element that is required either to justify the calculation methodology or to parameterize the model. Nodes in Figure 5-2 are named with the initials SC for source characterization, and are numbered sequentially from node SC 1 to SC 8. Nodes in Figure 6-6 are named with the initials DM for displacement model, and are numbered sequentially from node DM 1 to DM 6.

Each pathway through the logic trees in Figures 5-2 and 6-6 represents a complete and permissible set of model parameter inputs, and a hazard curve can be calculated to represent that pathway. The likelihood that the particular pathway and its resulting hazard curve are correct is indicated by the combined weight of epistemic branch values following that path. The mean hazard curve is calculated as the weighted sum of hazard for every possible pathway through the logic tree.

6.2.1 Source Characterization Logic Tree

The source characterization logic tree for the PFDHA is identical to the logic tree developed for the Waters Peak, Devils Gate, and Ione fault sources for input to PSHA (Figure 5-2); the logic tree and fault source parameters are described in Section 5.

The source characterization logic tree provides parameters needed to implement the first parts of equation (6-1) with the following exception. The conditional probability of principal rupture occurring adjacent to the site, represented by $\int_S f_{S|M}(s|m)\,ds$, is solved in the hazard code numerically by placing ruptures on the fault source plane based on magnitude and simple magnitude-area scaling (similar to PSHA codes). For the other terms of the equation—namely the rate of earthquakes and the magnitude PDF on the fault source—the source characterization is defined by fault location and source geometry (nodes SC 1, SC 3, and SC 4), the earthquake magnitude distribution (nodes SC 5 and SC 6), and the earthquake recurrence rate (nodes SC 7 and SC 8).

6.2.2 Fault Displacement Prediction Model Logic Tree

The fault displacement prediction model provides information to solve the later terms in equation (6-1) and the expanded terms in equation (6-2). A simplification to (6-1) that is used in this analysis is to recognize that the location of the primary fault zones are well defined adjacent to the dam (Figures 6-4 and 6-5), and treat *R* as a constant for each rupture (i.e., without aleatory variability).

The remaining terms are those in (6-2) and the logic tree to characterize uncertainties in these terms is presented in Figure 6-6. The first node in the displacement model, node DM 1, shows that the analysis is based on the displacement prediction model of Petersen et al. (2011), which was developed for strike-slip faults and relies on several California earthquakes and other, global earthquakes on strike-slip to strike-slip oblique faults. For this analysis, we consider using the Petersen et al. (2011) model with full weight (rather than weighting it and alternative models such as Youngs et al. (2003) for normal faulting) to be appropriate given the recognition that the Waters Peak and other local fault sources likely have a strong strike-slip component, and given that the Petersen et al. (2011) model has a more robust set of empirical data and equations appropriate to use for calculating secondary or distributed deformation hazard as compared to Youngs et al. (2003).

The progression of the displacement prediction model logic tree follows the order of terms in (6-2), and includes the following:

- conditional probability of surface rupture, $P[sr \neq 0|m]$, (node DM 2);
- conditional probability of displacement (in this case, secondary or distributed deformation) at the site, $P_{xy}[d \neq 0|s, z, r, sr \neq 0]$, (nodes DM 3 and DM 4); and
- displacement exceedance PDF (in this case, for secondary or distributed deformation), $P_{xy}[d \geq d_0|m, s, r, d \neq 0]$, (nodes DM 5 and DM 6).

6.2.2.1 Conditional probability of surface rupture

The first term, $P[sr \neq 0|m]$, is the conditional probability that some amount of surface rupture occurs as a result of an earthquake of magnitude m. Logic tree node DM 2 shows the implementation of this conditional probability.

The conditional probability of surface rupture is typically based on global empirical observations of earthquakes of varying magnitudes that have or have not produced surface rupture. As the outcome of surface rupture is binary (an earthquake either ruptures the surface or it does not), the probability can be represented through a logistic regression of the form:

$$P[sr \neq 0|m] = \frac{e^{a+bm}}{1+e^{a+bm}} \quad (6\text{-}3)$$

The logic tree shows two branch alternatives. The first branch, with a weight of [0.5], is the parameterization of the *a* and *b* constants developed by Wells and Coppersmith (1993) as presented in Youngs et al. (2003) (Table 6-2). This regression was developed from 276 worldwide earthquakes of various slip types, and it predicts that an earthquake of **M** 6.0 has a 45% chance of rupturing the surface, 70% for **M** 6.5, and 87% for **M** 7.0. The second branch, with an equal weight of [0.5], is shown as "Modified Takao et al. (2015)." The basis for this branch comes from Takao et al. (2015), who used the same functional form as (6-3) and fit *a* and *b* parameters using 107 inland crustal earthquakes in Japan of mostly reverse and strike-slip styles of faulting. They found a much steeper curve than the global Wells and Coppersmith (1993) data, with an only 7% probability of surface rupture from **M** 6.0, but a 91% probability from **M** 7.0 earthquakes. This result strongly suggests that regionalization is an important consideration for this conditional probability, and that the global average condition may not be an accurate, or best, model to use for any single site in particular.

Table 6-2. Logistic Regression Coefficients for the Conditional Probability of Surface Fault Rupture

REFERENCE AND DATASET	WEIGHT	a	*b*	P[*sr* ≠ 0], M 6.0	P[*sr* ≠ 0], M 6.5	P[*sr* ≠ 0], M 7.0
Wells and Coppersmith (1993), 276 worldwide earthquakes, all slip types	[0.5]	-12.51	2.053	0.45	0.70	0.89
Takao et al. (2015), 107 crustal earthquakes in Japan, strike-slip and reverse	--	-32.03	4.90	0.07	0.46	0.91
Modified Takao et al. (2015) for application to foothills faults	[0.5]	-30	5.2	0.77	0.98	1.0

Due to the surface rupture produced by the relatively low magnitude M_L 5.7 Oroville earthquake (California Department of Water Resources, 1979), we consider the probability of surface rupture as a function of magnitude to be greater for the foothills faults than the global average or from the Japan dataset. We keep the steep slope from the Takao et al. (2015) relationship, but modify the *a* and *b* values such that the probability of surface rupture is almost a certainty for earthquakes greater than or equal to **M** 6.5, and the probability of a **M** 6.0 earthquake generating surface rupture is greater than about 75% (Table 6-2). This modified Takao et al. (2015) parameterization is weighted [0.5] because it is not based on carefully considered data, but rather is defined on the more qualitative basis described above.

6.2.2.2 Conditional probability of distributed deformation at the site

The second term in equation (6-2), $P_{xy}[d \neq 0|s,z,r,sr \neq 0]$, is the conditional probability that some amount of surface displacement occurs at the study site (x,y) of site dimension z given principal rupture adjacent to the site (represented by s) and an earthquake that produces surface rupture ($sr \neq 0$). Logic tree node DM 3 shows that the conditional probabilities developed by Petersen et al. (2011) are used for the median model, and node DM 4 shows that uncertainty in the probabilities is treated epistemically, with branch alternatives for 90th, 50th, and 10th percentile probabilities.

The Petersen et al. (2011) empirical model was developed using data from several well-documented strike-slip earthquakes that documented both principal and distributed displacement (e.g., Figures 6-2 and 6-3). This probability (*P*) is represented through a regression of the form:

$$\ln(P) = a(z)\ln(r_p) + b(z) \quad (6\text{-}4)$$

where $a(z)$ and $b(z)$ are regression coefficients (dependent on cell size z) and r_p is the perpendicular distance from the site of interest to the primary rupture (Petersen et al., 2011, their Equation 20). Petersen et al. (2011) consider this model to be valid for values of r_p between

approximately 200 to 400 m and 2.5 km, depending on z. For distances less than 200 to 400 m, Petersen et al. (2011) provide fixed mean probabilities at interval distances based on interpolation. For our implementation, we replace the perpendicular distance r_p with closest distance r so that ruptures north or south of the perpendicular distance can contribute to hazard. For example, a line drawn perpendicular to fault strike from the southern end of the Ione fault source would not intersect the center point of Pardee Dam (Figure 6-5), and using a perpendicular distance criteria would result in ruptures on the Ione fault source having a zero contribution to displacement hazard at the site.

Node DM-4 presents the uncertainty in the median model for the probability of distributed deformation at the site of interest. Evaluation of the electronic supplement dataset provided in Petersen et al (2011) shows that the probability of displacement at a site off of the principal rupture varies greatly from earthquake rupture to earthquake rupture. Thus, the average of the earthquakes examined by Petersen et al. (2011) does not necessarily represent the average condition for any individual fault. It is unclear whether the probability of distributed displacement at Pardee Dam should be less than, about equal to, or greater than the dataset average. An argument that the probabilities should be less than the dataset average is that the Waters Peak, Devils Gate, and Ione faults are locally relatively straight and do not show much structural complexity along their traces (e.g., Figure 5-2). This simplicity may tend to minimize off-fault displacement during large earthquakes. An argument that the probabilities of off-fault displacement at the facility location may be higher than the dataset average is that Pardee Dam is located in the hanging wall side of the Waters Peak – Green Springs Run and Devils Gate fault sources, and evaluations of dip-slip fault ruptures, at least, clearly show a higher concentration of distributed displacement in the hanging wall block compared to the footwall block (Youngs et al., 2003).

Because of the uncertainty in how to center the conditional probability of distributed rupture for the project site, we adopt a 3-point uncertainty distribution with high, middle, and low branches representing the 90th, 50th, and 10th percentile probabilities from the Petersen et al. (2011) dataset (Figure 6-6). The 50th percentile probabilities use Equation (6-4) with published regression parameters. For the 90th and 10th percentile probabilities, we use the published regression parameters and standard deviation, and develop smoothed sets of interpolation point probabilities for the 90th and 10th percentile probabilities against the dataset provided with Petersen et al. (2011) as an electronic supplement at selected r distances. The weighting scheme of [0.4], [0.4], [0.2] for the 90th, 50th, and 10th percentile values, respectively, follows our judgment that the probabilities of secondary or distributed deformation at Pardee Dam from a rupture on the primary fault sources within 2 km of the dam are likely higher than the dataset average due to the dam's location in the hanging wall of the Waters Peak – Green Springs Run and Devils Gate fault sources, and due to the probable slip obliquity on the faults (Section 5). The probability levels, values and weights for the distributed displacement conditional probabilities used in the analysis at selected r distances are provided in Table 6-3.

Table 6-3. Values for Conditional Probability of Distributed Deformation for the 200 m × 200 m Cell Size at Selected Distances from Analysis of Data in Petersen et al. (2011)

Probability Level (Percentile)	Selected Point Probabilities $P(r_p)$						Branch Weight
	P(200)	P(300)	P(400)	P(800)	P(1200)	P(2000)	
90th	0.3235	0.2340	0.2148	0.1137	0.0712	0.0395	[0.4]
50th	0.1898	0.1100	0.0747	0.0309	0.0193	0.0107	[0.4]
10th	0.0560	0.0304	0.0200	0.0084	0.0052	0.0029	[0.2]

6.2.2.3 Displacement exceedance PDF for distributed deformation

The displacement exceedance model for distributed deformation, $P_{xy}[D \geq d|m, s, r, d \neq 0]$, is described under nodes DM 5 and DM 6 in the displacement model logic tree (Figure 4-2). Node DM 5 contains two alternative models from Petersen et al. (2011); both models are fit to a set of strike-slip earthquake data between approximately 20 m and 3 km from the principal rupture (Petersen et al., 2011). The first branch, with a weight of [0.3], is for a functional form that solves for distributed displacement *d* as a function of m and r. From equation 18 of Petersen et al. (2011), it is:

$$\ln(d) = 1.4016m - 0.1671\ln(r) - 6.7991 + 1.1193\varepsilon \quad (6\text{-}5)$$

where *d* is in centimeters and *r* is in meters. The regression standard deviation of 1.1193 is multiplied by the standard normal distribution function, ε, to represent event to event variability. The second branch under node DM 5 uses an alternative functional form that solves for normalized *d* over the average displacement of the rupture, D_{ave} , as a function of *r* :

$$\ln\left({}^{d}/_{D_{ave}}\right) = -0.1826\ln(r) - 1.5471 + 1.1388\varepsilon \quad (6\text{-}6)$$

This second branch is given a higher weight of [0.7] due to the greater flexibility of the model to explore uncertainty of distributed displacement amplitudes (through node DM 6). For both (6-5) and (6-6), the natural log standard deviations are used to capture aleatory variability in distributed displacement.

Node DM 6 explores equations to derive the average principal fault displacement as a function of magnitude, $D_{ave}(m)$, to provide the input required for implementing (6-6). Three branch alternatives are considered that explore epistemic uncertainty in average principal displacement for the fault sources (Figure 6-6). The branch alternatives are based on the published equation of Wells and Coppersmith (1994) constrained by global data of strike-slip ruptures. This equation has the form:

$$\log_{10} D_{ave} = bm + a + \tau\varepsilon \quad (6\text{-}7)$$

with τ representing the published standard deviation of the regression and ε representing the standard normal distribution. Best fit *a* and *b* values are listed in Table 6-4 as are the values for ε and τ. The upper (90th percentile) and lower (10th percentile) branches each are weighted [0.3] and the central (50th percentile) branch has a weight of [0.4] following Keefer and Bodily (1983).

Table 6-4. Parameters used for Average Principal Fault Displacement Estimations Based on Wells and Coppersmith (1994)

Probability (Percentile)	Parameters for $\log_{10} D_{ave} = bm + a + \tau\varepsilon$				Branch Weight
	b	*a*	τ	ε	
90th	0.90	-6.32	0.28	+1.28	[0.3]
50th	0.0482	-6.32	0.28	0	[0.4]
10th	0.0069	-6.32	0.28	-1.28	[0.3]

6.3 PFDHA Results

Probabilistic hazard results represent a generic "net displacement" hazard for Pardee Dam. The specific characteristics of the net displacement, including orientation, distribution, horizontal and vertical components, and coseismic slip versus afterslip, are beyond the scope of this simple hazard analysis. The probabilistic results are based on the PFDHA logic trees shown in Figures 5-2 and 6-6, and were calculated using LCI's hazard code TDISE. The hazard results are presented in three types of figures, as follows:

- Hazard curves showing total hazard for the facility shown in Figure 6-4, and contributions to total hazard by fault source;
- Hazard fractiles showing total epistemic uncertainty in the results captured in the logic trees;
- Hazard curves showing hazard sensitivity to examine the contribution to hazard uncertainty due to key logic tree uncertainties such as probability of activity, slip rate, Mchar, conditional probability of secondary displacement, and secondary displacement exceedance model.

6.3.1 Mean Hazard

The total mean hazard results of the PFDHA are presented in terms of mean annual frequency of exceedance (MAFE; in units of per year) as a function of net displacement amplitude in units of centimeters (panel a) and inches (panel b) (Figure 6-7). The total displacement hazard is the sum total of the mean hazard for each of the three fault sources considered, with the mean hazard for each source being the sum of all paths through the logic tree, with each path multiplied by its weight. The MAFE is the reciprocal of the average return period. Figure 6-7 also shows the mean displacement hazard for each of the three fault sources individually (the Waters Peak – Green Springs Run, Devils Gate, and Ione sources).

The total hazard curve is located below the 10^{-5} yr^{-1} MAFE hazard level, indicating that mean hazard is negligible at the 100,000 yr average return period (Figure 6-7). The largest contributor to total hazard is the Waters Peak fault source. The total hazard at the 10^{-6} yr^{-1} MAFE is approximately 9 cm (3.5 inches). For a displacement amplitude of 2 inches (~5 cm), the corresponding MAFE is approximately 1.7×10^{-6} yr^{-1}, corresponding to an average return period of about 590,000 years (Figure 6-7). Table 6-5 shows the hazard results at MAFEs of 10^{-5} and 10^{-6} yr^{-1}, and the MAFEs corresponding to displacements of 2 inches, 4 inches, and about 1 ft.

Table 6-5. Total Hazard Results from the PFDHA for Pardee Dam

MAFE (yr^{-1}) AND (CORRESPONDING RETURN PERIOD)	DISPLACEMENT	
	cm	inches
1×10^{-5} (100,000 yr)	- -	- -
1×10^{-6} (1,000,000 yr)	9	3.5
1.7×10^{-6} (590,000 yr)	5	2
9.0×10^{-7} (1,100,000 yr)	10	4
2.5×10^{-7} (4,000,000 yr)	30	12

6.3.2 Hazard Fractiles

As the field of PFDHA is relatively new, it is important to consider the uncertainty in the total mean hazard curve. Figure 6-8, panel (a) shows the mean hazard curve (black line) along with hazard fractiles in colored, solid lines at the 5th, 16th, 50th (median), 84th, and 95th percentiles. These fractile curves indicate the range of possibly correct hazard curves given the epistemic (or model) uncertainties in the logic trees. The 95th fractile, as an example, represents the hazard curve that would be exceeded by 5 percent of all possible paths (scaled by weight) through the logic tree. The 50th (or median) fractile represents a hazard curve that would be exceeded for about half of the possible paths through the logic tree. The weighted mean hazard curve falls between the median and 84th fractile hazard curves, as is common.

The hazard fractiles show that, even at the 95th fractile, the displacement hazard is on the order of 2×10^{-5} yr^{-1}, corresponding to an average return period of about 50,000 years, for net displacements of about 0.2 cm, or less than one tenth of an inch (Figure 6-8). At 1×10^{-5} yr^{-1}, the 95th fractile curve yields net displacements of about 2 cm, or less than one inch. This result suggests that the mean hazard results showing negligible hazard at the 10^{-5} hazard level (Table 6-5) is fairly robust even given the considerable epistemic uncertainties in the logic tree model.

6.3.3 Hazard Sensitivity

Figures 6-8, 6-9, and 6-10 examine how different elements of the PFDHA, as captured in the logic trees (Figures 5-2 and 6-6), impact uncertainty in the results. These sensitivity hazard curves are also called conditional hazard curves, as they show hazard curves given the condition that specific logic-tree branch values are given full weight (i.e., those values are assumed to be the *correct* values with no uncertainty). The greater the difference between the conditional hazard curve and the total mean hazard curve, the greater that model parameter (and the currently understood uncertainty) affects the hazard result. Figure 6-8, panel (b) shows the sensitivity to the fault source probability of activity (P(a)) parameter. The total mean hazard is shown as the solid black line. The dashed grey line shows the conditional hazard curve under the case where all three sources (Waters Peak – Green Springs Run, Devils Gate, and Ione) are modeled with a P(a) = 1.0.

Figure 6-9 shows two other hazard sensitivity plots from parameters in the fault source characterization logic tree (Figure 5-2). Fault slip rate (Figure 6-9, panel a) and Mchar (Figure 6-9, panel b) have fairly significant impacts on hazard uncertainty. These plots show the extreme cases whereby the "correct" logic tree values are the high (green curves), middle (red curves), or low (blue curves) branch values for all three fault sources. The large effect of fault slip rate on hazard results in not surprising given the direct scaling of the hazard curve with earthquake rate and the very large uncertainties in slip rate for these fault sources. The Mchar plots show a lesser contribution to hazard uncertainty, but an interesting effect whereby at low displacement amplitudes the lower Mchar values produce a greater rate of earthquakes (and higher MAFEs), but at larger displacement amplitudes the higher Mchar values correspond to higher MAFEs as the secondary displacement exceedances scale with earthquake magnitude (Equations 6-5, 6-6, and 6-7; Section 6.2.2). Sensitivities conducted on other nodes in the source characterization logic tree show smaller deviations from mean hazard than the ones in Figure 6-9.

The contribution to hazard uncertainty due to the fault displacement models (Figure 6-6) were also explored, with some of the more significant results shown in Figure 6-10. The uncertainty in conditional probability of distributed displacement at the site (Equation 6-4 and Table 6-3; Section 6.2.2) is explored in Figure 6-10, panel (a). This logic tree node has an enormous impact on hazard uncertainty and reflects the absence of available empirical data and poor predictive power of current models to anticipate the probability secondary displacement will occur at a specified location given the occurrence of a large earthquake on a nearby fault. The hazard sensitivity of distributed displacement exceedance (Equations 6-5 to 6-7) is explored in Figure 6-10, panel (b). The sensitivity curves show the two displacement prediction equations—based either as a function of magnitude and distance from a principal fault, $d(m,r)$ (Equation 6-5), or as secondary displacement normalized to average primary fault displacement as a function of distance, $d/D_{ave}(r)$ (Equation 6-6). These alternative models have a small but non-trivial difference on the hazard, but their similarity likely represents the fact that these two models rely on very few predictor variables and are derived largely from the same, limited dataset.

7.0 SUMMARY AND CONCLUSIONS

This surface fault rupture hazard and seismic source characterization for faults in the vicinity of Pardee Dam builds upon previous studies that recognized the reactivation of Mesozoic faults within the Foothills fault system. This study also incorporates new rupture models and investigative techniques to reevaluate the Waters Peak and other faults local to Pardee Dam. Earlier geological and seismological evaluations for critical facilities in the Sierra Nevada foothills were based on concepts introduced by projects that began in the 1970s. Major seismic hazard studies in the subject region included those in support of PG&E's proposed Stanislaus nuclear power plant (WCC, 1978), the proposed Auburn Dam by the US Bureau of Reclamation (Schwartz et al., 1977), EBMUD's Pardee Dam (ESA, 1992; HCG, 1998), USACE New Melones Dam (Biggar et al., 1978) and New Hogan Dam (Dames and Moore, 1993; USACE, 1995), and DWR following the (M_L) 5.7 Oroville earthquake (Morrison et al., 1976; California DWR, 1979). LCI's latest study builds upon this earlier work through the use of modern probabilistic seismic source characterization and paleoseismic techniques.

Results from this comprehensive analysis of the Waters Peak fault significantly improve the seismic community's understanding of hazards associated with surface fault rupture and strong ground shaking from the Waters Peak fault in the vicinity of Pardee Dam. This study also provides a valuable update to the seismic hazard contributions from other local faults that comprise the Foothills fault system, such as the Ione, Green Springs Run, Poorman Gulch, Haupt Creek and Slate Creek faults. In the summary below, we discuss the key findings from the paleoseismic study of the WPF, our updated seismic source model, and results from the probabilistic fault displacement hazard analysis.

Paleoseismic Investigation of the Waters Peak Fault

Three new trenches (LCI-T1 to -T3) on the WPF provide valuable information on the timing of the MRE and possible sense of slip. Collectively, the 2019 trenches (LCI-T1 to -T3) and previous trenches from Waters Peak North and South sites (USACE, 1995), indicate the WPF is *likely* inactive per the < 35 ka DSOD criteria (Fraser, 2001) for active faults in California. A distinct site-wide and predominantly eolian deposit (Unit 600) of early Modesto age (30 to 70 ka soil age) provides a key stratigraphic marker horizon to assess recency of activity. Evidence supporting a recent event that displaces the lower Modesto Unit 600 is: (1) in trench LCI-T1, generally poor and *unlikely*; (2) in trench LCI-T2, equivocal along an eastern fault strand, but *unlikely; and (3)* in trench LCI T-3, *unlikely;* as Unit 600 is unfaulted and undeformed. These new trench data support the previous findings of USACE (1995) that documented the WPF as a "non-capable" fault, and also support DSOD criteria for fault inactivity on the WPF. As such, our latest findings provide no compelling evidence to reclassify the WPF as active per DSOD criteria.

The trench exposures document the presence of late Pleistocene faulting. Similar to the findings of USACE (1995), we recognize clear evidence for late Pleistocene faulting with the vertical separation of Units 200 and 300 of Riverbank age across the WPF. This event (or events if faults

F1 and F2 ruptured independently) is interpreted as the MRE for this section of the WPF. Observations in trench LCI-T2 indicate a minimum of 47 cm of vertical separation of Riverbank to Turlock Lake age deposits. Kinematic observations of reverse faulting on more westerly-oriented fault strands (consistent with a restraining geometry) in trenches LCI-T2 and -T3, coupled with clear down-to-the-west displacement on fault(s) parallel to regional strike, suggest a greater contribution of lateral slip on the WPF in the late Quaternary than would be expected from structural observations in the Pardee Dam spillway and regional studies. Because the WPF is oriented sub-parallel to overall northwest direction of macroscopic dextral shear, paleoseismic evidence of a lateral slip component is not unexpected, and is accounted for in the updated seismic source model.

Updated Seismic Source Model for Faults Comprising Foothills fault system

Two types of seismic sources are considered in the updated seismic hazard analysis for Pardee Dam: (1) fault sources, and (2) areal source/background source zones. The updated seismic source model for Pardee Dam considered previously recognized fault sources within approximately 10 km of the dam, and focused on developing parameters useful for probabilistic seismic hazard analysis (PSHA). These data may also be considered for deterministic seismic hazard analysis (DSHA) by EBMUD (Table 5-1). Our analysis identified seven fault sources within 10 km of Pardee Dam that should be considered for inclusion in PSHA and may be reviewed and considered for DSHA. The study provides information on the seven sources, including their geologic and geomorphic basis for inclusion in the PSHA, geometry, evidence for late Cenozoic activity, evidence for recency of activity, style of faulting, and basis for slip rate in the current tectonic regime. The fault sources, listed in order of proximity to Pardee Dam, include the following:

Waters Peak – Green Springs Run	(0.2 km)
Devils Gate	(1.0 km)
Ione	(1.2 km)
Youngs Creek – Bowie Flat	(3.8 km)
Haupt Creek	(5.9 km)
Poorman Gulch – Rawhide Flat	(9.7 km)
Slate Creek	(10.2 km)

An areal (background) source zone model, coupled with instructions on how to implement the background model in the updated hazard analysis is provided as an appendix to this report. A Hazard Input Document (HID) was prepared that provides the EBMUD hazard analyst(s) with a complete description on the implementation of the background model and a listing of all the model components. The HID is a succinct summary of what is contained in the background model and provides the background logic tree parameters (nodes), alternative values (branches), and their weights (relative likelihood of each branch value being correct). The HID is provided in Appendix C.

Probabilistic Fault Displacement Hazard Analysis

The PFDHA calculated the hazard for surface-fault rupture to impact Pardee Dam, and focused on evaluating the hazard from secondary or distributed displacement from a surface-rupturing earthquake on the nearby Waters Peak – Green Springs Run, Ione, and Devils Gate faults. The source characterization logic tree for the PFDHA is identical to the logic tree developed for the Waters Peak, Devils Gate, and Ione fault sources for input to PSHA. The probabilistic hazard results are represented as a generic "net displacement" hazard for Pardee Dam.

The total mean hazard results of the PFDHA are presented in terms of mean annual frequency of exceedance (MAFE; in units of per year) as a function of net displacement amount. The total displacement hazard is the sum total of the mean hazard for each of the three fault sources considered, with the mean hazard for each source being the sum of all paths through the logic tree, with each path multiplied by its weight. The MAFE is the reciprocal of the average return period. The PFDHA results indicate that the total mean hazard curve lies below the 10^{-5} yr^{-1} MAFE hazard level, indicating that mean hazard is negligible at the 100,000 yr average return period. For a displacement amplitude of 2 inches (~5 cm), the corresponding MAFE is approximately 1.7×10^{-6} yr^{-1}, corresponding to an average return period of about 590 thousand years. The PFDHA results indicate that the surface fault displacement hazard associated with secondary or distributed faulting at Pardee Dam is very low to negligible. The displacement hazard associated with any particular portion of Pardee Dam, such as the powerhouse, is even lower than the hazard calculated for the entire dam based on the smaller footprint dimension.

8.0 REFERENCES CITED

AMEC Environment & Infrastructure Inc., 2012, Technical Memorandum No. 1: Summary of Geologic/Geotechnical Site Conditions and Recommendations for Foundation Properties and Rock Springs, 9 p., Appendix A in Jacobs Associates, 2013, Pardee Outlet Tower Seismic Evaluation, report to East Bay Municipal Utility District

Bateman, P.C., and Wahrhaftig, C., 1966, Geology of the Sierra Nevada, in Bailey, E. A., ed., Geology of Northern California, Volume 190, California Division of Mines and Geology Bulletin, p. 107-172.

Biasi, G. P., and S. G. Wesnousky (2016). Steps and gaps in ground ruptures: Empirical bounds on rupture propagation, Bull. Seismol. Soc. Am. 96, 1110–1124

Biggar, N., Cluff, L.S., and Ewoldsen, H., 1978, Geologic and seismologic investigations, New Melones Dam project, California: unpublished report by Woodward-Clyde Consultants to U.S. Army Corps of Engineers, 246 p.

Birkeland, P.W., 1999. Soils and Geomorphology. Oxford Univ. Press, New York. 430 pp

Bonilla, M.G., 1970, Surface faulting and related effects, in Wiegel, R. L., ed., Earthquake Engineering, Englewood Cliffs, N. J., Prentice-Hall, p. 47-74.

Borchardt, G. A., Rice, S. and Taylor, G., 1980a, Paleosols overlying the Foothills fault system near Auburn, California: California Division of Mines and Geology Special Report 149. Originally released as CDMG Open File Report 78-16 SF, 125 p.

Bryant, W.A., 1983, Southern Foothills fault system, Amador, Calaveras, El Dorado, and Tuolumne Counties: California Division of Mines and Geology Fault Evaluation Report FER-148, 12 p.

Busacca, A.J., 1982, Geologic history and soil development, northeastern Sacramento Valley, California: University of California Davis, Ph.D. thesis, 348 p.

Busby, C.J., Hagan, J.C., Putirka, K., Pluhar, C.J., Gans, P., Wagner, D.L., Rood, D., DeOreo, S.B., and Skilling, I., 2008, The ancestral Cascades arc: Cenozoic evolution of the central Sierra Nevada (California) and the birth of the new plate boundary, *in* Wright, J.E., and Shervais, J.W., eds., Ophiolites, Arcs, and Batholiths: Geological Society of America Special Paper 438.

California Department of Water Resources, 1979, The August 1, 1975 Oroville earthquake Investigations, Bulletin 203-78, 669 pages and multiple plates.

Chen, R.C., Dawson, T.E., and Will, C.J., 2013, Quantifying surface fault rupture location uncertainty for lifeline crossings, Final Technical Report, U.S. Geologic Survey National Earthquake Hazards Reduction Program Award G11AP20040, 51p.

Clark, L.D., 1960, Foothills fault system, western Sierra Nevada, California: Geological Society of America Bulletin, v. 71, p. 483–496.

Clark, L.D., 1964, Stratigraphy and Structure of Part of the Western Sierra Nevada Metamorphic Belt, California, United States Geological Survey Professional Paper 410, 75p.

Cornell, C.A., 1968, Engineering seismic risk analysis, Bulletin of the Seismological Society of America, v. 58, p. 1583–1606.

Cornell, C.A. and Vanmarcke, E.H., 1969, The major influences on seismic risk: Proceedings of the 4th World Conference on Earthquake Engineering, Santiago, Chile.

Dames and Moore, 1993, Photogeologic and imagery analysis for the geologic and seismologic investigation, New Hogan Dam, Calaveras County, California, unpublished consulting report to the United States Army Corps of Engineers, Sacramento District

Earth Sciences Associates, 1992, Raised Pardee Dam Additional Storage Alternative Geotechnical Investigation, unpublished consulting report dated June 1992, prepared for EBMUD.

Edelman, S.H., and Sharp, W.D., 1989, Terranes, early faults, and pre-Late Jurassic amalgamation of the western Sierra Nevada metamorphic belt, California: Geological Society of America Bulletin, v. 101, p. 1420-1433.

Federal Emergency Management Agency, 2013, LiDAR Dataset for Calaveras County, 1-m resolution, data obtained from the California Geological Survey, April 2019.

Fraser, W.A., 2001, Fault Activity Guidelines, California Division of Safety of Dams, 11p.

Gray, B., Graehl, N., Bozkurt, S., Baldwin, J. and Clahan, K., Seamless Photomosaic Trench Logging Using Trench-Based Photogrammetry Methods: Workflow and Case-Studies, 7th International INQUA Meeting on Paleoseismology, Active Tectonics and Archeoseismology (PATA), 30 May to 3 June, 2016, Crestone, Colorado, USA

Gutierrez, C.I., Holland, P.J., and O'neal, M.D., 2019, Preliminary Geologic Map of the Ione 7.5' Quadrangle, Amador County, California, vers. 1.0, California Geological Survey.

Hanks, T.C., and Bakun, W.H., 2014, M-logA models and other curiosities: Bulletin of the Seismological Society of America, v. 104, p. 2604-2610.

Harden, J.W., 1987, Soils Developed in Granitic Alluvium near Merced, California, U.S. Geological Survey Bulletin 1590-A, Soil Chronosequences in the Western United States, 76p.

Harden, J. W., and Marchand, D. E. (1977). The soil chronosequence of the Merced River. In "Soil Development, Geomorphology and Cenozoic History of the Northeastern San Joaquin Valley and Adjacent Areas, California: Guidebook for Joint Field Sessions, Soil Science Society of America, and Geological Society of America" (M. J. Singer, Ed.) pp. 22-38. Univ. of California Press. Davis.

Harden, J. W., and Marchand, D. E. (1980). Quaternary stratigraphy and interpretation of soil data from Auburn, Oroville, and Sonora areas along the Foothills fault system, western Sierra Nevada, California, U.S. Geological Survey Open File Report, p. 80-305, 56 p.

Harden J.W., and Taylor, E.T., 1987, A quantitative comparison of soil development in four climatic regimes, Quaternary Research, v. 20, no. 3, p 342-359

HCG Pardee Project Team, HDR Engineering, Christensen Associates, and GEI Consultants (HCG), 1998, Preliminary Design Report, Consultant Report submitted to East Bay Municipal Utility District (EBMUD), June 1998.

Henry, C.D., 2014, personal communication reported by Holland et al. (2015) regarding the age of the Campbell Creek Tuff member of the Valley Springs Formation

Henry, C.D. and John, D.A., 2013, Magmatism, ash-flow tuffs, and calderas of the ignimbrite flareup in the western Nevada volcanic field, Great Basin, USA, *Geosphere*, vol. 9, no. 3, 58p.

Holland, P.J., and O'Neal, M.D., 2019, Preliminary Geologic Map of the Jackson 7.5' Quadrangle, Amador and Calaveras Counties, California, vers. 1.0, California Geological Survey.

Holland, P.J., Gutierrez, C.I., and O'Neal, M.D., 2015, Preliminary Geologic Map of the Valley Springs 7.5' Quadrangle, Amador and Calaveras Counties, California, vers. 1.0, California Geological Survey.

Idriss, I.M., Archuleta, R.J., and Abrahamson, N.A., 2018, Evaluation of Earthquake Ground Motions: Engineering Guidelines for the Evaluation of Hydropower Projects – Chapter 13, prepared for Division of Dam Safety and Inspections, Office of Energy Projects, Federal Energy Regulatory Commission (FERC), Washington DC, 100 p.

Janda, R.J., 1966, Pleistocene history and hydrology of the upper San Joaquin River, California: Berkeley, University of California, Ph.D. thesis, 425 p.

Janda, R.J., 1965, Quaternary alluvium near Friant, California, in International Association for Quaternary Research Guidebook for Field Conference I, northern Great Basin and California: Lincoln, Nebraska Academy of Sciences, p. 128-133.

Jennings, C.W., and Bryant, W.A., 2010, Fault activity map of California, California Geological Survey Geologic Data Map No. 6, map scale 1:750,000.

Keefer, D.L., and Bodily, S.E., 1983, Three-point approximations for continuous random variables: Management Science, v. 29, p. 595–609.

Klinger, Y., 2010, Relation between continental strike-slip earthquake segmentation and thickness of the crust: Journal of Geophysical Research, v. 115, B07306.

Lettis Consultants International, Inc. (LCI), 2019, Pardee Dam Foothills fault system study, draft Waters Peak fault trenching work plan, report prepared for East Bay Municipal Utility District as a component of the Pardee Dam Foothills fault system study, 19 p. plus figures

Louderback, G.W., 1928, Geological report on Pardee Dam site, unpublished report to East Bay Municipal Utility District.

Leonard, M., 2010, Earthquake fault scaling: Self-consistent relating of rupture length, width, average displacement, and moment release: Bulletin of the Seismological Society of America, v. 100, p. 1971–1988.

Marchand, D.E., 1977, The Cenozoic history of the San Joaquin Valley and the adjacent Sierra Nevada as inferred from the geology and soils of the eastern San Joaquin Valley, in Singer, M.H., ed., Soil development, geomorphology, and Cenozoic of the northeastern San Joaquin Valley and adjacent areas, California: Soil Science of America-Geological Society of America joint field session, 1977, guidebook, p. 39-50.

Marchand, D.E., and Allwardt, A., 1981, Late Cenozoic stratigraphic units, northeastern San Joaquin Valley, California: U.S. Geological Survey Bulletin 1470, 70 p.

Morrison, P.W., Stump, B.W., and Uhrhammer, R., 1976, The Oroville earthquake sequence of August 1975: Bulletin of the Seismological Society of America, v. 66, p. 1065-1084.

O'Neal, M.D., Holland, P.J., and Gutierrez, C.I., 2015, Preliminary Geologic Map of the Wallace 7.5' Quadrangle, Amador, Calaveras, and San Joaquin Counties, California, vers. 1.0, California Geological Survey.

Pacific Gas & Electric Company (PG&E), 2017, Geology, Tectonics, and Seismic Source Characterization for the PG&E Hydroelectric Territory, unpublished report prepared by PG&E Geosciences Department, March.

Page, W.D., 1994, Review of fault trenches, New Hogan Dam, Calaveras County, independent peer review report of USACE (1995) paleoseismic studies, submitted to USACE on August 16, 1994

Page, W.D., and Sawyer, T.L., 2001, Use of geomorphic profiling to identify Quaternary faults within the Northern and Central Sierra Nevada, *in* Engineering Practice in Northern California, California Division of Mines and Geology, Bulleting 210, edited by Ferriz, H. and Anderson., R., 19 pages and 45 plates.

Page, W.D., and Sawyer, T.L., 2007, Overview of late Cenozoic faulting in the Sierra Nevada Foothills (including a reassessment of faults near New Bullards Bar Dam): unpublished consulting report submitted to the California Division of Safety of Dams, dated September 7, 2007.

Petersen, M.D. and Chen, R., 2018, Fault displacement hazard for strike-slip faults: Proceedings of the 11th National Conference in Earthquake Engineering, Earthquake Engineering Research Institute, Los Angeles, CA, 12 p.

Petersen, M.D., Dawson, T.E., Chen, R., Cao, T., Wills, C.J., Schwartz, D.P., Frankel, A.D., 2011, Fault displacement hazard for strike-slip faults: Bulletin of the Seismological Society of America, v. 101, p. 805–825.

Prentice, C. S., P. Mann, A. J. Crone, R. D. Gold, K. W. Hudnut, R. W. Briggs, R. D. Koehler, and P. Jean, 2010, Seismic hazard of the Enriquillo–Plantain Garden fault in Haiti inferred from paleoseismology: Nature Geosciences, v. 3, p. 789–793, doi:10.1038/ngeo991.

Rizzo, 2018, Eighth FERC Part 12D Independent Consultant Safety Inspection, Pardee Dam and Hydroelectric Facility, FERC Project No. 2916-CA, State Dam No. 31-004, NATDAM NO. CA00164, Revision 0.

Schwartz, D.P., Swan F.H., Harpster, R.E., Rogers, T.H., and Hitchcock, D.E., 1977, Surface faulting potential as part of the earthquake evaluation studies of the Auburn Dam area, Auburn-Folsom South Unit, Central Valley Project, California. Vol. 2: unpublished report from Woodward-Clyde Consultants to U.S. Bureau of Reclamation, Denver, 135 p.

Shlemon, R.J., 1994, New Hogan Dam Fault Study Investigations, Supplemental Technical Review for U.S. Army Corps of Engineers, Sacramento District, March, 1994 *in* U.S. Army Corps of Engineers, 1995, Geologic and Seismologic Investigation (Fault Study), New Hogan Dam and Reservoir (New Hogan Lake), Calaveras River, California.

Snow, C.A., and Scherer, H., 2006, Terranes of the western Sierra Nevada foothills metamorphic belt, California: A critical review: International Geology Review, v. 48, 46-62.

Streig, A.R., Rubin, C.M., Chen, W-S, Chen, Y-G., Lee, L-S., Thompson, S.C., Madden, C., and Lu, S-T., 2007, Evidence for prehistoric coseismic folding along the Tsaotun segment of the Chelungpu fault near Nan-Tou, Taiwan: Journal of Geophysical Research, v. 112, B03S06, doi:10.1029/2006JB004493.

Swan, F.H., III, and Hanson, K., 1977, Quaternary geology and age dating, in Woodward-Clyde Consultants, Earthquake evaluation studies of the Auburn Dam area, v. 4: report for the U.S. Bureau of Reclamation, Denver, 83 p. plus appendices.

Takao, M., Annaka, T., and Kurita, T., 2015, Establishment of evaluation formulae for probabilistic fault displacement hazard analysis (PFDHA) in Japan: Best Practices in Physics-based Fault Rupture Models for Seismic Hazard Assessment of Nuclear Installations, Vienna, Austria, Nov. 18-20, 2015, 16 p.

Terra/Geopentech, 2010, Camanche embankments safety review, unpublished consultant's report

United States Geological Survey and California Geological Survey (USGS and CGS), 2006, Quaternary Fault and Fold Database of the United States: Updated in 2018, url http://earthquake.usgs.gov/hazards/qfaults/; site accessed 2/15/2018.

Unruh, J.R., 1991, The uplift of the Sierra Nevada and implications for late Cenozoic epeirogeny in the western Cordillera: Geological Society of America Bulletin, v. 103, p. 1395-1404.

U.S. Army Corps of Engineers, 1995, Geologic and Seismologic Investigation (Fault Study), New Hogan Dam and Reservoir (New Hogan Lake), Calaveras River, California.

Wagner, D.L., Jennings, C.W., Bedrossian, T.L., and Bortugno, E.J., 1981, Geologic map of the Sacramento quadrangle: California Division of Mines and Geology, 1:250,000 scale.

Wagner, D.L. and Saucedo, G.J., 1990. Age and stratigraphic relationships of Miocene volcanic rocks along the eastern margin of the Sacramento Valley, California. *In* Ingersoll, R.V. and Nilsen, T.V. eds. 1990, Sacramento Valley Symposium and Guidebook: Pacific Section S.E.P.M., Vol. 65, p. 143-151.

Wakabayashi, J., 2013, Paleochannels, stream incision, erosion, topographic evolution, and alternative explanations of paleoaltimetry, Sierra Nevada, California: Geosphere, v. 9, no. 2, p. 191-215.

Wakabayashi, J., and Kemp, C. D., 2015, North Fork Feather River-Yellow Creek Divide, From Mohawk Valley to Caribou Junction, Middle and North Forks of the Feather River,

northeastern California: Friends of the Pleistocene, Pacific Cell, Annual Fieldtrip Guidebook, p. 223¬-230.

Wells, D.L. and Coppersmith, K.J., 1993, Likelihood of surface rupture as a function of magnitude: Seismological Research Letters, v. 64, p. 54 (abstract).

Wells, D.L. and Coppersmith, K.J., 1994, New Empirical Relationships among Magnitude, Rupture Length, Rupture Width, Rupture Area, and Surface Displacement: Bulletin of the Seismological Society of America, v. 84, p. 974–1002.

Wesnousky, S.G., Scholz, C.H., Shimazaki, K., and Matsuda, T., 1983, Earthquake frequency distribution and the mechanics of faulting, Journal of Geophysical Research, v. 88, p. 9331–9340.

William Lettis and Associates (WLA), 1994, Seismotectonic Evaluation, New Hogan Dam, Calaveras County, California, *in* U.S. Army Corps of Engineers, 1995, Geologic and Seismologic Investigation (Fault Study), New Hogan Dam and Reservoir (New Hogan Lake), Calaveras River, California.

Woodward-Clyde Consultants (WCC), 1977, Earthquake Evaluation Studies of the Auburn Dam Area, by Schwartz, D.P., Swan, F.H., Harpster, R.E., Rogers, T.H., and Hitchcock, D.H., Auburn-Folsom South Unit, Central Valley Project, California, Consultant's report to the U.S. Bureau of Reclamation, Denver, Colorado, Submitted July 1977, 411 p.

Woodward-Clyde Consultants (WCC), 1978, Foothills fault system study: Stanislaus Nuclear Project, Site Suitability/ Site Safety Report: Consultant's report to Pacific Gas and Electric Company, San Francisco, Appendix C.4, v. 6, 166 p. plus tables and figures.

Yeats, R.S. and Huftile, G.J., 1995, The Oak Ridge fault system and the 1994 Northridge earthquake: Nature, v. 373, p. 418–420.

Youngs, R.R., Arabasz, W.J., Anderson, R.E., Ramelli, A.R., Ake, J.P., Slemmons, D.B., McCalpin, J.P., Doser, D.I., Fridrich, C.J., Swan, F.H. III, Rogers, A.M., Yount, J.C., Anderson, L.W., Smith, K.D., Bruhn, R.L., Knuepfer, L.K., Smith, R.B., dePolo, C.M., O'Leary, K.W., Coppersmith, K.J., Pezzopane, S.K., Schwartz, D.P., Whitney, J.W., Olig, S.S., and Toro, G.R., 2003, A methodology for probabilistic fault displacement hazard analysis (PFDHA): Earthquake Spectra, v. 19, p. 191–219.

Zandt, G., Gilbert, H., Owens, T.J., Ducea, M., Saleeby, J., and Jones, C.H., 2004, Active foundering of a continental arc root beneath southern Sierra Nevada in California: Nature, v. 431, p. 41-46.

Tables

Table 5-1. Summary Activity Information and Simplified Source Parameters for Local Fault Sources

Fault Source Name [Distance from Pardee Dam]	Youngest Activity Documented [Confidence]	Oldest Inactivity Documented [Confidence]	DSOD Activity Category	Slip Rate (Preferred)	Dip and Dip Direction (Preferred)	Depth to Bottom of Faulting (Preferred)	Earthquake Magnitude (Preferred Mchar)
Waters Peak – Green Springs Run [0.2 km]	Late Riverbank to Early Modesto[1] (50 to 125 ka) [Likely]	Early Modesto[1] (30 to 70 ka) [Likely]	Inactive	0.01 mm/yr	65°NE	15 km	**M** 6.4
Devils Gate [1.0 km]	Late Cenozoic[2] [Probable]	-none-	Conditionally Active	0.02 mm/yr	75°SW	10 km	**M** 6.0
Ione [1.2 km]	Cenozoic[2] [Likely] Latest Pleistocene to Holocene[3,4] [Possible]	Latest Pleistocene to early Holocene[3,4] [Possible] Late Holocene [Likely]	Active or Conditionally Active	0.03 mm/yr	70°SW	15 km	**M** 6.2
Youngs Creek – Bowie Flat [3.8 km]	Late Cenozoic[5] [Likely]	Latest Pleistocene to early Holocene[4,6] (8 to 14 ka) [Probable]	Conditionally Active	0.002 mm/yr	70°NE	15 km	**M** 6.4
Haupt Creek [5.9 km]	Mesozoic[5] [Likely]	Late Cenozoic[5] [Probable]	Inactive	0.0006 mm/yr	70°NE	15 km	**M** 6.2
Poorman Gulch – Rawhide Flat [9.7 km]	Early Modesto[5,6] (30 to 70 ka) [Probable]	Latest Pleistocene to early Holocene[5,6] (8 to 14 ka) [Probable]	Active	0.009 mm/yr	70°NE	15 km	**M** 6.4
Slate Creek [10.2 km]	Mesozoic[2] [Likely] Late Cenozoic[2] [Possible]	Early Modesto to Riverbank[3,4] (30 to >100 ka) [Possible]	Inactive or Conditionally Active	0.01 mm/yr	70°NE	15 km	**M** 6.2

Note: Fault source parameter uncertainties, expressed as logic-tree values and weights, are in Figure 5-2. Fault activity designations (Fraser, 2001): Active = rupture in the last 35 ka, Conditionally Active = Quaternary fault with unknown displacement history in last 35 ka, Inactive = consistently shown to have no ruptures in the last 35 ka. Sources of activity information: 1 = this report (see Table 4-1); 2 = Dames and Moore (1993); 3 = Page (1994); 4 = WLA (1994); 5 = WCC (1978); 6 = Page and Sawyer

(2007). Note that chronologic descriptors *early* and *late* are used throughout this table to indicate age; Text and Table 4-1 use the corollary stratigraphic descriptors *upper* and *lower* to indicate sequential order of deposits.

Table 4-1. Field Descriptions of Trench T-2 Soils and Age Correlations[1]

Unit Number	Soil Horizons			Color (moist)	Structure[2]	Clay films[3]	Plasticity[4]	Stratigraphic Correlation with Waters Peak North Trench 3		Estimated Soil Series based on Comparison with Regional Soil Chronosequences (Marchand and Allwardt, 1981; Harden and Taylor, 1983; Harden, 1987)	LCI Preferred Soil Age
	LCI-T1	LCI-T2	LCI-T3					Trench 3 Unit Number (Sheet 4 of USACE, 1995)	Estimated Soil Series (USACE, 1995)		
800	Ap/AB Bw	Ap ABw Bwt	Ap A/Ap AB	10YR 5/2 to 7.5YR 4/3 5YR 4/4 7.5YR 4/4	1,f,sabk to 1,c,pl 1,f,gr to m 0.5,vf,sabk to 0.5,vf,gr	none none v1,n,co	non non non to sl	1	Holocene	post-Modesto	0 to 10 ka
700a		2 Bwt		7.5YR 4/4	1,vf,pr	v1,n,br co	non to sl	-[6]	-[6]	upper Modesto	5 to 30 ka
700	Bw2	BwA/Bwtj	Bw/Bwtj	7.5YR 4/4 (to 5YR 4/4)[5]	1,f,gr-sabk	none	non to sl	2	Holocene		
600	2 Btb1	3 Btb1	2 Btb1	10YR 3/2 to 7.5YR 4/3	2.5,m,abk-pr	2,n,pf po co	mod	3	Modesto	lower Modesto	30 to 70 ka
500		3 Btb2 3 Bt2b2	3 Btb2 3 Bt2b2	7.5YR 4/4 10YR 3/3	2,f,abk 1.5,vf,sabk	3,mk,pf po co 2,n,pf co	mod sl	3a / 3b	Modesto	upper Riverbank	50 to 125 ka
400		4 Bwtb3 4 Btb3	4 Btb3	2.5YR 4/6 10YR 4/6	2.5,vf,abk 2.5,f,sabk	4,n,pf br po co 4,n,pf co	sl sl	4 / 4a / 5	Riverbank or Older	upper Riverbank	>80 ka
300	3 Btb2	5 Bt2b3	5 Bt2b3	10YR 5/6	2.5,f,sabk	4,n,pf co	sl	4a	Riverbank or Older	upper / middle Riverbank	>80 ka
200		6 Btb4	6 Btb4	2.5Y 6/6 to 2.5Y 4/3	2,m,pr	4,mk,pf ss	high	6	Riverbank or Older	middle Riverbank / Turlock Lake	>80 ka

[1]Soils descriptors and codes adapted from Harden and Taylor (1983) and Harden (1987), according to standard methods and nomenclature (Birkeland, 1999).

[2]Structure codes: (m - massive, sg - single grained, 1 - weak, 2 - moderate, 3 - strong; vf - very fine, f - fine, m - medium, c - coarse, vc - very coarse; gr - granular, pl - platy, pr - prismatic, cpr - columnar, abk - angular blocky, sabk - subangular blocky)

[3]Clay films codes: (0 - none, v1 - very few, 1 - few, 2 - common, 3 - many, 4 - continuous; n - thin, mk - moderately thick, k - thick; pf - ped face coatings, br - bridging grains, po - pore linings, w - waves or lamellae, co - coats on clasts, ss - slickensides)

[4]Plasticity codes: (non - nonplastic, sl - slightly plastic, mod - moderately plastic, high - highly plastic)

[5]More reddish soil color from east end of LCI-T1, interpreted to be imparted from oxidation of underlying bedrock

Table 4-3: Structural Measurements of the Waters Peak Fault and Adjacent Bedrock

Location	Trench	Wall	Description	Measurement Type	Measurement Number on Trench Log	STRIKE	DIP	DIP DIRECTION	RAKE	PLUNGE DIRECTION	CONFIDENCE RANK
Southern Waters Peak Fault Trenches T-2 and T-3 (LCI, 2019)	LCI-T2	S	fault (secondary)	cross-trench	S1	011	67	E			
	LCI-T2	S	fault (secondary)	cross-trench	S2	004	90				
	LCI-T2	S	foliation shear	cross-trench	S3	343	65	E			
	LCI-T2	S	foliation shear	cross-trench	S4	002	76	E			
	LCI-T2	S	joint	exposed plane	S5	255	90				
	LCI-T2	S	foliation shear	cross-trench	S6	001	74	E			
	LCI-T2	S	fault (secondary)	cross-trench	S7	346	59	E			
	LCI-T2	S	foliation shear / joint	exposed plane	S8	182	39	W			
	LCI-T2	S	western fault strand	cross-trench	S9	344	86-90	E			
	LCI-T2	S	joint	exposed plane	S10	206	85	W			
	LCI-T2	S	eastern fault strand	cross-trench	S11	138	61-72	W			
	LCI-T2	S	eastern fault stand	exposed plane	S12	128	69	W	67	S	Moderate (B)
	LCI-T2	S	eastern fault stand	exposed plane	S13	129	68	W	64	S	High (A)
	LCI-T2	S	foliation shear	cross-trench	S14	349	51	E			
	LCI-T2	S	foliation shear	cross-trench	S15	344	57	E			
	LCI-T2	S	foliation shear	exposed plane	S16	342	49	E			
	LCI-T2	S	foliation shear	exposed plane	S17	345	53	E			
	LCI-T2	S	joint	exposed plane	S18	128	51	W			
	LCI-T2	S	foliation shear (?)	cross-trench	S19	139	81	W			
	LCI-T2	S	joint	exposed plane	S20	216	88	W			
	LCI-T2	S	foliation shear	exposed plane	S21	334	46	E			
	LCI-T2	S	fault (secondary)	cross-trench	S22	342	70-77	E			
	LCI-T3	S	foliation shear	exposed plane	S1	311	56	E			
	LCI-T3	S	western fault stand	cross-trench	S2	334	75-80	W			
	LCI-T3	S	western fault stand	cross-trench	S3	332	82	E			
	LCI-T3	S	eastern fault strand	cross-trench	S4	133	84	W			
	LCI-T3	S	eastern fault strand (?)	cross-trench	S5	130	83	W			
	LCI-T3	S	foliation shear	exposed plane	S6	321	55	E			
	LCI-T3	S	foliation shear	cross-trench	S7	327	51	E			
	LCI-T3	N	foliation shear	exposed plane	S8	344	52	E			

Location	Trench	Wall	Description	Measurement Type	Measurement Number on Trench Log	STRIKE	DIP	DIP DIRECTION	RAKE	PLUNGE DIRECTION	CONFIDENCE RANK
Northern Waters Peak Trenches (LCI-T1)	LCI-T1	S	foliation shear	cross-trench	S1	355	76	E			
	LCI-T1	S	foliation shear	cross-trench	S2	356	76	E			
	LCI-T1	S	foliation shear	cross-trench	S3	003	70	E			
	LCI-T1	S	foliation shear	cross-trench	S4	352	44	E			
	LCI-T1	N	western fault strand	cross-trench	S5	357	64	E			
	LCI-T1	S	foliation shear	cross-trench	S6	359	78	E			
	LCI-T1	S	eastern fault strand	cross-trench	S7	338	58	E			
	LCI-T1	S	eastern fault strand	cross-trench	S8	168	60	W			
	LCI-T1	S	eastern fault strand	cross-trench	S9	332	85-90	E			
	LCI-T1	S	foliation shear	cross-trench	S10	350	80	E			
	LCI-T1	S	foliation shear	cross-trench	S11	348	72	E			
	LCI-T1	S	foliation shear	cross-trench	S12	340	50	E			
	LCI-T1	S	western fault strand	cross-trench	S13	320	65	E			
	LCI-T1	N	western fault strand	exposed plane	S14	358	62	E			
	LCI-T1	S	western fault strand	cross-trench	S15	340	51	E			
USACE North Trench T-3 (USACE, 1995)	USACE-T3		joints			059	86	NW			
	USACE-T3		joints			082	57	SW			
	USACE-T3		cleavage			317	49	NE			
	USACE-T3		joints			075	58	SE			
	USACE-T3		joints			015	43	NW			
	USACE-T3		cleavage / foliation			062	64	SE			
	USACE-T3		joint			335	52	NE			
	USACE-T3		slaty cleavage			328	42	NE			
	USACE-T3		joint			045	18	SE			
	USACE-T3		joint			310	75	SW			
USACE South, Trench T-3 (USACE, 1995)	USACE-T3 (South)		Primary fault strand			337	66	NE	42	NE	Unknown
Pardee Spillway			primary fault			325	66	NE	64	SE	Very High (A+)
			primary fault (western)			335	56	NE	61	SE	Moderate (B)
			bedrock fault			307	57	NE	72	SE	Moderate (B)*
			fault (secondary)			334	69	NE	76	SE	Moderate (B)*

Figures

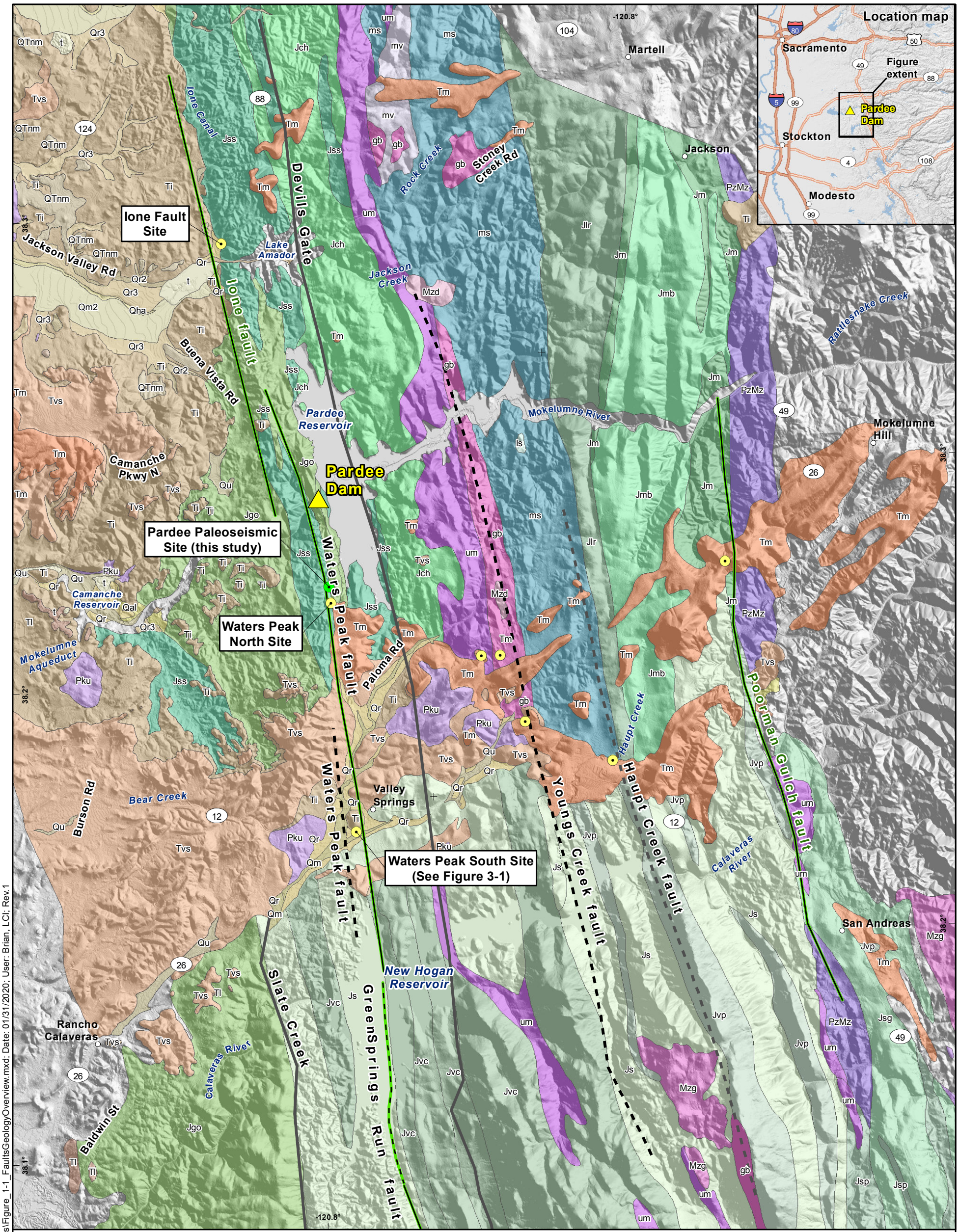

EXPLANATION

- 2019 Study location
- Previous paleoseismic trench sites (USACE, 1995; WCC, 1978)

Quaternary Faults (modified from USGS, 2018):
Solid where certain, dashed where approximate, colored by age.
- < 130,000 years
- < 1.6 million years
- Late Cenozoic or older fault

Geologic Units:
Quaternary
- **Qr** - Riverbank Formation
- **Qu** - Undifferentiated surficial deposits

Tertiary
- **Tm** - Mehrten Formation
- **Ti** - Ione Formation
- **Tvs** - Valley Springs Formation

Jurassic
- **Jss** - Salt Springs Slate
- **Jch** - Copper Hill Volcanics
- **Jmb** - Brower Creek Volcanics
- **Jgo** - Gopher Ridge Volcanics
- **Jlr** - Logtown Ridge Formation

Paleozoic
- **ms** - Metasedimentary rocks

Plutonic Rocks
- **Mzd** - Mesozoic dioritic rocks
- **gb** - Gabbroic rocks
- **um** - Ultramafic rocks

Note:
- See Figure 5-1 for complete seismic source map

Geologic Map Sources:
- Bartow et al. (1979)
- Bryant, W.A. (1983)
- Clark et al. (1963)
- Wagner et al. (1981)

Other sources:
- 10 m hillshaded DEM from USGS (2013)

0 1 2 mi.
0 2 4 km

Map projection and scale: NAD 1983 UTM Zone 10N, 1:90,000

Regional Geologic and Fault Activity Map

EBMUD PARDEE DAM FAULT HAZARD STUDY

Lettis Consultants International, Inc. | Figure **1-1**

File path: S:\1772_Pardee\Figures\January Report Figures\Figure_1-1_FaultsGeologyOverview.mxd; Date: 01/31/2020; User: Brian, LCI; Rev.1

Pardee Dam

Pardee Spillway

Phyllite seam

Mokelumne Tunnel

Chemical Plant

Waters Peak fault

Mokelumne River

Pardee Reservoir

Sandretto Rd

Site 5 (This study)

Site 6 (This study)

Waters Peak North Site (USACE, 1995)

LCI T-1

LCI T-2

LCI T-3

USACE T-1

USACE T-2

USACE T-3

af

Jgo

Jss

Qc

Qal

Qt

Qaf

Qls

Jgoa

Ei

OMvsc

Pl

Mpm

H_2O

Location map

Figure Extent

Buena Vista

Amador

Pardee Reservoir

Camanche

Calaveras

Campo Seco

Paloma

Camanche

8

EXPLANATION

Mokelumne tunnel

Exploration data

LCI trench (This study)

USACE trench (1995)

Geologic symbols

5 foot contour

Ephemeral stream

Contact; dashed where approximate, dotted where concealed

Fault, Quaternary inactive; dashed where approximate, dotted where concealed

Fault, Quaternary active; dashed where approximate, dptted where concealed

Phyllite seam (compiled from previous work); location approximate

Geologic Units

H_20	water
af	artificial fill
Aaf	allvial fan (anthropogenic)
Qt	fluvial terrace
Qc	colluvium
Qal	alluvium
Qls	Landslide
Qaf	alluvial fan
Pl	Laguna Formation
Mpm	Mehrten Formation
OMvsc	Valley Springs Formation conglomerate
Ei	Ione Formation
Jss	Salt Springs Slate
Jgo	Gopher Ridge Volcanics
Jgoa	Amphibolite facies

Notes:

- Geology compiled from Holland et al. (2015), ESA (1992), and original mapping completed for this study. Quaternary geology mapped near Sites 5 and 6 only.
- Quaternary geology shown for paleoseismic sites only.

N W E S

0 500 1,000 ft

0 200 400 m

Map projection and scale: NAD 1983 UTM Zone 10N, 1:8,500

Geologic Map of the Waters Peak Fault near Pardee Dam

EBMUD PARDEE DAM FAULT HAZARD STUDY

LCI Lettis Consultants International, Inc.

Figure **1-2**

File path: S:\1772_Pardee\Figures\January Report Figures\Figure_1-2_WatersPeak.mxd; Date: 01/29/2020; User: Brian, LCI; Rev.1

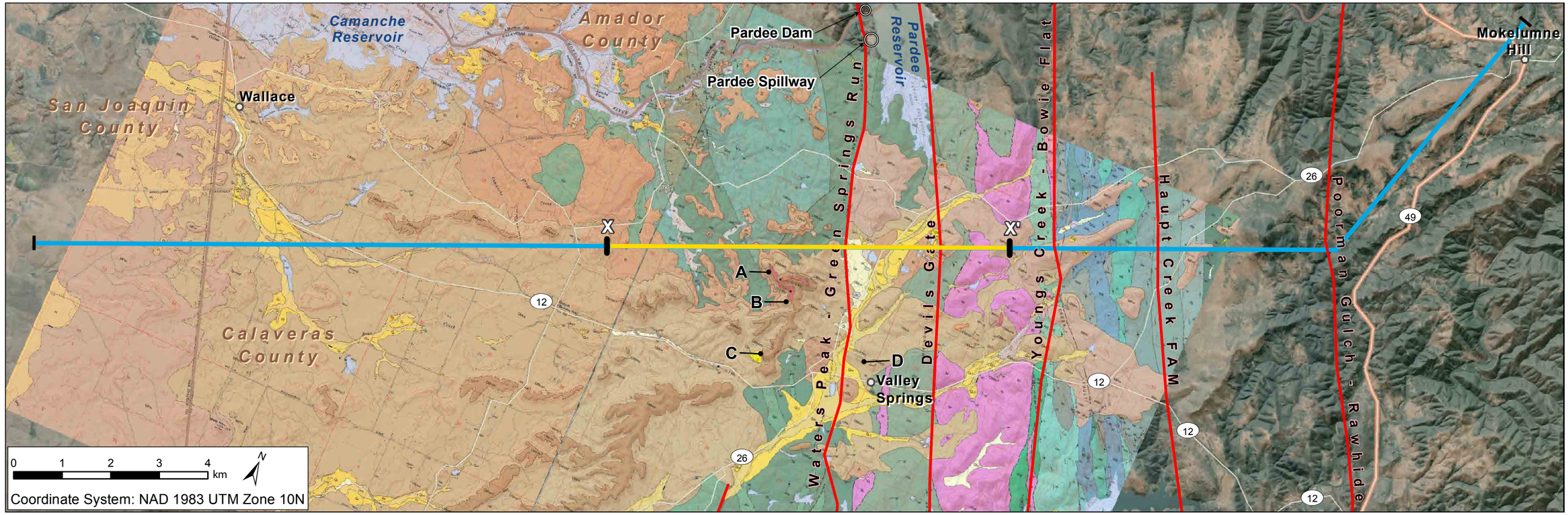

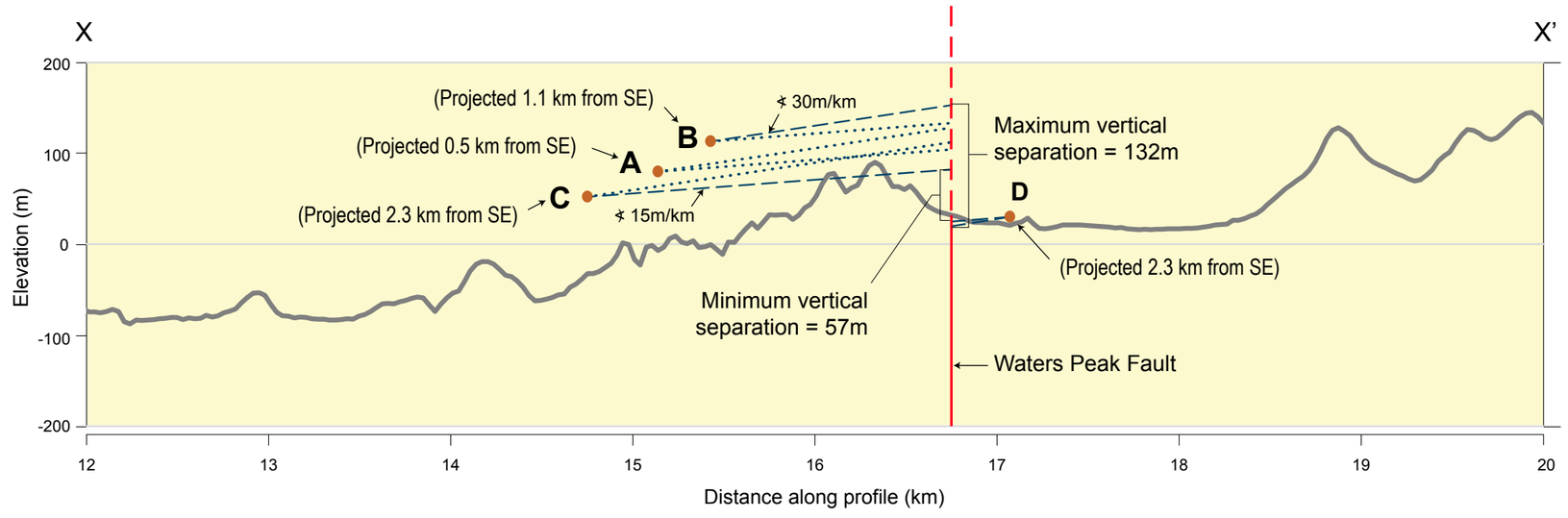

EXPLANATION

- Point locations at base of Campbell Creek Member
- Fault sources of Page and Sawyer (2001) Profile 31
- Approximate location of complete profile
- Location of profile excerpt presented in this figure
- Topographic profile (from 1m DEM, Calaveras County)
- Select Geologic Units (See Figure __ for explanation of all Units)
  - MPm – Miocene Mehrten Formation
  - OMvs – Oligocene Valley Springs Formation
  - OMvscc – Campbell Creek Member, Valley Springs Formation

Profile scale:
Vertical: 1 in = 160m
Horizontal: 1 in = 800m

Sources:
- Geology compiled from CGS 24k maps of the Wallace (Oneal et al., 2015) and Valley Springs (Holland et al., 2015) Quadrangles.
- Imagery basemap from ESRI.

Map and Geologic Profile of Campbell Creek Tuff Across the Waters Peak Fault

EBMUD PARDEE DAM FAULT HAZARD STUDY

Lettis Consultants International, Inc. | Figure **1-3**

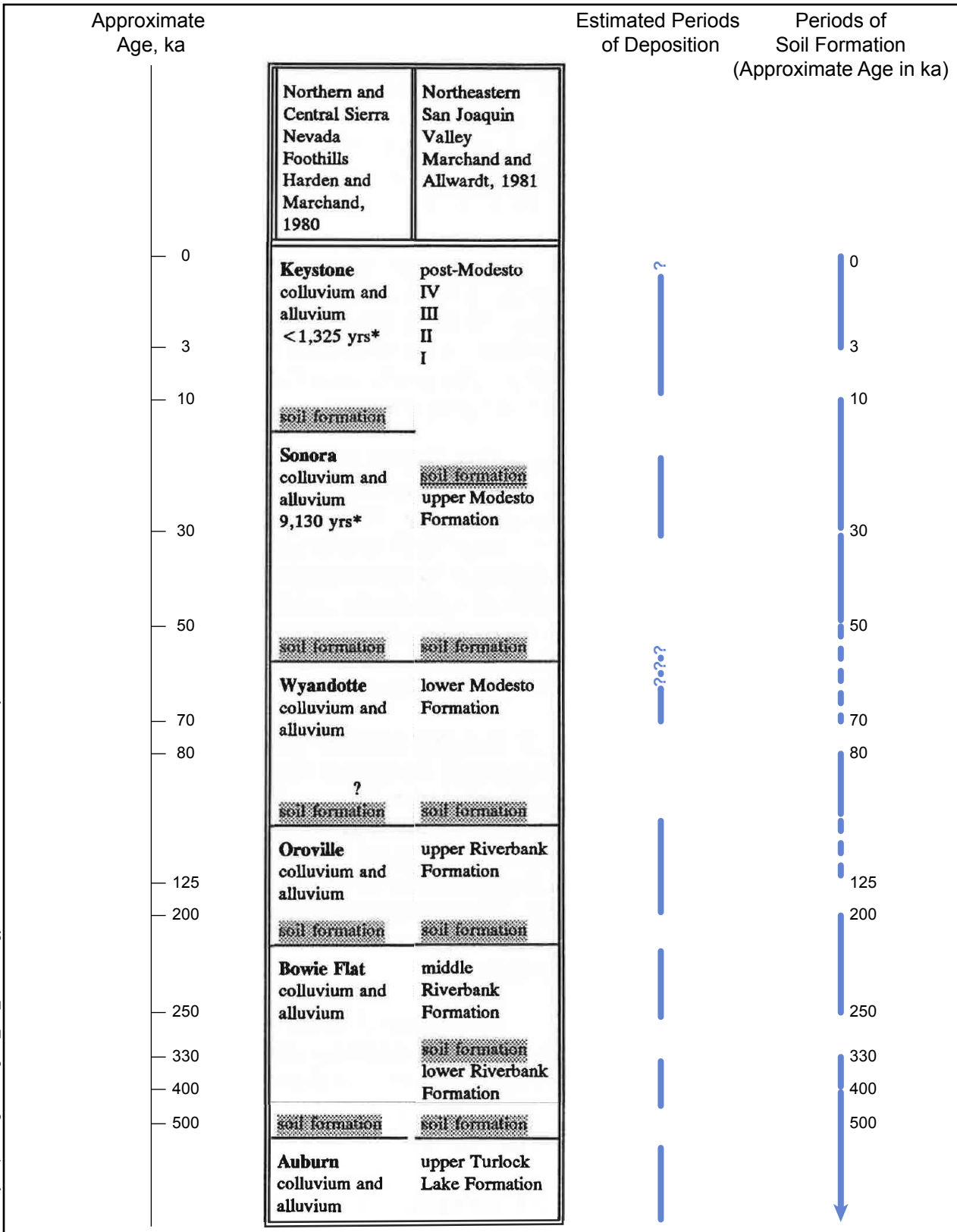

Notes:

- All periods of deposition must pre-date or coincide with their associated formation.
- Approximate age not to scale.
- Modified from Harden & Marchand (1980) and Marchand & Allwardt (1981)

Summary of Central Sierra Nevada Soil Chronology

EBMUD PARDEE DAM FAULT HAZARD STUDY

Lettis Consultants International, Inc. | Figure **2-1**

File path: S:\1772_Pardee\Figures\January Report Figures\Figure_2-1_Chronology.ai; Date: 11/18/2019; User: Whitney Newcomb, LCI; Rev.1

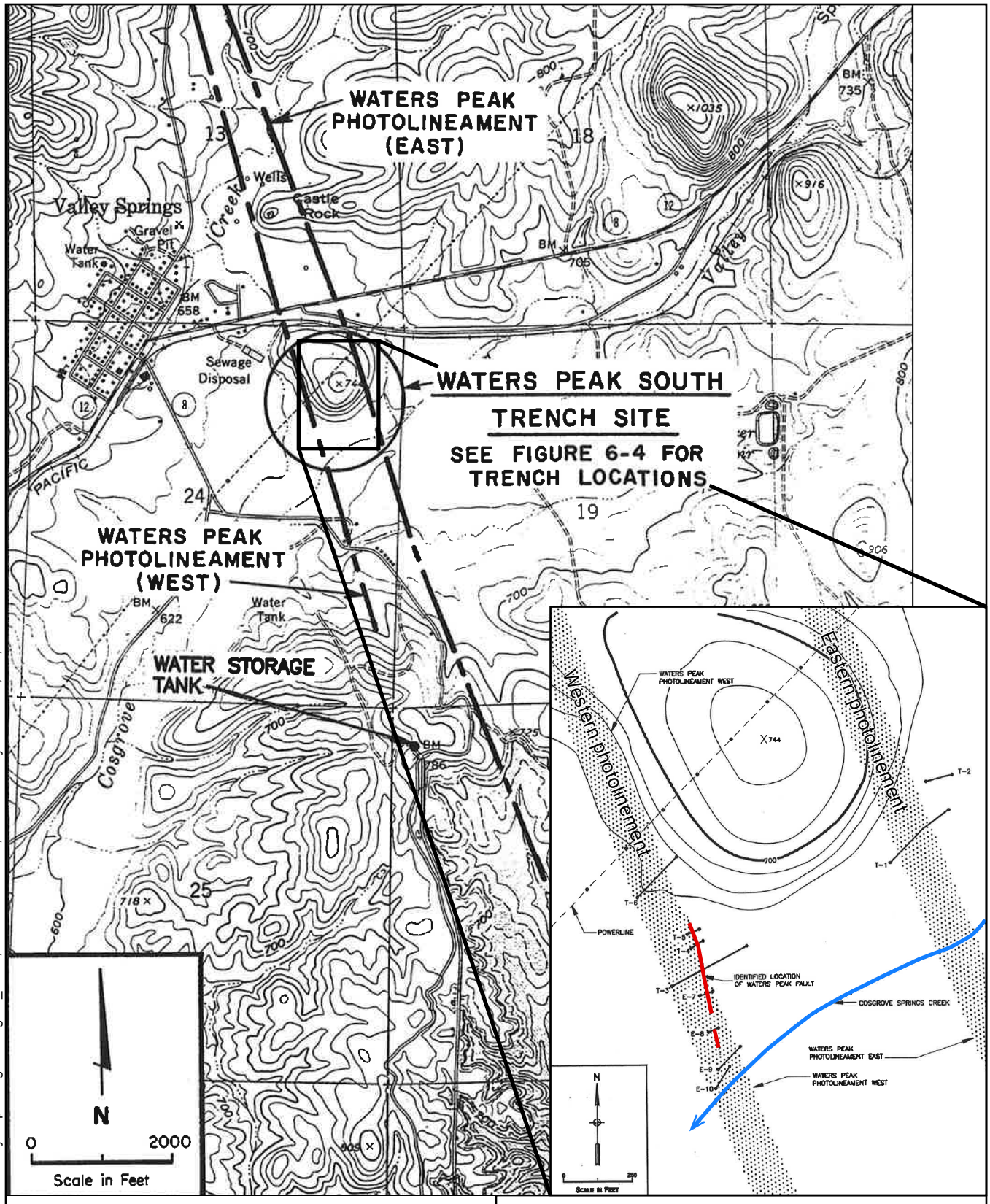

Source:
• Modified from USACE (1995) Figures 6-3 & 6-4.

Waters Peak South Site Map (USACE, 1995)

EBMUD PARDEE DAM FAULT HAZARD STUDY

LCI **Lettis Consultants International, Inc.** | Figure **3-1**

File path: S:\1772_Pardee\Figures\January Report Figures\Figure_3-1.ai; Date: 11/22/2019; User: Whitney Newcomb, LCI; Rev.1

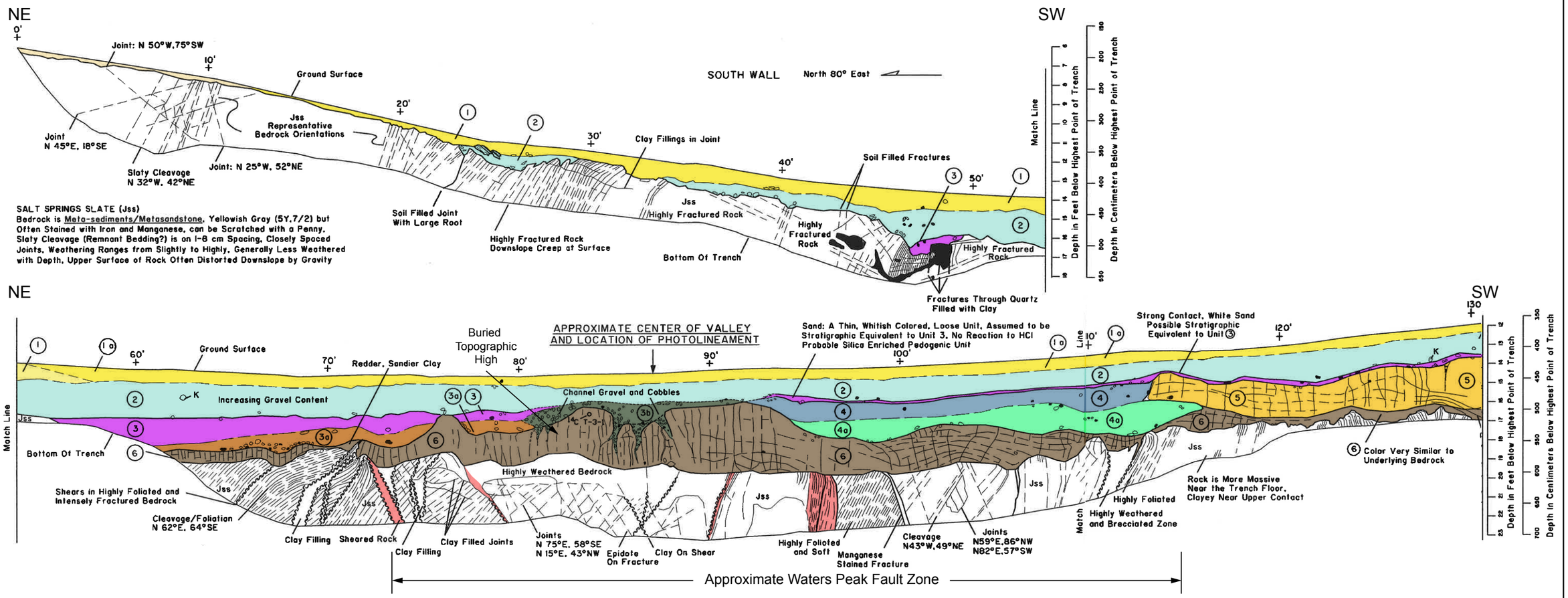

LCI Unit — **FIELD CLASSIFICATIONS OF SOIL (ASTM D 2488-84)** (Colors Designated from Munsell Soil Color Charts)

Holocene Deposits

800 — (1) Qc3 Sandy Fat Clay (CH), Brown to Dark Brown when Moist (7.5YR, 4/4). Approx. 60% High Plasticity Fines, 30% Fine to Coarse, Subangular to Subrounded Sand, 10% Subangular Gravel to 3 Inches, High Dry Strength High Toughness, Low Dilatancy, but Not Very Dense, Dry, Abundant Roots

800 — (1a) Qc3 Sandy Fat Clay (CH), Similar to Unit 1 Except Mottled Dark Yellowish Brown (10YR, 4/4) to Strong Brown (7.5YR, 5/6), Porous, Not Very Dense, Dry, Abundant Roots

700/700a — (2) Qc2 Sandy Fat Clay (CH), Brown to Dark Brown when Moist (7.5YR, 4/4), Approx. 50-70% Medium Plasticity Fines, 25-40% Fine to Coarse, Subangular to Subrounded Sand, 0-10% Subangular to Rounded Gravel to 3 Inches, Medium Dry Strength and Toughness, Low Dilatancy, Porous, Dry, Abundant Quartz

Modesto Age Deposits

600 — (3) Qc1 Fat Clay with Sand (CH), Dark Grayish Brown when Moist (10YR, 4/2), Approx. 70% High Plasticity Fines, 20% Fine to Coarse, Subangular to Subrounded Sand, 10% Subangular to Subrounded Gravel to 3 Inches, High Dry Strength, High Toughness, Low Dilatancy, Dry, Abundant Quartz

LCI Unit

500 — (3a) QcO Clayey Sand with Gravel (SC), Brown when Moist (10YR, 4/3), Approx. 50% Fine to Coarse, Subangular to Subrounded Sand, 30% Subangular to Subrounded, 20% Medium to High Plasticity Fines, 20% by Volume Cobbles to 6 Inches, Coarse Fraction Mostly Quartz and Meta-Sediments

500 — (3b) QcO Poorly Graded Gravel with Clay and Sand (Gp-GC), As Above (3a) except 50% Gravel, 30% Sand

Riverbank Age or Older Deposits/Residual Soils

400 — (4) Sandy Lean Clay with Gravel (CL), Dark Reddish Gray when Moist (5YR, 4/2), Approx. 50% Medium Plasticity Fines, 40% Fine to Coarse, Subangular to Subrounded Sand, 10% Subangular to Subrounded Gravel to 1.5 Inches, Mostly Quartz and Meta-Sediments

300 — (4a) Sandy Lean Clay with Gravel (CL), Dark Reddish Brown when Moist (5YR, 3/4), Similar to Unit 4, Except Slightly More Gravel

(5) Sandy Fat Clay (CH), Reddish Brown when Moist (5YR, 4/3), Approx. 60-80% Medium Plasticity Fines, 20-40% Very Fine to Coarse, Subangular to Subrounded Sand, Abundant Quartz, Unit is Very Dense, Horizontal and Vertical Parting Planes

Fracture Fills (Lettis, 1995)

LCI Unit

Show Slickensides From Shrink/Swell, Some Roots Near Upper Contact

200 — (6) Sandy Lean Clay (CL), Olive Brown (2.5Y, 4/3) to Dark Yellowish Brown (10YR, 4/4) when Moist, Approx 60% Medium Plasticity Fines, 40% Very Fine to Coarse, Subangular to Subrounded Sand, Grains are Mostly Quartz and Feldspars, Numerous Fragments of Bedrock Near Base of Unit, Some Gravel Found in Desiccation Cracks, Unit may have Weathered from Underlying Bedrock

100 — Jss - Jurassic Age; Salt Springs Slate

Notes:
See Figures 1-1 and 1-2 for location (Waters Peak North Site).
Figure modified from USACE (1995).
Unit colors correspond to LCI-T2 and T-3

Waters Peak Trench T-3 (USACE, 1995)
South Wall

EBMD PARDEE DAM FAULT HAZARD STUDY

Lettis Consultants International, Inc. | Figure **3-2**

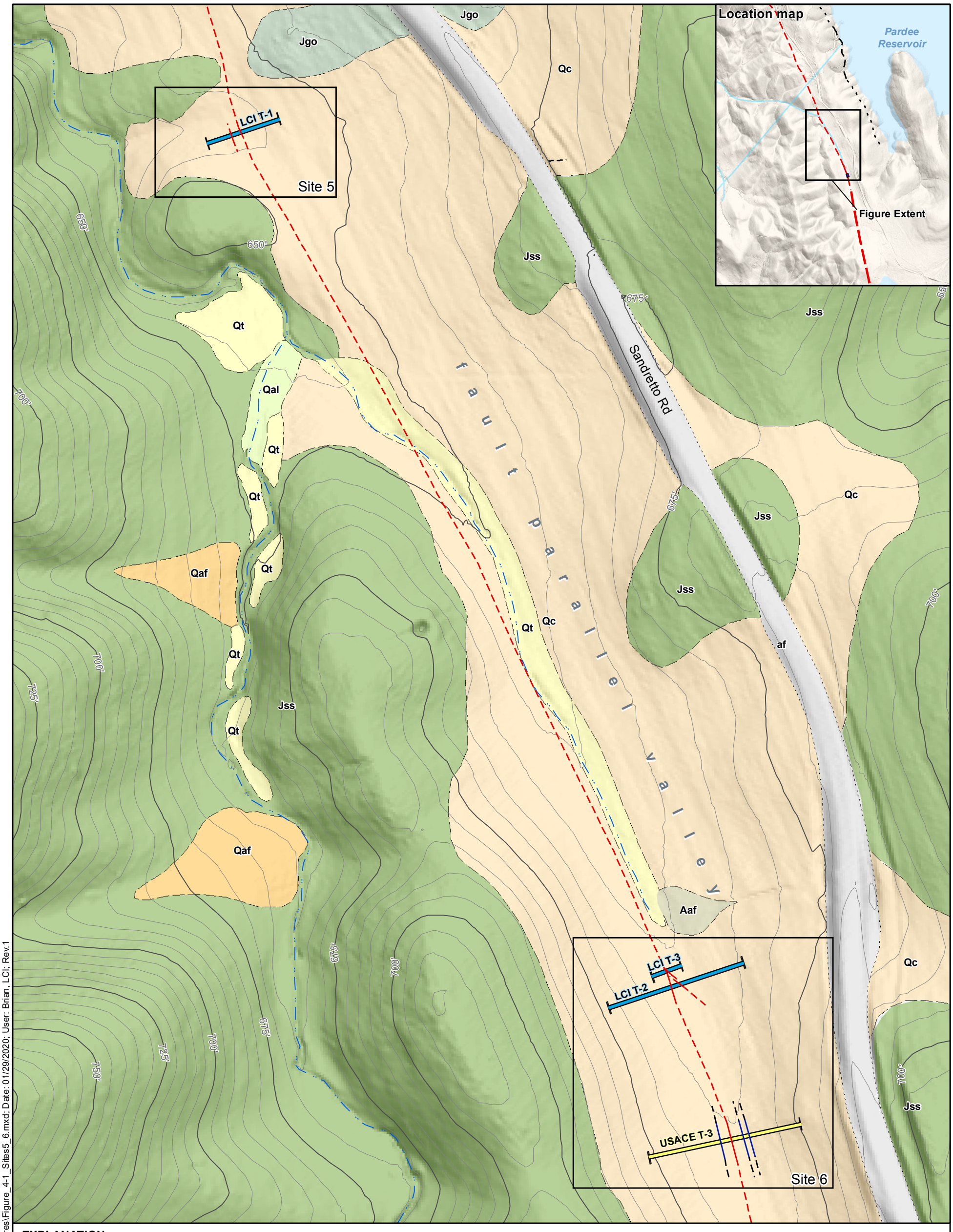

EXPLANATION

Exploration data
- LCI 2019 trench
- USACE trench (1995)

Geologic symbols
- ephemeral stream
- Contact; dashed where approximate, dotted where concealed
- Fault, Quaternary inactive; dashed where approximate, dotted where concealed
- Fault, Quaternary active; dashed where approximate, dotted where concealed
- 5 foot contour

Geologic Units
- H20 water
- af artificial fill
- Aaf allvial fan (anthropogenic)
- Qt fluvial terrace
- Qc colluvium
- Qal alluvium
- Qaf alluvial fan
- Mpm Mehrten Formation
- Jss Salt Springs Slate
- Jgo Gopher Ridge Volcanics

Notes:
Geology compiled from Holland et al. (2015), ESA (1992), and original mapping completed for this study.

N W E S

0 100 200 ft
0 40 80 m

Map projection and scale: NAD 1983 UTM Zone 10N, 1:1,500

Geologic and Geomorphic Map of Sites 5 and 6

EBMUD PARDEE DAM FAULT HAZARD STUDY

Lettis Consultants International, Inc. | Figure **4-1**

File path: S:\1772_Pardee\Figures\January Report Figures\Figure_4-1_Sites5_6.mxd; Date: 01/29/2020; User: Brian, LCI; Rev.1

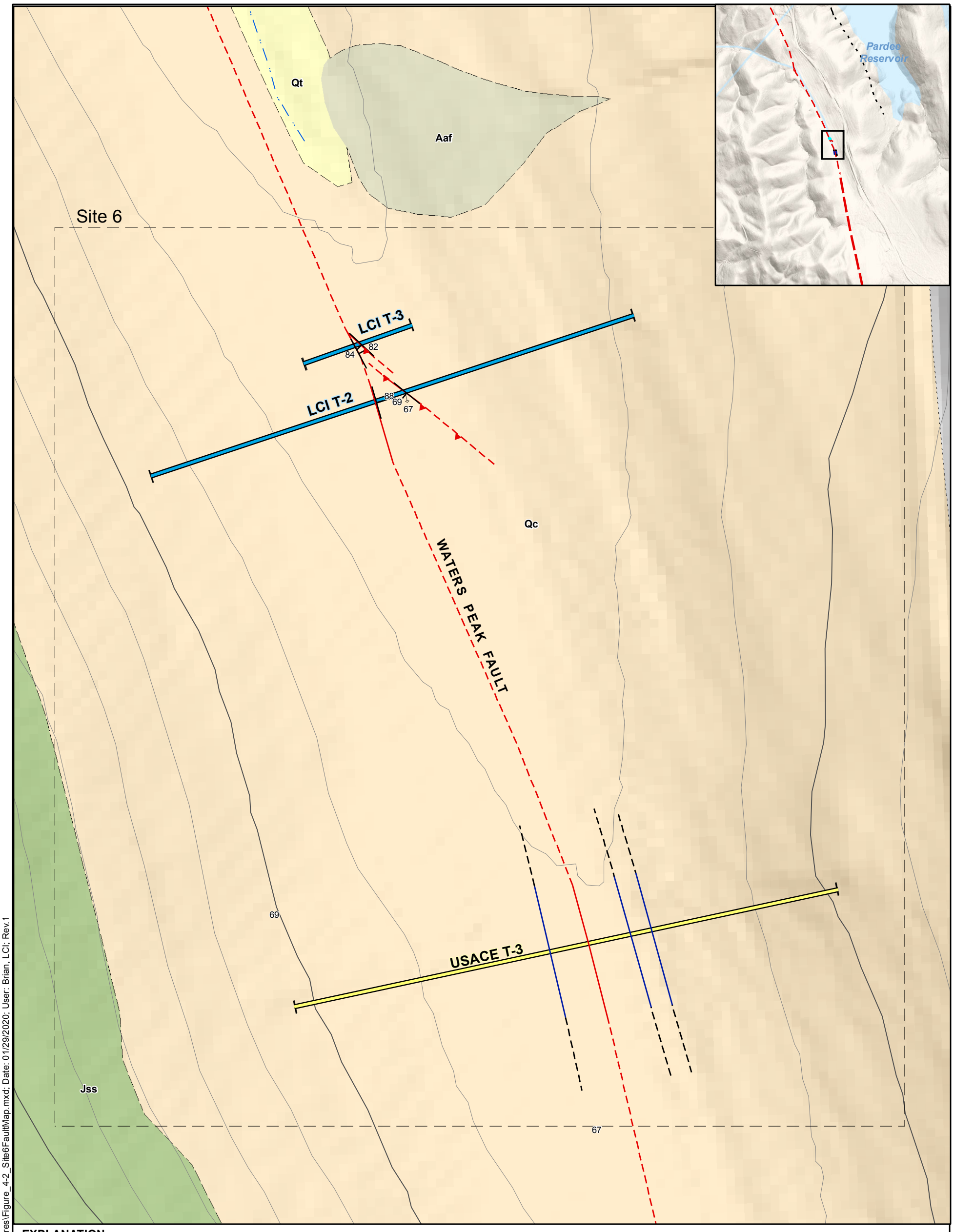

EXPLANATION

Fault attitude, dip and rake (68, 74)

Fault attitude, dip only (68)

Exploration data

- LCI 2019 trench
- USACE trench (1995)

Geologic symbols

- ephemeral stream
- Contact; dashed where approximate, dotted where concealed
- Fault, Quaternary inactive; dashed where approximate, dotted where concealed
- Fault, Quaternary active; dashed where approximate, dptted where concealed

5 foot contour

Geologic Units

H20	water
af	artificial fill
Aaf	allvial fan (anthropogenic)
Qt	fluvial terrace
Qc	colluvium
Qal	alluvium
Qaf	alluvial fan
Mpm	Mehrten Formation
Jss	Salt Springs Slate
Jgo	Gopher Ridge Volcanics

Notes:
Geology compiled from Holland et al. (2015), and original mapping completed for this study.

0 40 80 ft

0 10 20 m

Map projection and scale: NAD 1983 UTM Zone 10N, 1:421

Map of Site 6 Fault Locations and Projections

EBMUD PARDEE DAM FAULT HAZARD STUDY

Lettis Consultants International, Inc. | Figure **4-2**

File path: S:\1772_Pardee\Figures\January Report Figures\Figure_4-2_Site6FaultMap.mxd; Date: 01/29/2020; User: Brian, LCI; Rev.1

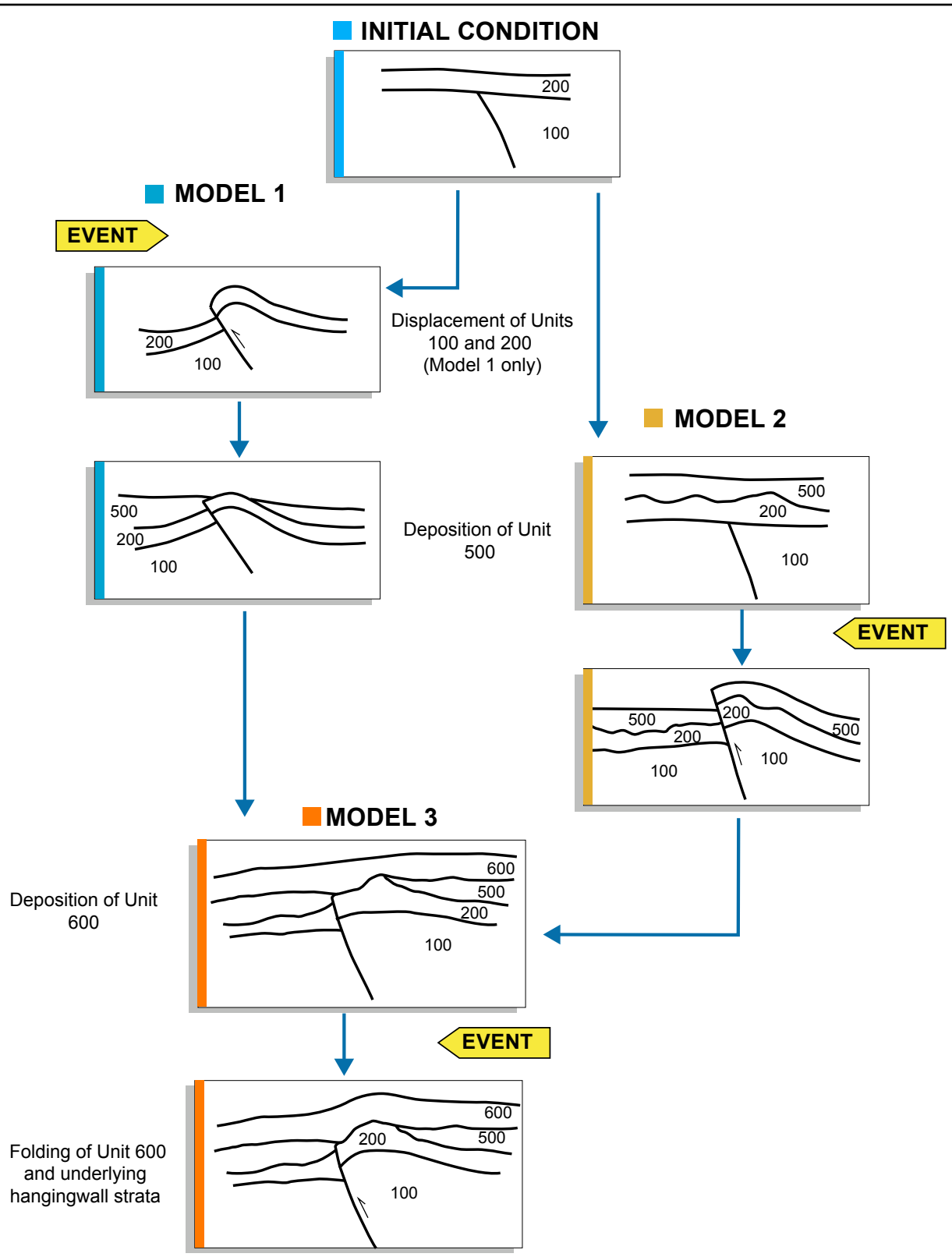

Event Models for LCI-T2 F2

EBMUD PARDEE DAM FAULT HAZARD STUDY

Lettis Consultants International, Inc. | Figure **4-3**

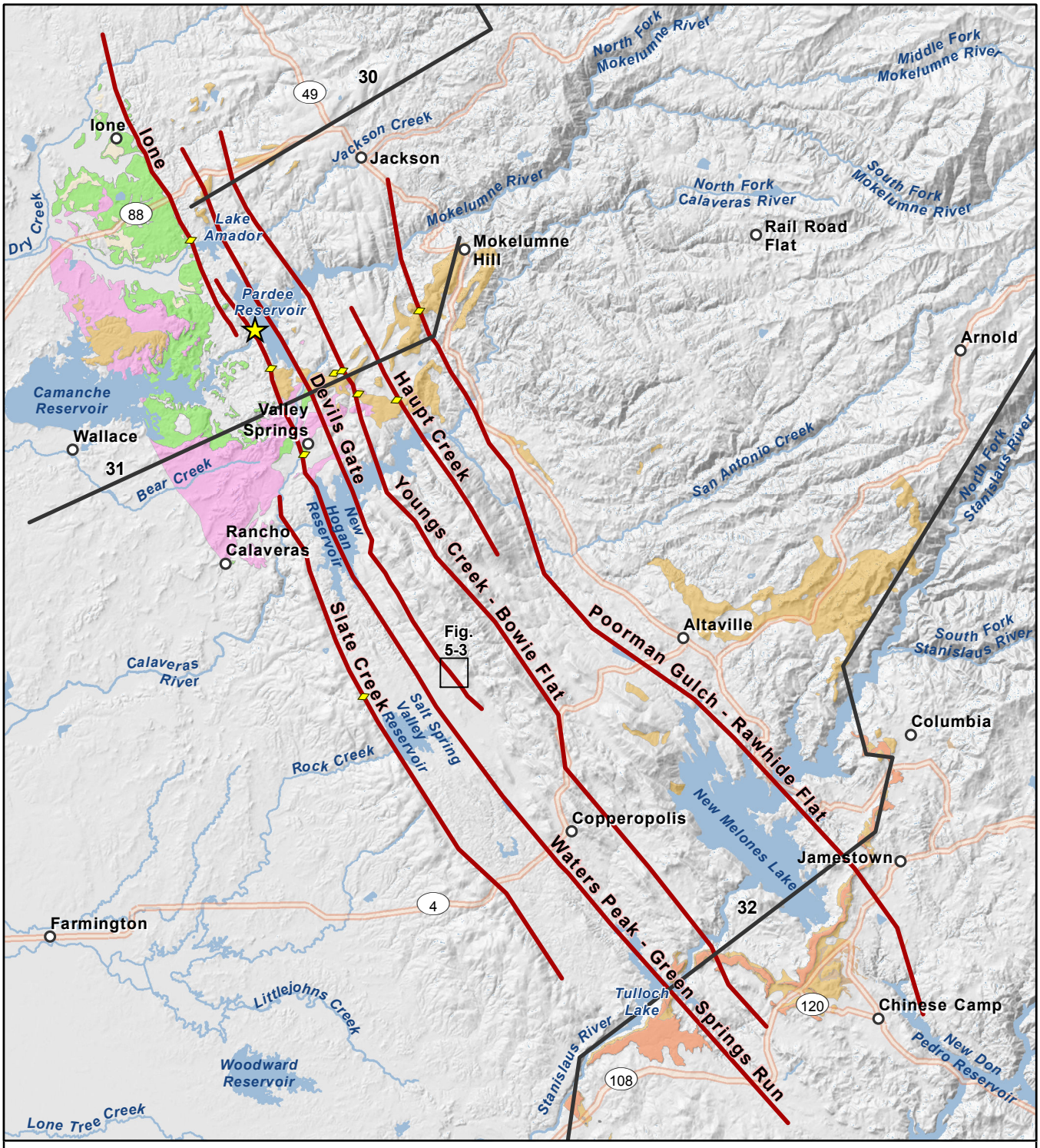

EXPLANATION:

- Project site
- Fault source
- 31 — Profile (Page and Sawyer, 2001)
- Trench location

Tertiary Units

- Tm - Mehrten Formation (Miocene)
- Tml - Table Mountain Latite (Miocene)
- Tvs - Valley Springs Formation (Oligocene)
- Ti - Ione Formation (Eocene)

Sources:
30 m hillshaded DEM from DFG (2002)
Geology compiled by LCI (2018) from WCC (1978) and others

N

0 5 10 mi

0 5 10 20 km

Map projection and scale: NAD 1983 UTM Zone 10N, 1:350,000

Local Fault Sources, Pardee Dam

EBMUD PARDEE DAM FAULT HAZARD STUDY

Lettis Consultants International, Inc.

Figure **5-1**

File path: S:\1772_Pardee\Figures\January Report Figures\Figure_5-1_local-sources-map.mxd; Date: 01/23/2020; User: steve, LCI; Rev.1

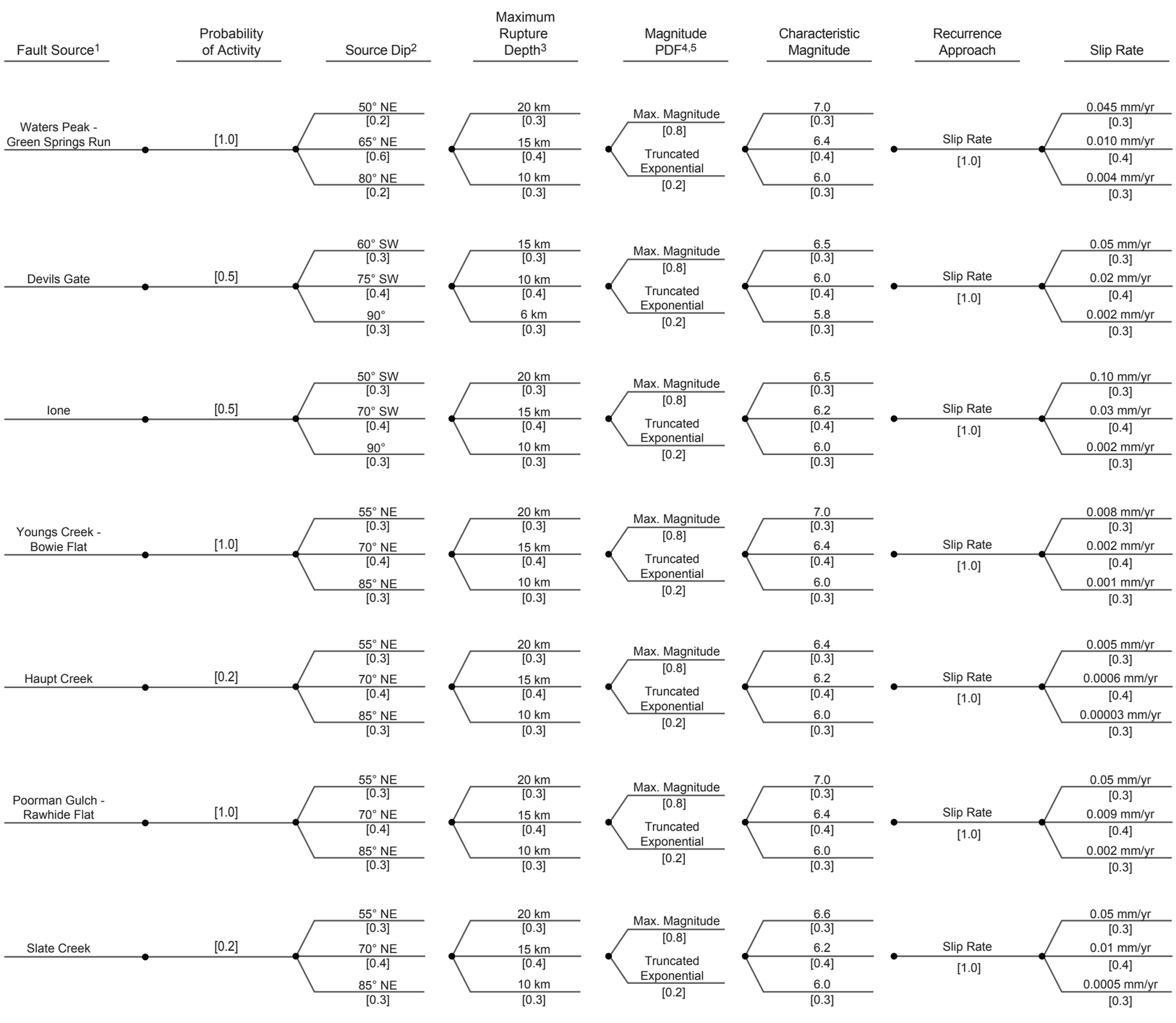

Notes:
1. Faults listed in order of distance from Pardee Dam. See Figure 5-1 for fault source locations. All sources considered to be strike-slip-normal oblique faults, with sub-equal components of strike-slip and dip-slip movement.
2. Source dip represents average dip through the seismogenic crust.
3. Top of rupture for all sources is 0 km; the maximum rupture depths are equal to maximum rupture thicknesses.
4. Maximum Magnitude model has a fixed standard deviation of 0.12 and an upper magnitude truncation of 2 standard deviations (maximum magnitude = characteristic magnitude + 0.24 magnitude units).
5. Tuncated Exponential model has a fixed *b* value of 0.8 and a maximum magnitude = characteristic magnitude + 0.5 magnitude units (a fixed offset)

Source Characterization Logic Tree for Local Pardee Dam Fault Sources

EBMUD PARDEE DAM FAULT HAZARD STUDY

LCI Lettis Consultants International, Inc. | Figure **5-2**

EXPLANATION

- - - - - Devils Gate fault

N

0 500 1,000 Feet

0 100 200 400 Meters

Map projection and scale: NAD 1983 UTM Zone 10N, 1:10,000

Note:
-Indicated scarp measurement (X m) represents interpreted vertical displacement of geomorphic surface rather than true scarp height.

Sources:
• 1 m hillshaded DEM from Calaveras County LiDAR data.
• Imagery from ESRI.

Geomorphic Evidence Suggestive of Late Quaternary Fault Activity from LiDAR and Orthophoto Data, Devils Gate Fault

EBMUD PARDEE DAM FAULT HAZARD STUDY

Lettis Consultants International, Inc.

Figure **5-3**

File path: S:\1772_Pardee\Figures\January Report Figures\Figure_5-3_DevilsGateLidar.mxd; Date: 01/29/2020; User: Brian, LCI; Rev.1

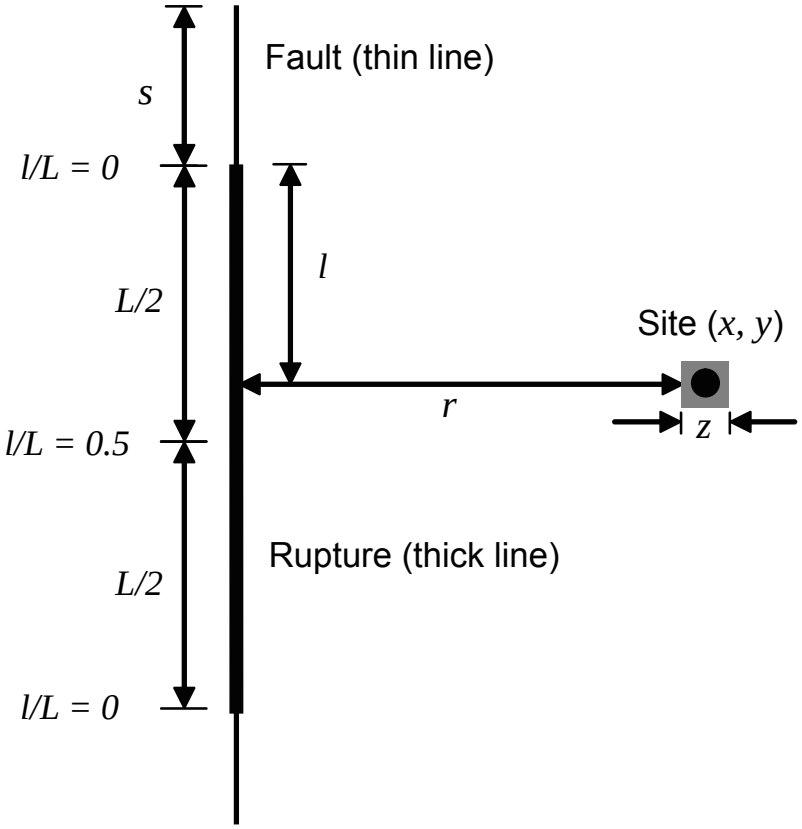

Variables used in the fault-displacement hazard analysis:

x,y	Site coordinates (center point)
z	Dimension of the site area considered for probability of fault rupture
r	Distance from the site to the mapped fault trace
l	Distance from the nearest point on the rupture to the closest end of the rupture
L	Total rupture length
s	Distance from the end of the rupture to the end of the fault

Definition of PFDHA Variables, Earthquake Magnitude Approach (After Petersen et al., 2011)

EBMUD PARDEE DAM FAULT HAZARD STUDY

Lettis Consultants International, Inc. | Figure **6-1**

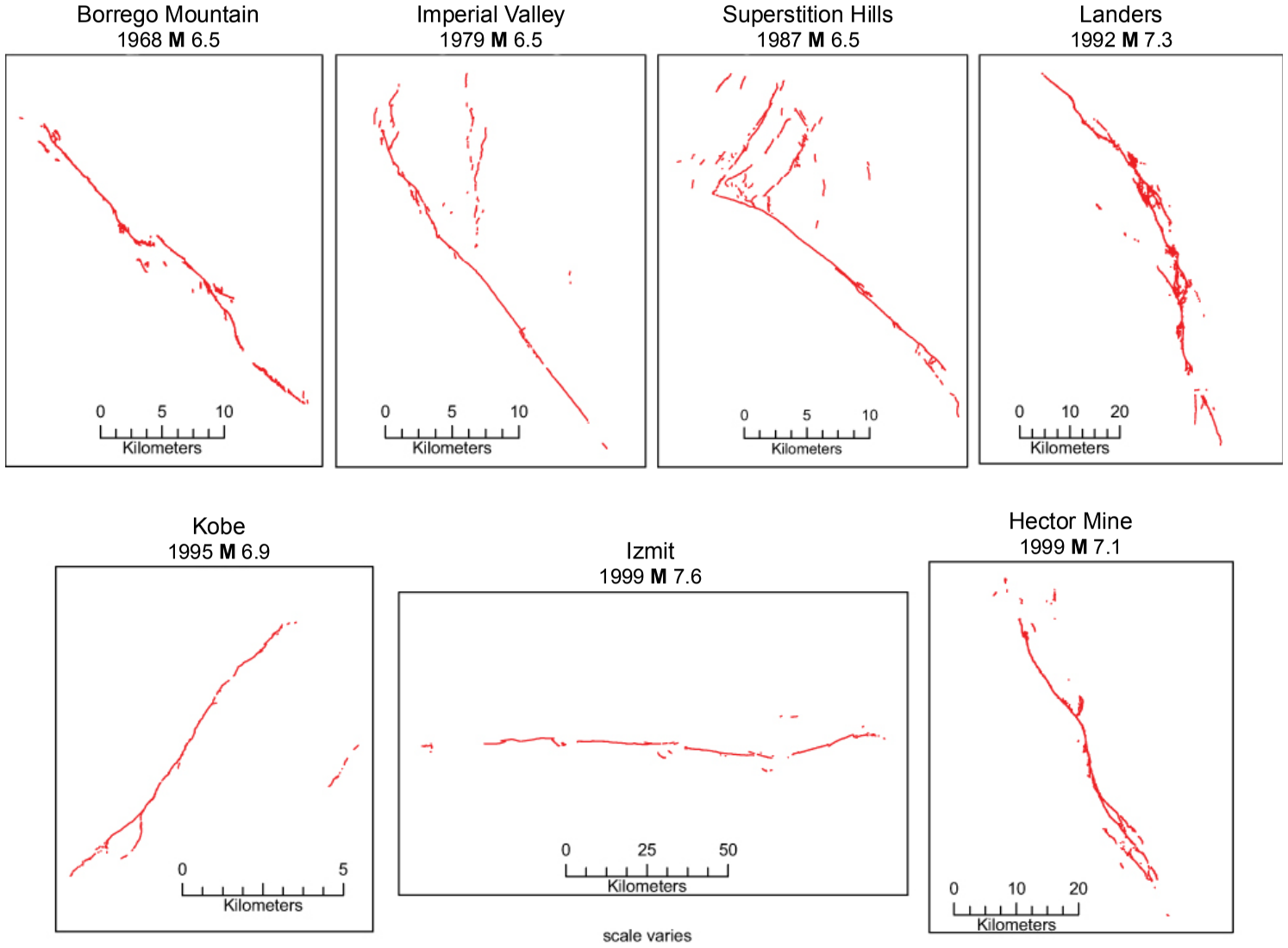

Note: From Figure S1 of Petersen et al. (2011)

Examples of Historic Strike-Slip Surface Ruptures (After Petersen et al., 2011)

EBMUD PARDEE DAM FAULT HAZARD STUDY

Lettis Consultants International, Inc. | Figure **6-2**

File path: S:\1772-Pardee\Figures\Figure_6-2.ai; Date: 1/22/2020; User:Steve T., LCI

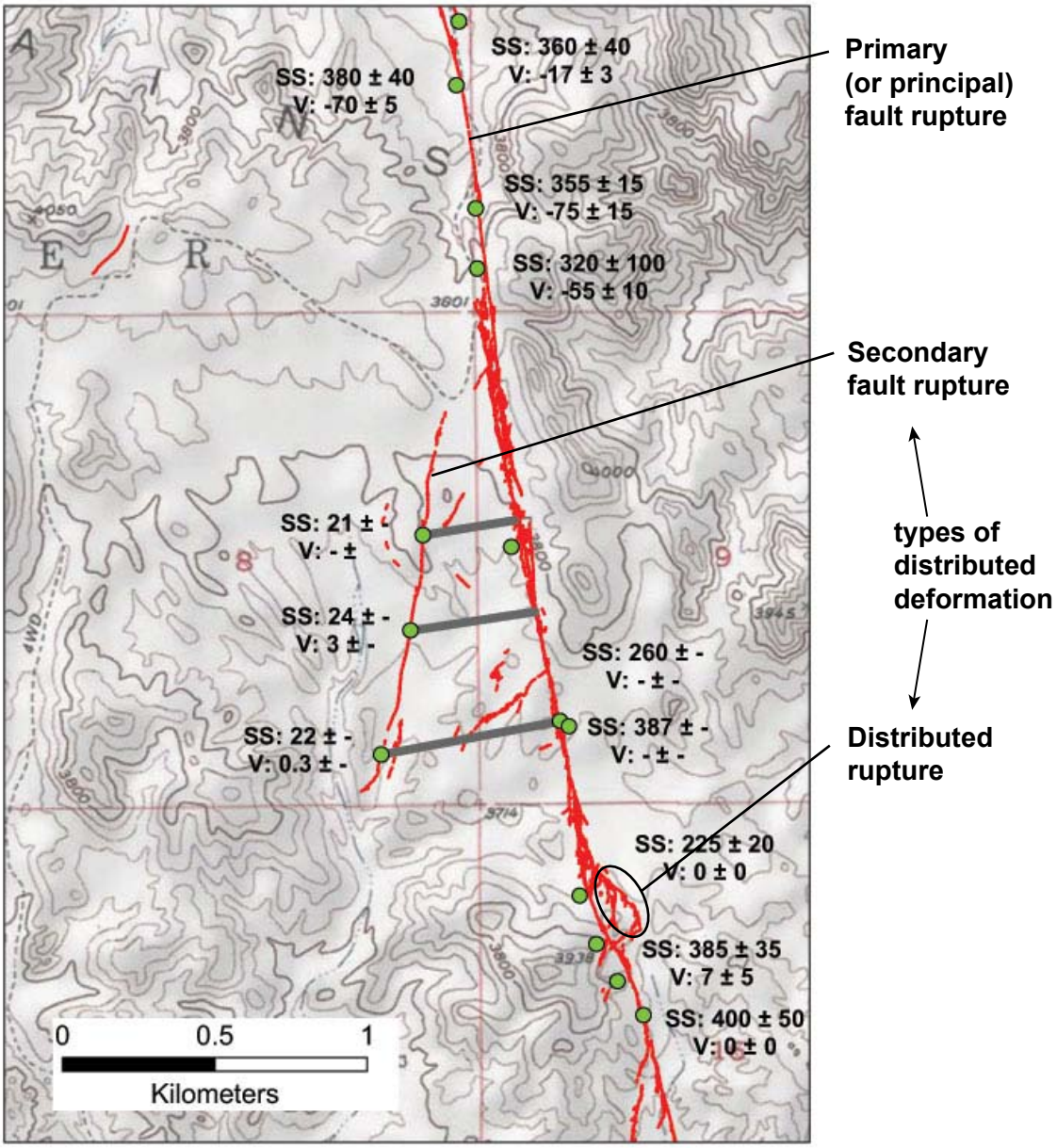

EXPLANATION

SS: Lateral component of slip in centimeters

V: Vertical component of slip in centimeters

Slip measurements

Distance from secondary rupture to primary rupture

Note: From Figure S2 of Petersen et al. (2011)

Example of Primary, Secondary, and Distributed Fault Rupture, Hector Mine Earthquake (After Petersen et al., 2011)

EBMUD PARDEE DAM FAULT HAZARD STUDY

Lettis Consultants International, Inc.

Figure **6-3**

File path: S:\1772-Pardee\Figures\Figure_6-3.ai; Date: 1/22/2020; User:Steve T., LCI

EXPLANATION

Waters Peak fault

Hazard location (approximate center point of Pardee Dam foundation)

N W E S

0 200 400 ft

0 50 100 m

Map projection and scale: NAD 1983 UTM Zone 10N, 1:3,000

Center Point For Calculating Displacement Hazard to Pardee Dam Relative to the Waters Peak Fault Source

EBMUD PARDEE DAM FAULT HAZARD STUDY

Lettis Consultants International, Inc. | Figure **6-4**

File path: S:\1772_Pardee\Figures\January Report Figures\Figure_6-4.mxd; Date: 01/21/2020; User: steve, LCI; Rev.1

EXPLANATION

Fault Source in PFDHA

Hazard location (approximate center point of Pardee Dam foundation)

N W E S

0 2,000 4,000 ft

0 500 1,000 m

Map projection and scale: NAD 1983 UTM Zone 10N, 1:24,000

Source:
• Imagery from ESRI.

Hazard Calculation Cell Center Point Relative to Waters Peak, Devils Gate, and Ione Fault Sources

EBMUD PARDEE DAM FAULT HAZARD STUDY

Lettis Consultants International, Inc.

Figure **6-5**

File path: S:\1772_Pardee\Figures\January Report Figures\Figure_6-5.mxd; Date: 01/21/2020; User: steve, LCI; Rev.1

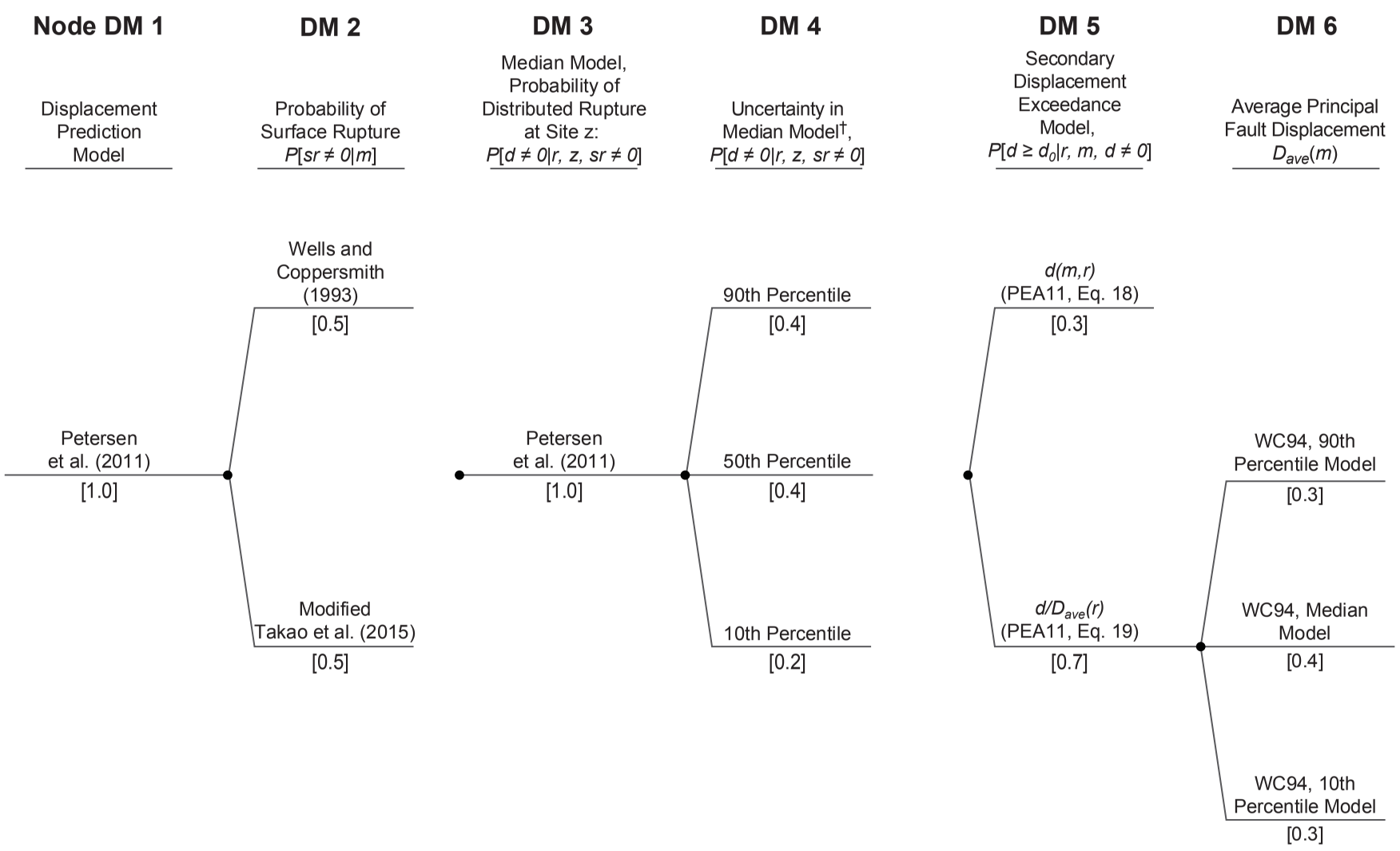

† Values based on PEA11 data. See Table 6-3.

Abbreviations:
- PEA11 = Petersen et al. (2011)
- WC94 = Wells and Coppersmith (1994)

Displacement Prediction Model Logic Tree

EBMUD PARDEE DAM FAULT HAZARD STUDY

LCI Lettis Consultants International, Inc. | Figure **6-6**

(a) Total Hazard Curves (Centimeters)

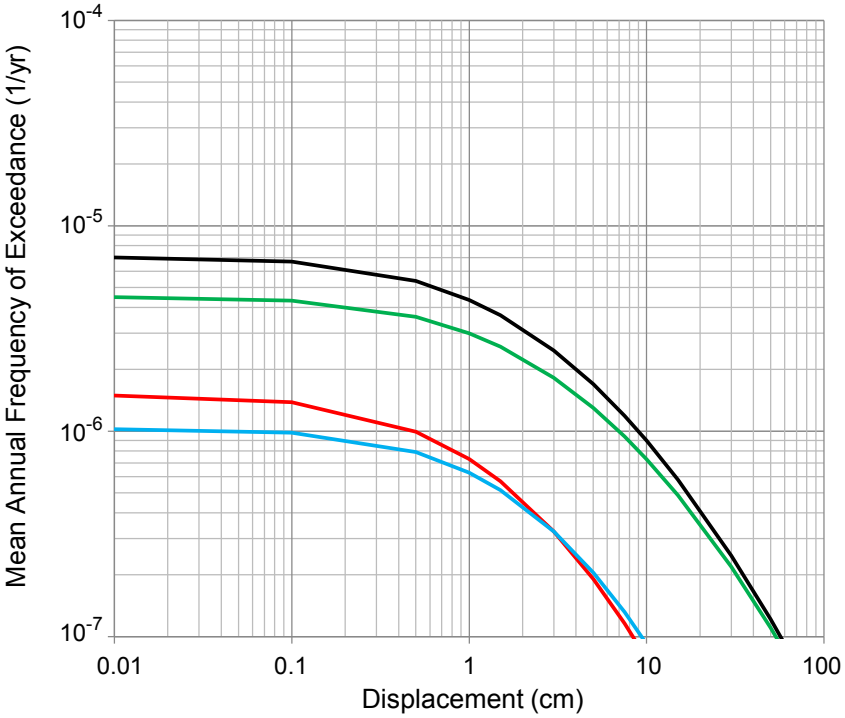

(b) Total Hazard Curves (Inches)

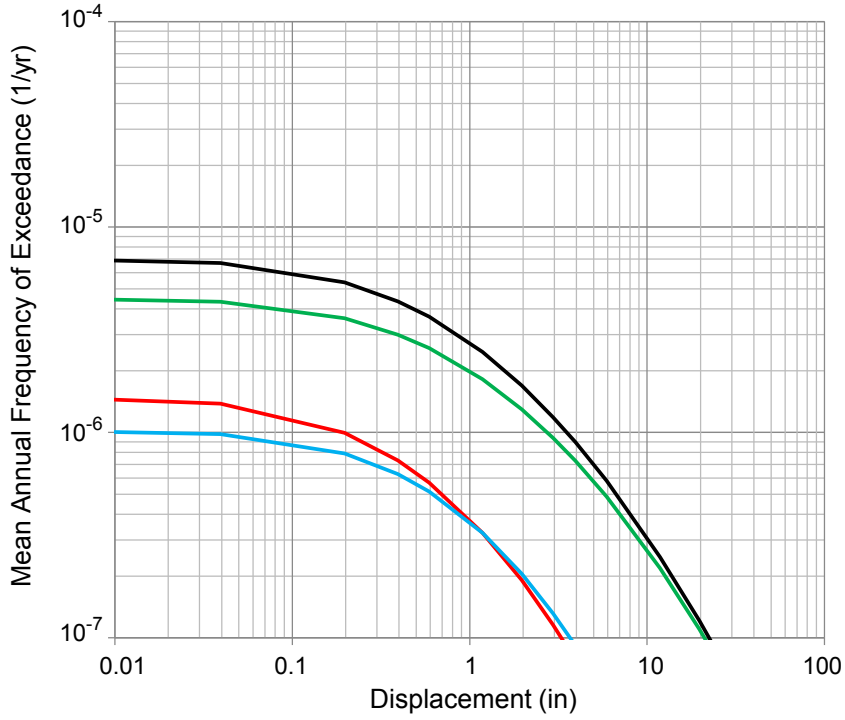

EXPLANATION

- Total Hazard
- Individual Source Contributions:
- Waters Peak - Green Springs Run
- Devils Gate
- Ione

Total Displacement Hazard Curves for Pardee Dam and Contribution by Fault Source (a) Centimeters and (b) Inches

EBMUD PARDEE DAM FAULT HAZARD STUDY

Lettis Consultants International

Figure **6-7**

File path: S:\1772_Pardee\Figures\January Report Figures\Figure_6-7.ai; Date: 01/21/2020; User:Jch., LCI

(a) Mean and Fractile Hazard (Centimeters)

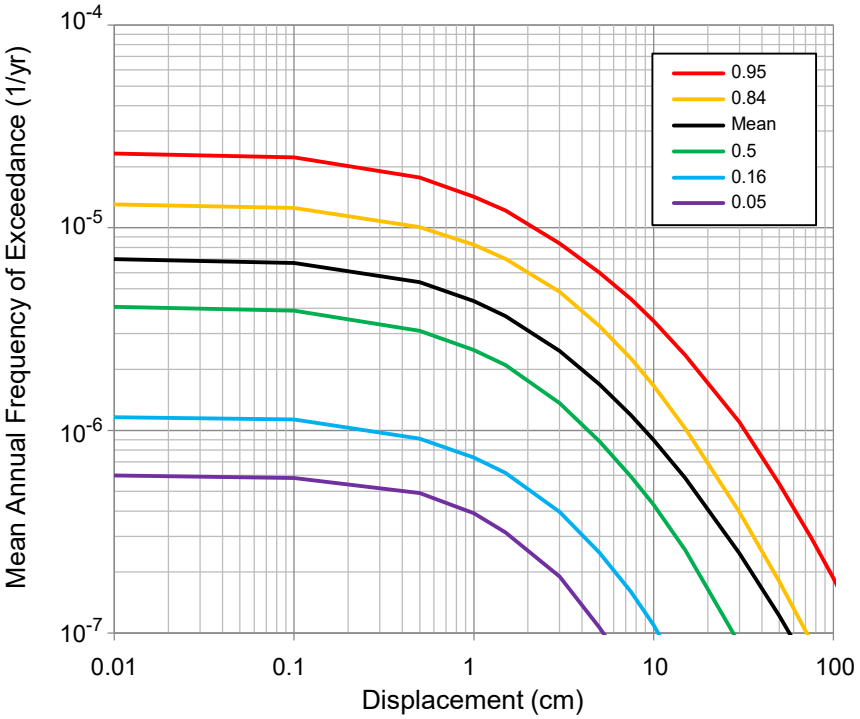

(b) Hazard Sensitivity, Probability of Activity (Centimeters)

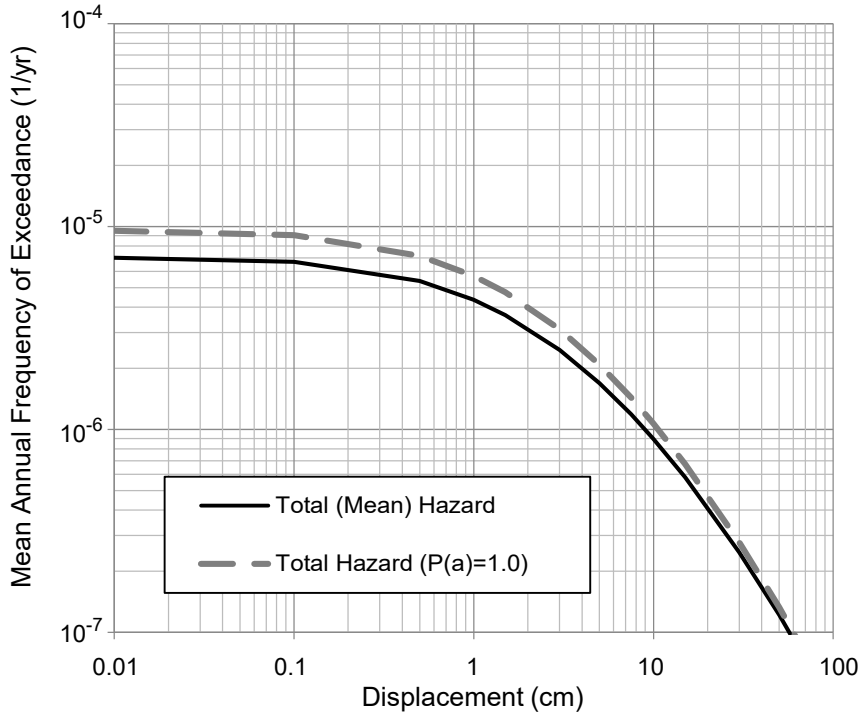

EXPLANATION

- Total (Mean) Hazard
- Hazard Fractile, Percentile Indicated on Plot
- Conditional Hazard, P(a) = 1 for All Sources

Notes:
- Figures 6-4 and 6-5 show location of 50 m cell relative to fault sources

Fractile Hazard and Hazard Sensitivity Curves: (a) Mean and Hazard Fractiles, (b) Sensitivity for Probability of Activity

EBMUD PARDEE DAM FAULT HAZARD STUDY

Lettis Consultants International

Figure **6-8**

(a) Hazard Sensitivity, Slip Rate

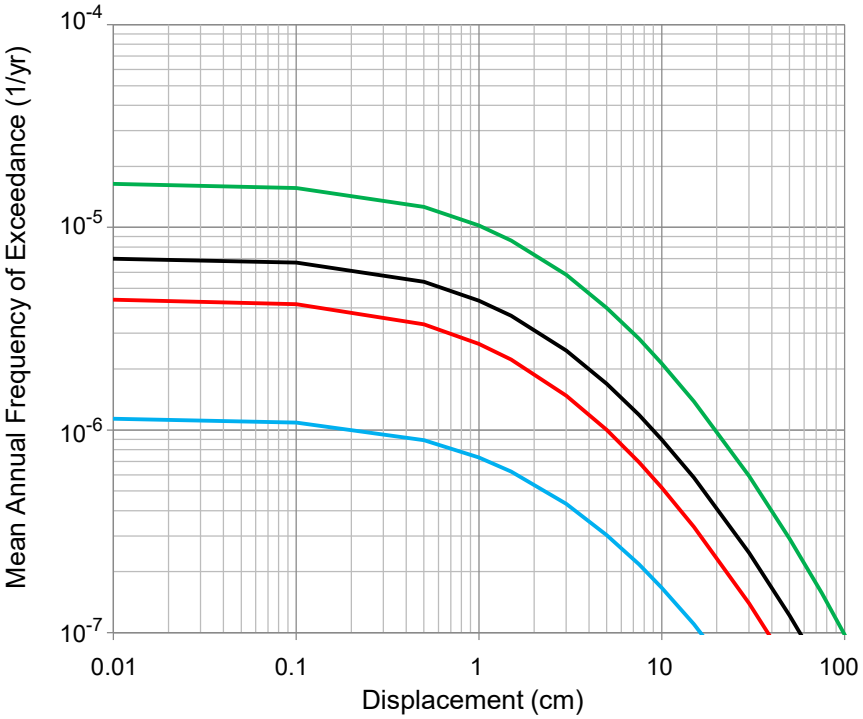

(b) Hazard Sensitivity, Characteristic Magnitude (All Sources)

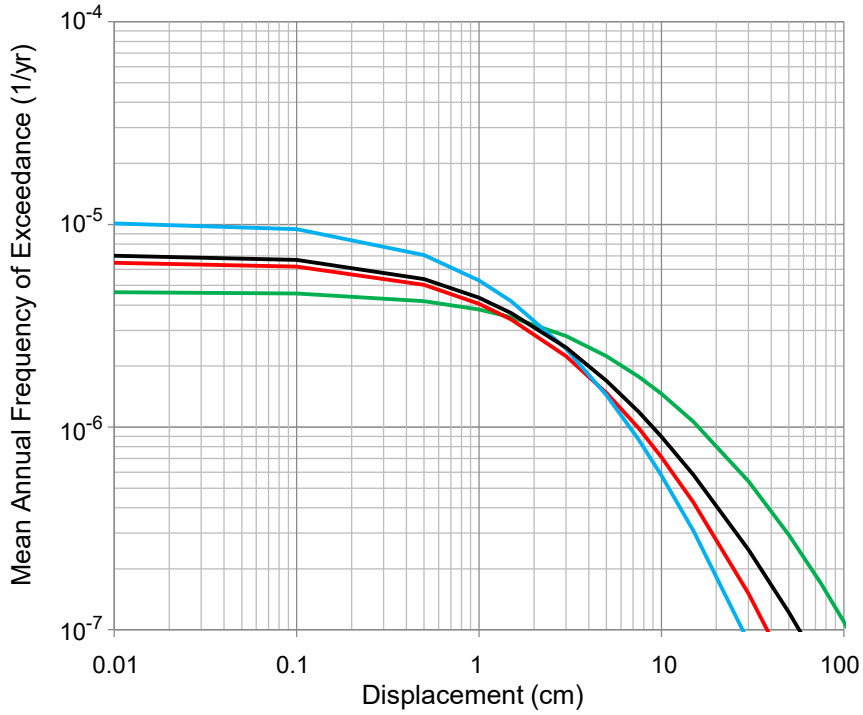

EXPLANATION

- Total (Mean) Hazard
- Conditional Hazard:
  - High logic-tree branch value
  - Middle logic-tree branch value
  - Low logic-tree branch value

Notes:
- Figure 5-2 shows fault source characterization logic-tree branch values for Waters Peak - Green Springs Run, Devils Gate, and Ione fault sources

Hazard Sensitivity Curves, Fault Source Characterization: (a) Slip Rate, (b) Characteristic Magnitude

EBMUD PARDEE DAM FAULT HAZARD STUDY

Lettis Consultants International

Figure **6-9**

(a) Hazard Sensitivity, Conditional Probability of Distributed (Secondary) Deformation

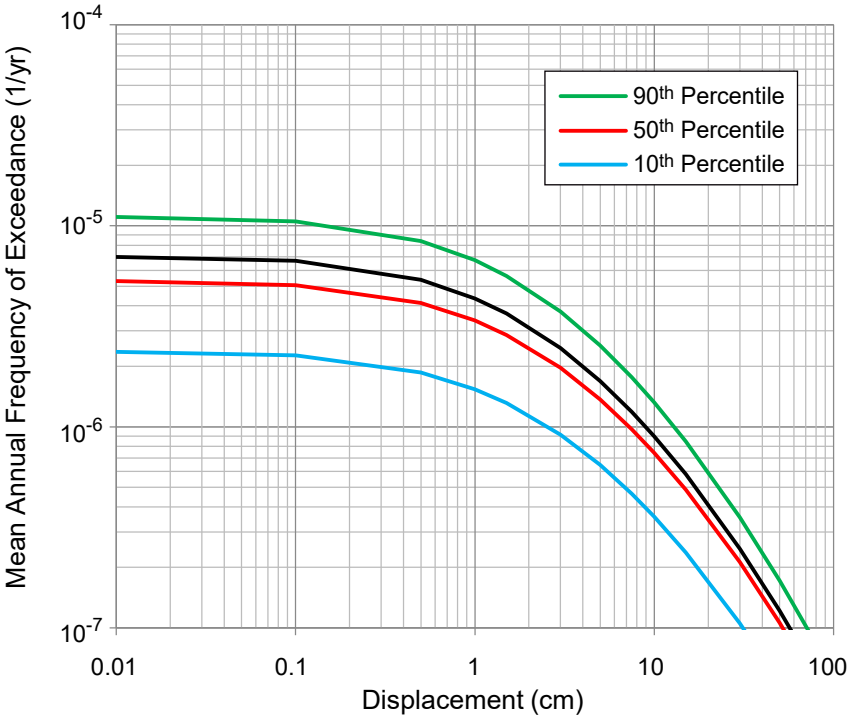

(b) Hazard Sensitivity, Distributed (Secondary) Displacement Exceedance Equation

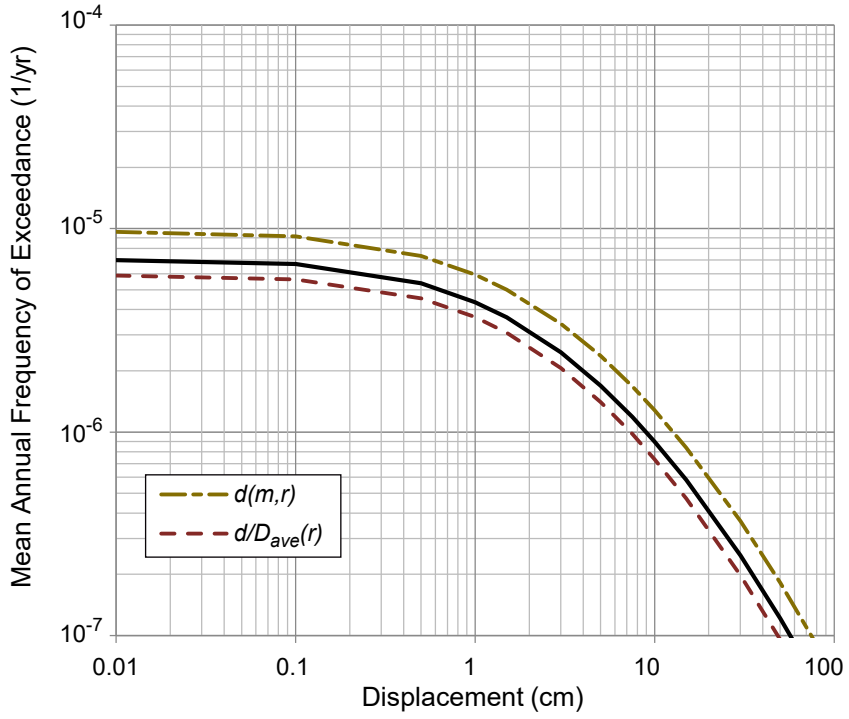

EXPLANATION

- Total (Mean) Hazard
- Conditional Hazard:
  - High logic-tree branch value
  - Middle logic-tree branch value
  - Low logic-tree branch value

Notes:
- Figure 6-6 shows fault displacement model logic-tree branch values used for Waters Peak - Green Springs Run, Devils Gate, and Ione fault sources

Hazard Sensitivity Curves, Fault Displacement Model Logic Tree: (a) Conditional Probability of Secondary Displacement, (b) Secondary Displacement Exceedance Equation

EBMUD PARDEE DAM FAULT HAZARD STUDY

Lettis Consultants International

Figure **6-10**

File path: S:\1772_Pardee\Figures\January Report Figures\Figure_6-10.ai; Date: 01/21/2020; User: Jch., LCI

Plates

Trench LCI-T1 South Wall

Uninterpreted

Trench LCI-T1 South Wall

Interpreted

View to northwest from the east-facing topographic high. Trench LCI-T1 is in the middle part of photograph.

View is to the west-southwest of trench LCI-T1.

UNITS DESCRIPTION

800 — Unit 800: sandy silt with gravel, yellow brown (10YR 6/4) to reddish yellow (7.5YR 6/6); silt 60-70%, <10% clay, <10% sand, <10% clasts, few large clasts; massive; weak to slightly tough and soft; friable, non-plastic, non to slightly cohesiveness; granular to platy soil texture, weak angular blocky to platy peds; abundant fine to medium rootlets and roots; basal contact is irregular and clear to sharp (modern Ap with duripan – **Holocene Colluvium [Keystone/Sonora])**.

700 — Unit 700: sandy silt with gravel, yellowish brown (10YR 6/4), reddish brown (5YR5/4) to yellowish red (5YR5/6); 60-80% silt; <10% clay; <10% fine to medium-grained sand; 10% gravel; clasts of 2-4 cm common and up to 10 cm in length; common slate clasts with few quartzite gravel; poorly sorted; non-plastic, medium dry strength, slightly cohesive to friable; common rootlets and filaments; common bioturbation and soil mixing; silt coatings on peds and clasts; discontinuous basal stone line; basal contact sharp **(Late Pleistocene to Holocene [Sonora/Upper Modesto])**.

600 — Unit 600: clayey silt with sand and fine gravel, very dark grayish brown (10YR3/2) to brown (7.5YR5/2); 60% silt; 10-20% fine-to coarse-grained sand, 15-20% fine gravel; clasts typically 1-2 cm and up to 5 cm, subangular to tablular, moderately weathered, moderately sorted, few rounded quartzite clasts; majority clasts are slate; massive; high dry strength, slightly to moderately plastic, moderately cohesive, hard; very few small pores, very few rootlets; basal contact diffuse over 10-20 cm, planar to wavy; strong Bt-horizon with subangular to blocky peds developed in alluvium **(Late Pleistocene Colluvium with Aeolian [Lower Modesto])**.

500 — Unit 500: sandy silt with gravel and clay, brown (7.5 YR 5/4 to 4/4) to dark yellow brown (10YR 4/4) with 10% clay, 20% very fine-to coarse-grained sand, and 10-15% fine gravel; clasts of 1-2 cm common and up to a few of 15 cm in length; gravel subangular to angular, few subrounded, clasts moderately weathered, moderately to poorly sorted, few subangular quartzite clasts with common slate; gravel forms discontinuous basal stone line; massive; moderately hard; moderately to slightly plastic; moderately cohesive; very high dry strength; high toughness; roots up to 5 cm, few small pores, small subangular blocky peds with some clay coatings; wavy to irregular, clear basal contact **(Late Pleistocene Colluvium to Alluvium [Lower Modesto/Riverbank])**.

100 — Unit 100: Slate, aphanitic, greenish gray (10Y 5/1; Gley 1) to grayish brown (2.5Y 5/2) to very dark greenish gray when fresh (10Y 3/1; Gley 1), moderately weathered to slightly weathered, intensely fractured along foliation, weakly to moderately foliated with steep to vertical NE dipping foliation, exfoliates into tabular spindles and thin blocks **(Jurassic Salt Springs slate)**.

105 — Unit 105: Slate and volcanics, brecciated and highly/completely weathered; olive gray with mottles of reddish yellow (7.5YR 6/6); grains and clasts are elongated within shear zone parallel to foliation; primarily composed of Salt Springs slate but also contains blocks of Gopher Ridge volcanics within a sheared matrix **(Fault Zone Material)**.

110 — Unit 110: Porphyritic volcanic, greenish gray (5GY 5/1, Gley 1) to light greenish gray (10Y 7/1; Gley 1) and light gray (2.5 Y 7/2), with moderately weathered medium to large phenocrysts; strongly foliated with mineral alignment parallel to foliation; moderately hard to hard, moderately to intensely weathered; moderately to intensely fractured; MnO and FeO staining along joint faces, clay infilling along joint surfaces, exfoliates into massive and occasional tabular/planar clasts **(Jurassic Gopher Ridge volcanics)**.

Note:

Refer to Table 4-3 for structural measurements noted on log.

EXPLANATION

- Trench Boundary
- Contact — *Dashed where approximate; Queried where uncertain; Dotted where concealed*
- Soil Contact
- Fault — *Dashed where approximate; Queried where uncertain; Dotted where concealed*
- Shears
- Fractures
- Clasts
- OSL Sample *(Retained for future analysis)*
- S1 Structural Measurement

Soil Profile (SP): AP/Ab, Bw, Bw2, 2Btb1, 3Btb2, R

PLATE 1

Photomosaic and Log of Trench LCI-T1 South Wall

Waters Peak Fault

Lettis Consultants International, Inc.

EBMUD PARDEE DAM
FOOTHILLS FAULTS SYSTEM STUDY

Trench LCI-T2 South Wall

Uninterpreted

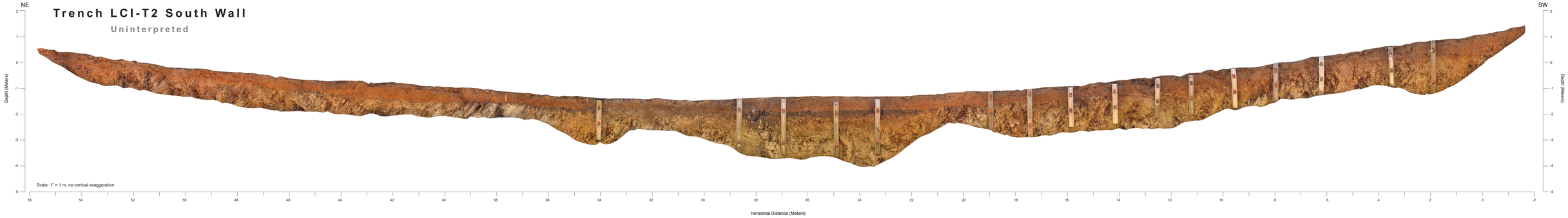

Trench LCI-T2 South Wall

Interpreted

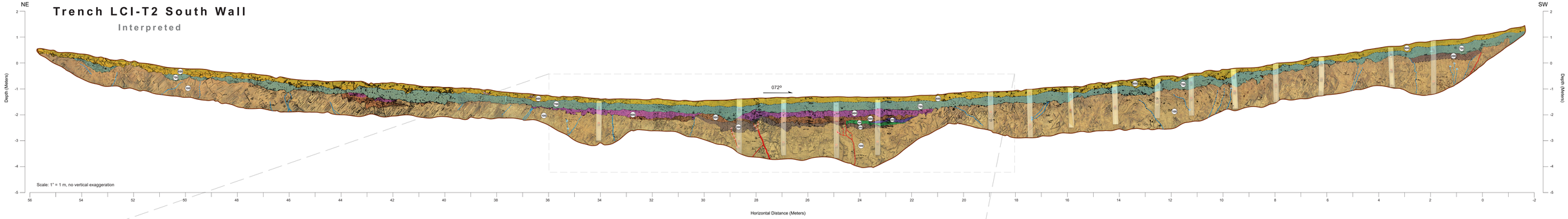

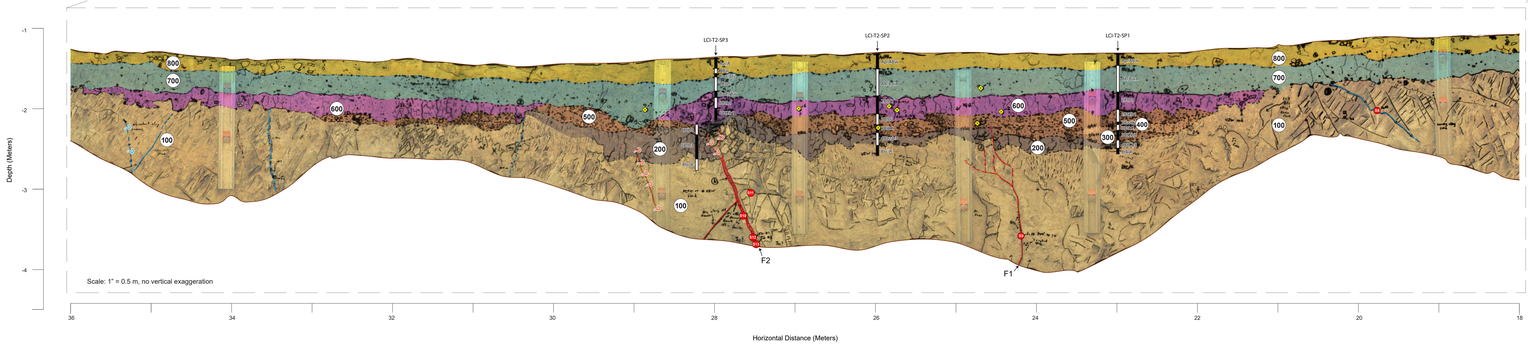

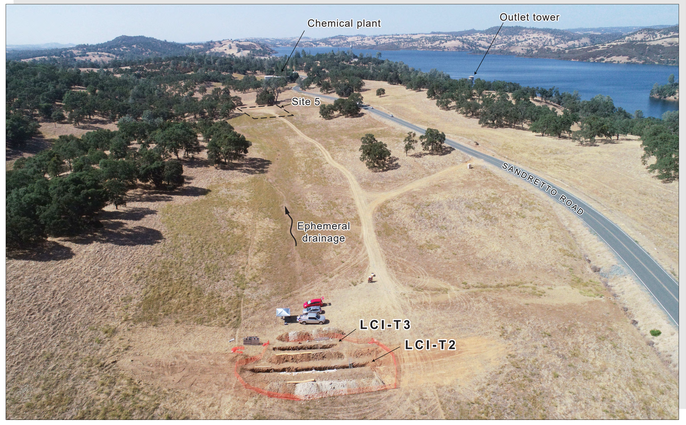

Aerial view looking northwest along the linear valley coincident with the Waters Peak fault. Photo documents partial backfilling of trench. Trench LCI-T2 formerly extended farther to northeast and southwest prior to date of photograph.

UNITS DESCRIPTION

Unit 800 : silt with sand and trace of gravel, pink (7.5 YR 7/3) to strong brown (7.5YR 5/6); 10% medium- to coarse-grained sand, 10% gravel, <5% clay; gravel is fine to pebble-sized, angular to rounded; dry strength is weak to moderate, non-plastic, peds are medium to large, abundant root filaments and pores; peds are blocky to platy; abundant bioturbation and krotovina; contact wavy to irregular, and diffuse across 5-15 cm (modern Ap with duripan – **Holocene Colluvium [Keystone/Sonora]**).

Unit 700: silt with sand and gravel, brown (7.5 YR 4/4) and weakly mottled in upper part of unit to strong brown (7.5 YR 5/6) to reddish yellow (5Y 6/8); 5% clay, 10% fine-grained sand, 10-15% fine to coarse gravel, angular to rounded, with moderately to strongly weathered clasts, trace quartzite clasts; massive; low plasticity, dry strength is weak to moderate; slightly hard to slightly cohesive; peds are small to medium-sized, weakly developed, root pores common, intensely bioturbated, abundant krotovinas, trace MnO nodules 2-3 mm thick; weak to absent clay films; planar to locally irregular basal contact, abrupt to diffuse over 5-10 cm **(Late Pleistocene to Holocene [Sonora/Upper Modesto])**.

Unit 600: clayey silt with sand and trace of gravel, very dark grayish brown (10 YR 3/2) to dark yellow brown (10YR4/4) [dark brown (7.5YR3/3) when wet]; FeO staining and mottline reddish brown (5YR4/4); 50% silt, 15-25% clay, 5-20% fine-to coarse-grained sand; gravel rare, predominantly rounded with some angular quartzite; massive; weakly to moderately plastic, hard, dense; small-to medium-sized peds, FeO-staining on ped faces; MnO nodules up to 3 mm; thin clay films; pores rare to absent; basal contact irregular to diffuse over 5-10 cm; well-developed Bt-horizon developed in deposit **(Late Pleistocene Alluvium mixed with Aeolian [Lower Modesto])**.

Unit 500: gravelly, clayey silt with sand, brown (7.5YR5/4); 40% silt, 20% clay; 30% fine to coarse gravel (up to cobble-sized); 10% medium to very coarse-grained sand; weak normally graded to slight fining upward; clasts consist of quartzite, andesite, slate (derived from Mehrten Fm to south); FeO and MnO staining of clasts; clay coatings are discontinuous to continuous on clasts; slightly to moderately plastic, slightly to moderately cohesive; hard, stiff, dense; few small pores and few small roots; fine subangular blocky peds with well-developed clay coatings and clay bridges; basal contact planar and inclined to east well developed Bt horizon developed in deposit **(Late Pleistocene Alluvium [Riverbank])**.

Unit 400: sandy clayey silt to sandy silty clay with gravel, yellowish red (5YR4/6) to brown (7.5YR5/4); 35% silt; 35% clay; 25% fine-to coarse-grained sand; 5% fine gravel; fines upward; clasts of varied composition (including from Mehrten Fm to south) are weathered to slightly weathered; dense, very hard, slightly cohesive, slightly plastic, no dilatancy; few to no roots; very few pores; clay films coat subangular blocky peds and clasts, continuous; abundant cutans and vertical desiccation cracks; soil contact is wavy and diffuse and gently inclined to east; soil developed within fluvial overbank deposits **(Late Pleistocene Alluvium [Riverbank])**.

Unit 300: sandy clayey gravel, brown (7.5YR5/4); 40% gravel; 30% clay; 20% silt; and 20% sand; clasts are of variable composition (derived from Mehrten Fm to south); very hard, dense, slightly plastic, slightly cohesive; subangular blocky peds with continuous clay coatings; FeO and MnO staining common; highly weathered clasts; roots and pores absent; desiccation cracks along clasts margins; clear basal contact **(Late Pleistocene Alluvium [Riverbank])**.

Unit 200: silty gravely clay, yellow brown (10YR5/4); 70% clay, 10% silt; 20% fine to medium gravel with sand matrix; clasts predominantly composed of weathered slate with some rare quartzite; cohesive; plastic to fat clay; prismatic peds with soil cutans (slickensides) on surfaces; clasts coated in clay films; MnO staining; roots and pores absent; desiccation cracks wide, open, and widely-spaced; saprolite developed in bedrock **(Pedogenic clay an Saprolite [Pre-Riverbank])**.

Volcanic sandstone to slate; grayish brown (2.5Y 5/2) to yellowish brown (10YR 5/4); weakly to strongly foliated, fine-to medium-grained sand with trace of quartzite clasts; grains are weakly elongated parallel to foliation; structure is blocky, moderately to intensely weathered, FeO staining on joint surfaces **(Jurassic Salt Springs slate [Metasandstone facies]).

Notes:
1. Refer to Table 4-3 for structural measurements noted on log.
2. Undrafted logs from the south wall of the this trench are presented in Appendix A.
3. Log of fault F2 represents the preferred (model 1) interpretation of faulting.

EXPLANATION

- Trench Boundary
- Contact (*Dashed where approximate; Queried where uncertain; Dotted where concealed*)
- Soil Contact
- Fault (*Dashed where approximate; Queried where uncertain Dotted where concealed*)
- Shears
- Fractures
- Clasts
- OSL Sample (*Retained for future analysis*)
- Structural Measurement

Soil Profile (SP)

↓	
47ka	
Bw	
Bw2	
28ka	
Bt1	
38ka	
R	

PLATE 2
Photomosaic and Log of Trench LCI-T2 South Wall
Waters Peak Fault

Lettis Consultants International, Inc.

EBMUD PARDEE DAM
FOOTHILLS FAULTS SYSTEM STUDY

Trench LCI-T3 South Wall

Uninterpreted

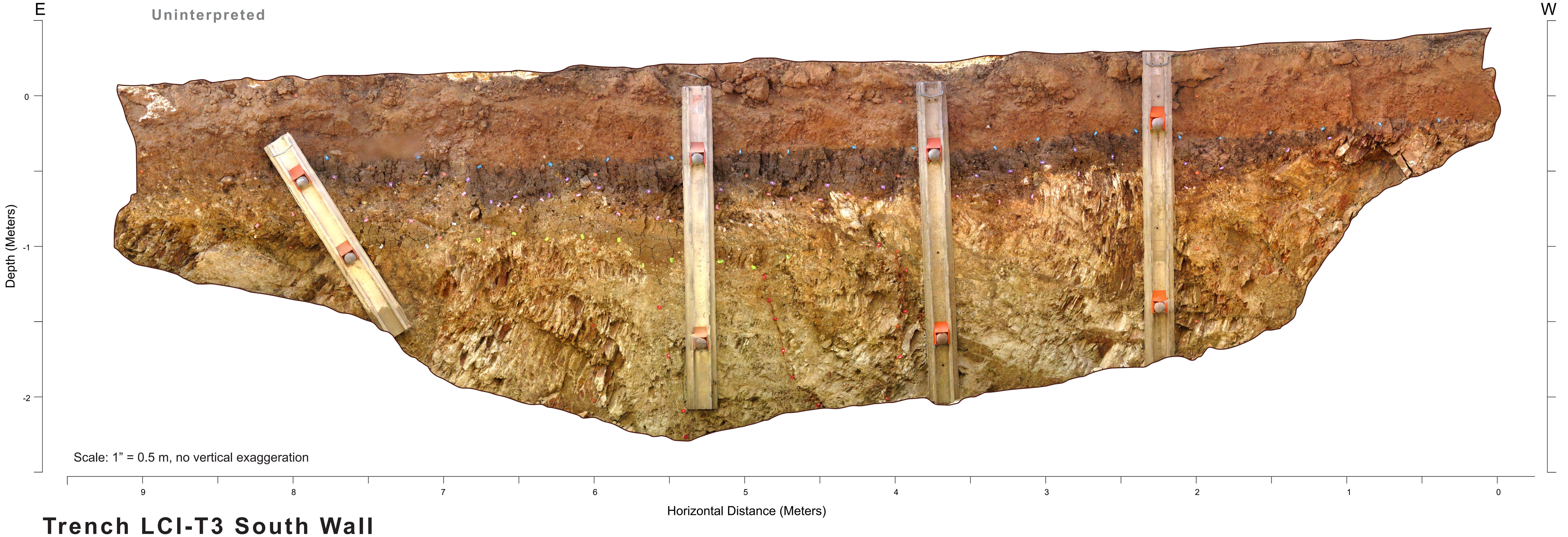

Trench LCI-T3 South Wall

Interpreted

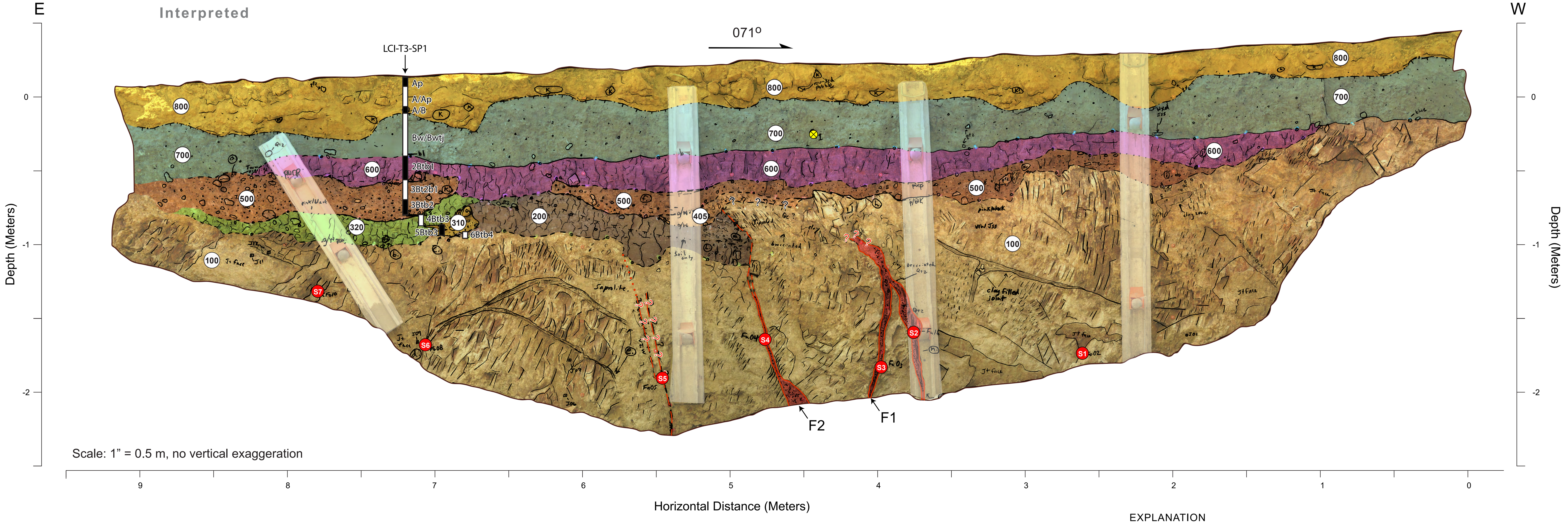

Note:
Refer to Table 4-3 for structural measurements noted on log.

UNITS DESCRIPTION

800 — Unit 800: silt with sand and trace of gravel, pink (7.5 YR 7/3) to strong brown (7.5YR 5/6): <5% clay, 10% fine-to coarse-grained sand, 10% gravel; clasts fine-to pebble-sized, angular to rounded; dry strength weak to moderate, non-plastic, soil peds are medium to large blocky to platey; abundant root filaments and pores; abundant bioturbation and krotovinas; basal contact wavy to irregular, and diffuse over 5-15 cm; upper part of deposits consists of an agricultural hard-pan (modern Ap with duripan – **Holocene Colluvium [Keystone/Sonora]**).

700 — Unit 700: silt with sand and gravel, brown (7.5 YR 4/4); weakly mottled in upper part of unit to strong brown (7.5 YR 5/6) to reddish yellow (5Y 6/8); 5% clay, 10% fine-grained sand, 10-15% fine to coarse gravel; clasts are angular to rounded and moderately to strongly weathered, trace quartzite clasts; massive; low plasticity, dry strength is weak to moderate; slightly hard to slightly cohesive; soil pads are small to medium, weakly developed; root pores common; intensely bioturbated and abundant krotovinas; trace MnO nodules up to 2-3 mm thick; weak to absent clay films; planar to locally irregular basal contact that is abrupt to diffuse over 5-10 cm **(Late Pleistocene to Holocene [Sonora/Upper Modesto])**.

600 — Unit 600: clayey silt with sand and gravel, very dark gray (10YR 3/1); 20% clay; 15-20% fine-to medium-grained sand; 15% fine to coarse, fine to pebble-sized gravel; clasts are angular to subrounded, and consist of slate and quartzite; generally massive; low to medium plasticity, very stiff to hard, dry strength medium to high; medium-sized blocky soil peds with few thin clay films; some to many rootlets, few small pores; 1-2 mm sized MnO nodules; basal contact is wavy and diffuse over 4-6 cm **(Late Pleistocene Alluvium mixed with Aeolian [Lower Modesto])**.

500 — Unit 500: gravelly and sandy silt with clay, brown (10YR 4/3); 15-20% fine-to coarse-grained sand, 15% clay 20-30% fine to very coarse gravel; rare small cobbles of angular to subangular slate and metasandstone, some quartzite as large as coarse gravel; massive yet fines upward and poorly sorted; low to medium plasticity, very stiff to hard, high dry strength; few dessication cracks; some clasts have thin clay films; rare rootlets and rare small pores; basal boundary is wavy to irregular, and diffuse over 2-3 cm where overlies bedrock and abrupt where overlies saprolite **(Late Pleistocene Alluvium [Riverbank])**.

405 — Unit 405: gravelly and sandy silt, brown (10YR 6/3); <15% fine to coarse-grained sand, <10% clay, 30% fine to very coarse gravel; clasts consist primarily of slate and metasandstone, angular to subangular with abundant FeO and Mno staining; low to medium plasticity, high dry strength, stiff to very stiff, soil peds of fine to medium blocky; some clay films on clasts; abundant FeO and Mno staining along fractures; many rootlets and many small pores; bedrock-derived colluvial clasts oriented subhorizontal or rotated approximately 20 degrees from horizontal; basal contact is wavy, and abrupt to diffuse **(Late Pleistocene Colluvium [Riverbank]**).

320 — Unit 320: sandy clay with gravel, yellowish brown (10YR 5/4); 10-20% fine-to medium-grained sand with trace of coarse-grained sand; 15% silt and clay; 10% fine to very coarse gravel (up to 50 cm in diam) with majority < 10 cm; clasts are subrounded to subganular, some of quartzite, but most common is slate; low to medium plasticity, stiff to medium stiff, high dry strength; fine-to medium-sized blocky peds; rare small pores, some rootlets, basal boundary is wavy and diffuse over 3-5 cm; clay films on most clasts and ped faces **(Late Pleistocene Alluvium [Riverbank])**.

310 — Unit 310: sandy silt with gravel, yellowish brown (10YR 5/4); 30% fine to coarse-grained sand with most fine to very fine-grained sand, <5-10% clay, 20% fine to coarse gravel up to 0.6 m in length; clasts are rounded to subangular, moderately weathered, lithics of slate, metasandstone and quartzite; MnO nodules present; low plasticity, low to medium dry strength; soil ped faces along clast boundaries and lined with clay films, clay films coat many clasts; basal contact is wavy to diffuse over 1 to 4 cm **(Late Pleistocene Alluvium [Riverbank])**.

200 — Unit 200: gravelly clay with silt, yellowish brown (10YR 5/4) to brown (7.5YR4/3); ; 5-10% fine-grained sand; 10% fine to coarse gravel in upper part of unit and 20% in lower part of unit; clasts are angular to subrounded with some quartzite; low to medium plasticity; medium stiff to stiff; high dry strength; clasts have thin clay films, fine to coarse blocky peds; rare rootlets and rare small pores; basal boundary is wavy to diffuse up to 7 cm; saprolite developed in bedrock **(Saprolite [Riverbank/Turlock Lake])**

100 — Unit 100: slate to fine-grained metasandstone, light greenish gray (Gley 1 7/10); dry fine-grained and aphanitic ground mass; moderately to highly weathered; strong to medium strong, intensely to very highly weathered; very intensely to moderately fractured; primarily fractured along foliation; abundant FeO and MnO staining along joint faces; thin 1 mm-thick clay films along some joint faces **(Mesozoic Salt Springs slate)**

Aerial view of trenches LCI-T2 and LCI-T3 looking west southwest.

EXPLANATION

- Trench Boundary
- Contact — *Dashed where approximate; Queried where uncertain; Dotted where concealed*
- Soil Contact
- Fault — *Dashed where approximate; Queried where uncertain; Dotted where concealed*
- Shears
- Fractures
- Clasts
- OSL Sample — *(Retained for future analysis)*
- S1 Structural Measurement

Soil Profile (SP)

AP/Ab
Bw
Bw2
2Btb1
3Btb2
R

PLATE 3
Photomosaic and Log of Trench LCI-T3 South Wall
Waters Peak Fault

Lettis Consultants International, Inc.

EBMUD PARDEE DAM
FOOTHILLS FAULTS SYSTEM STUDY

File path:S:\1772_Pardee\Agis\Illustrator\T_3_S_1inch_0.5m.ai; Date: 11/20/2019; User: JCh, LCI.

Appendix A

Undrafted Logs of LCI Paleoseismic Trenches

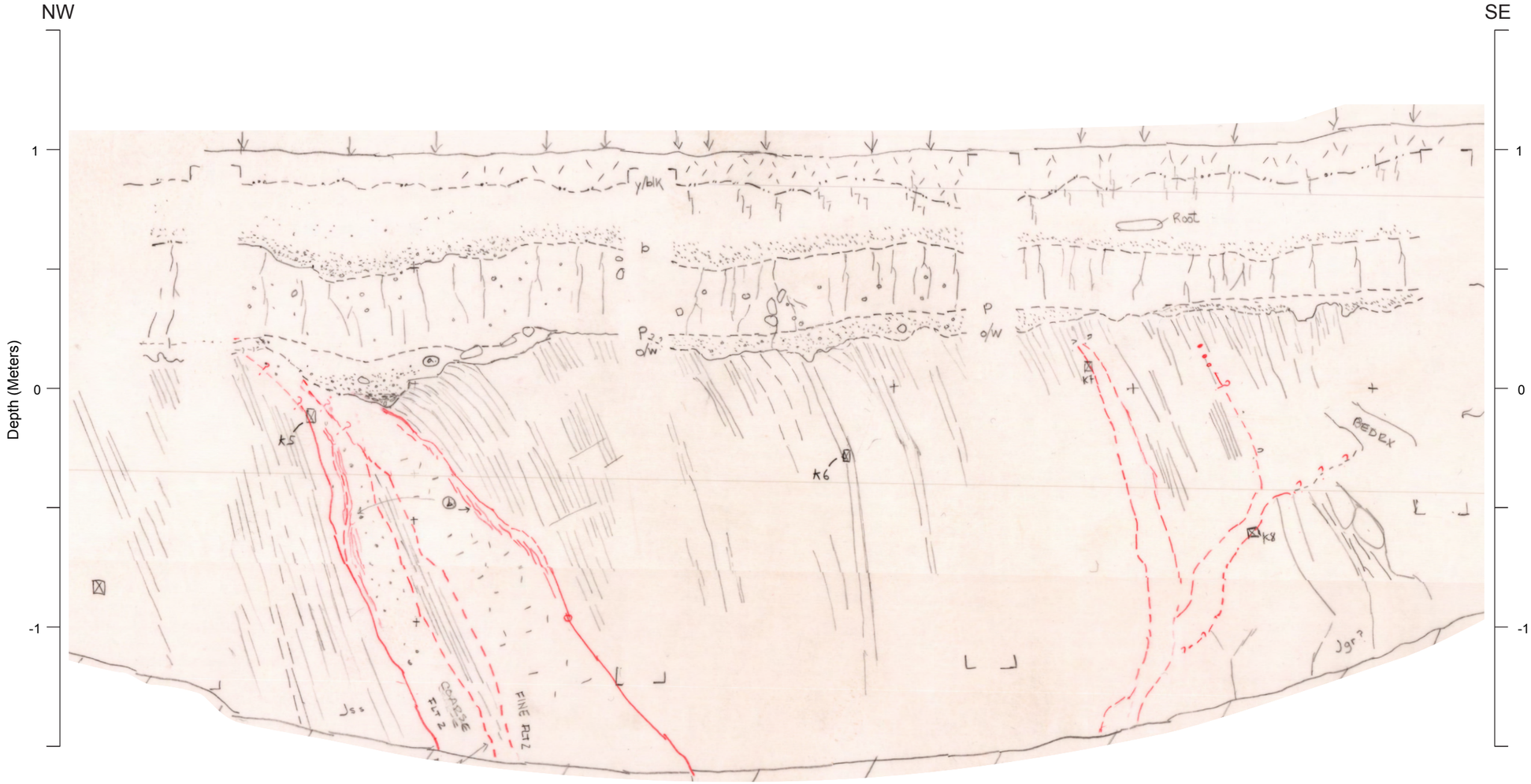

Scale: 1” = 0.5 m, no vertical exaggeration

9 10 11 12 13 14

Horizontal Distance (Meters)

Field Log of Trench LCI-T1
North Wall

EBMUD PARDEE DAM FAULT HAZARD STUDY

Lettis Consultants International, Inc. | Figure **A-1**

File path: S:\1772_Pardee\Figures\November Report Figures\Fig_A_1_Trench_T1_N_maylar.ai; Date: 11/20/2019; User: Jch

NW

SE

-1

-2

-3

-4

Depth (Meters)

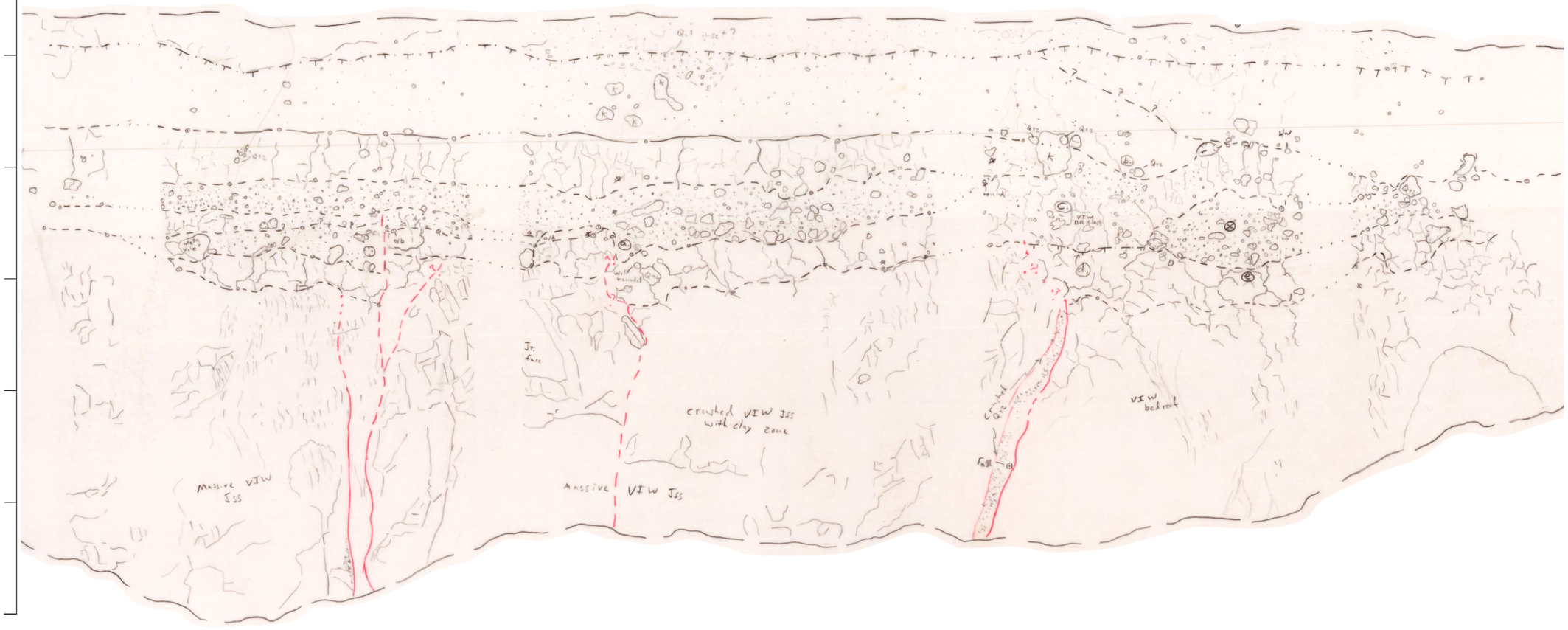

Scale: 1” = 0.5 m, no vertical exaggeration

22 24 25 26 27 28 29

Horizontal Distance (Meters)

Field Log of Trench LCI-T2
North Wall

EBMUD PARDEE DAM FAULT HAZARD STUDY

Lettis Consultants International, Inc. | Figure **A-2**

File path: S:\1772_Pardee\Figures\November Report Figures\Fig_A_2_Trench_T2_N_maylar.ai; Date: 11/20/2019; User: Jch

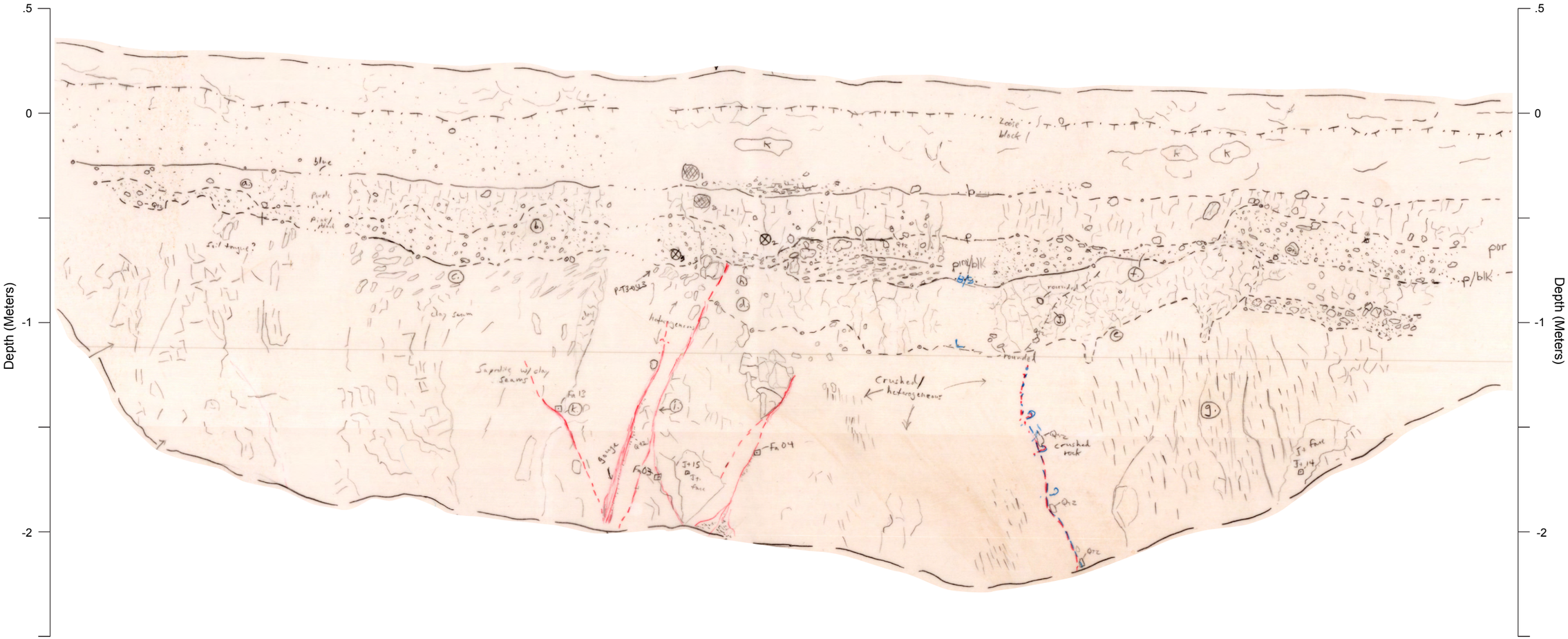

Field Log of Trench LCI-T3
North Wall

EBMUD PARDEE DAM FAULT HAZARD STUDY

Lettis Consultants International, Inc. | Figure **A-3**

File path: S:\1772_Pardee\Figures\November Report Figures\Fig_A_3_Trench_T3_N_maylar.ai; Date: 11/20/2019; User: Jch

Appendix B

Results of Bulk Radiocarbon Analysis

BetaCal 3.21

Calibration of Radiocarbon Age to Calendar Years

(High Probability Density Range Method (HPD): INTCAL13)

(Variables: d13C = -25.8 o/oo)

Laboratory number **Beta-536775**

Conventional radiocarbon age **4780 ± 30 BP**

95.4% probability

(95.4%)	3642 - 3519 cal BC	(5591 - 5468 cal BP)

68.2% probability

(60.4%)	3587 - 3530 cal BC	(5536 - 5479 cal BP)
(7.8%)	3636 - 3628 cal BC	(5585 - 5577 cal BP)

P-T2-BULK1

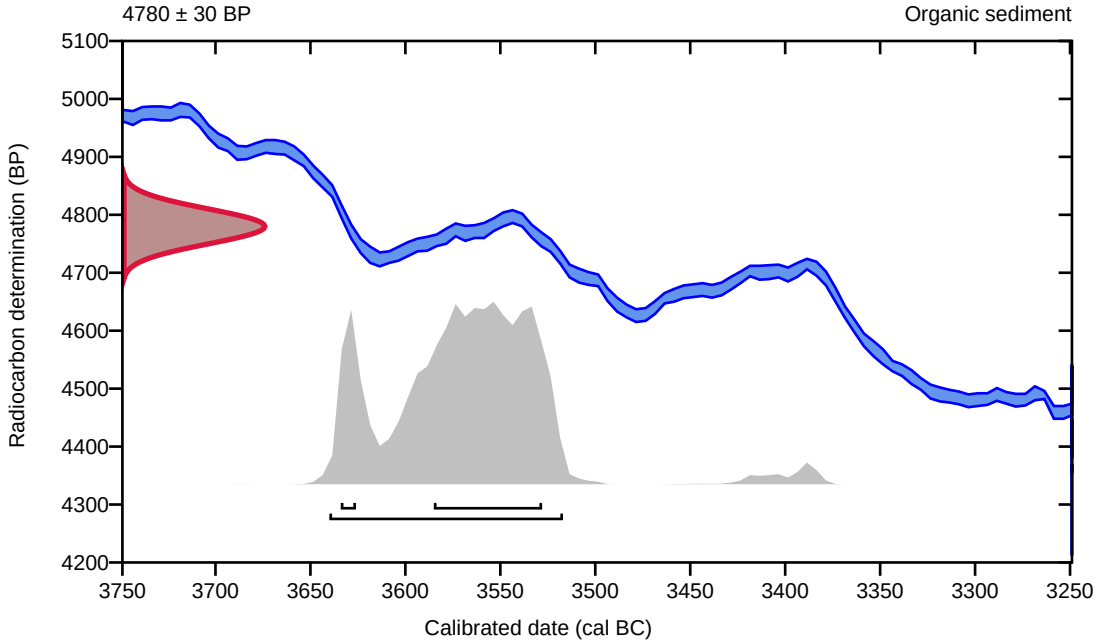

Database used

INTCAL13

References

References to Probability Method

Bronk Ramsey, C. (2009). Bayesian analysis of radiocarbon dates. Radiocarbon, 51(1), 337-360.

References to Database INTCAL13

Reimer, et.al., 2013, Radiocarbon55(4).

Beta Analytic Radiocarbon Dating Laboratory

4985 S.W. 74th Court, Miami, Florida 33155 • Tel: (305)667-5167 • Fax: (305)663-0964 • Email: beta@radiocarbon.com

Appendix C

Background Source Zone Model, Hazard Input Document (HID)

Appendix C
Background Source Zone Model, Hazard Input Document (HID)
EBMUD Pardee Dam

Prepared for:

East Bay Municipal Utility District
375 11th Street
MS 610
Oakland, CA 94607

Prepared by:

Lettis Consultants International, Inc.

January 31, 2020

TABLE OF CONTENTS

LIST OF TABLES

LIST OF FIGURES

ATTACHMENTS

1.0 INTRODUCTION

This Hazard Input Document (HID) describes the areal seismic source zone model ("background model") developed for probabilistic seismic hazard analysis (PSHA) for East Bay Municipal Utility District's (EBMUD) Pardee Dam. This background model encompasses the 150 km radius surrounding Pardee Dam (Figure 1-1).

The purpose of this HID is to provide the hazard analyst(s) with a complete description of how to implement the background model and a listing of all the model components. The HID is a succinct summary of what is in the background model and provides the background logic tree parameters (nodes), alternative values (branches), and their weights (relative likelihood of each branch value being correct).

Although the intention of this HID is to provide complete instructions for implementing the background model, we understand that the hazard analyst reviewing this document may find that it is missing information or that the instructions are unclear, ambiguous, or questionable. In order for the HID to be an effective tool for documenting the hazard calculation, we request that the hazard analysts review the HID carefully prior to running the model. We request that the hazard analysts note any of the following:

- Instances where the HID did not provide a complete instruction
- Instances where the HID instructions are vague or unclear
- Instances where the model implemented by the hazard analysts deviated from the HID

In any of the above cases, we recommend that the hazard analysts document what decisions were made and the values used in the model. With the exception of Section 2.5, the HID does not justify the technical basis for the model approach, parameters, values, or weights.

2.0 AREAL (BACKGROUND) SEISMIC SOURCE ZONES

Background earthquakes are those events that do not appear to be associated with known geologic structures. These earthquakes occur on crustal faults that exhibit no surficial expression (buried faults) or are unmapped due to inadequate studies. We model the hazard from background earthquakes through six areal source zones. Figure 2-1 shows the source zones as well as a 150 km radius buffer around Pardee Dam. Each source zone has a unique ID that is used in the Haz45 fault file *PardeeFlt_v3.DAT* and grid files (Figure 2-1 and Table 2-1). The Haz45 fault file is provided as Attachment 1, and the grid files are provided as Attachment 2. The six areal source zones are delineated based on similar seismotectonic characteristics such as style(s) of faulting, seismogenic thickness, estimated maximum earthquake magnitude (for earthquakes not occurring on the fault sources within that areal source zone), and historic and instrumental seismicity rate. The six areal source zones are: Coast Ranges (CR) Zone, Coast Ranges/Great Valley Boundary (CRGVB) Zone, Mammoth/Long Valley/Mono-Inyo Volcanic

(MLVMI) Zone, Sierra Nevada/Great Valley (SNGV) Zone, Southern Sierra/Tehachapi (SST) Zone, and the Walker Lane (WL) Zone (Table 2-1).

The logic tree structure to capture epistemic uncertainty in the background model is identical for all six source zones. This structure is shown in Figure 2-2. Each source zone is modeled in the *PardeeFlt_v3.DAT* fault file with nine "seg models". These nine seg models, which represent epistemic uncertainty in the recurrence parameters, are grouped based on the approach to characterizing the spatial distribution of seismicity. The first approach (seg model one) models uniform seismic source zones, where earthquakes are assumed to occur randomly and uniformly within each zone. The second approach (seg models two through nine) models gridded seismicity, where locations of past seismicity are assumed to be likely locations of future seismicity (stationarity; captured by smoothing the catalog seismicity and having spatially variable rates defined over a grid of points). In both approaches, eight sets of recurrence parameters are implemented. Note that for the uniform seismic source zone branch, all eight sets of recurrence parameters are within the uniform seg model one. For the gridded seismicity approach, each set of eight recurrence parameters requires its own seg model given the format of HAZ45.2. The resulting weights for each of these eight seg models (two through nine) are 0.0625, which is the weight of the gridded seismicity branch (0.5) times the weight of the recurrence parameters (0.125). These recurrence parameters and how they were calculated are described further in Sections 2.4 and 2.5.

In total, the background model contains 240 unique paths through four nodes the logic tree: two approaches to modeling the spatial distribution of seismicity, three seismogenic thicknesses, five maximum magnitudes, and eight sets of recurrence parameters (Figure 2-2). The logic tree is constructed such that there are no correlations between parameters other than the combinations of recurrence parameters (*b*-value and rate at M_{min} and greater).

The logic tree nodes in Figure 2-2 are discussed below in Sections 2.1 through 2.4.

2.1 Style of Faulting

The style of faulting for each source zone is defined by the frequency of strike-slip, normal, and reverse fault types. Although the style of faulting in the source zones is considered aleatory, the frequency of strike-slip, normal, and reverse fault types is modeled epistemically in the fault file, where frequencies are treated as weights. These values are provided in the *PardeeFlt_v3.DAT* fault file and Table 2-1.

2.2 Depth to Top, Seismogenic Thickness, and Depth PDF

Five of the six source zones are modeled with a depth to the top of rupture of 2 km. The Mammoth/Long Valley/Mono-Inyo Volcanic Zone is modeled with a depth to top of rupture of 1 km. Each individual source zone has three weighted values for seismogenic thickness in units of kilometers. These values are provided in the *PardeeFlt_v3.DAT* fault file and Table 2-1 and are based on the depth distribution of catalog seismicity. For all zones, the three seismogenic thicknesses are assigned the same weights of [0.3], [0.4], and [0.3], with the second listed seismogenic thickness value always representing the preferred value. Note that the maximum

depth of rupture is equal to the seismogenic thickness plus the depth to the top of rupture. The depth probability density function (PDF) modeled for all source zones is a uniform distribution.

2.3 Magnitude-Frequency Distribution and Maximum Magnitudes

The magnitude PDF for all source zones is a doubly truncated exponential distribution, which requires a definition of minimum magnitude (M_{min}), maximum magnitude (M_{max}), *b*-value, and rate (at M_{min} and greater). For all source zones, M_{min} is fixed at 5.0. Each source zones has five branch values for M_{max} with weights of [0.101], [0.244]. [0.310], [0.244], and [0.101] (Table 2-1). The M_{max} values are provided in the *PardeeFlt_v3.DAT* fault file.

2.4 Recurrence Parameters and Spatial Distribution of Seismicity

Recurrence parameters (*b*-values and rates) were calculated using the historical seismicity record and the program ABSMOOTH. Each source zone has eight alternative sets of recurrence parameters based on the eight alternative "realizations" calculated from ABSMOOTH (Figure 2-2). The same eight sets of recurrence parameters are implemented in the uniform seismicity approach and the gridded seismicity approach. The recurrence parameter values and weights are described in Section 2.5.

In the gridded seismicity approach, each of the eight sets of recurrence parameters consists of *b*-values and rates for 0.2-degree cells (except for the Mammoth/Long Valley/Mono-Inyo Volcanic Zone, which used 0.1-degree cells) across the background source zone extent. In the uniform seismicity approach, the same eight alternative *b*-values and rates for each source zone are implemented; however, unlike the gridded seismicity approach, the rates are allocated uniformly (equally) across a given source zone. The eight *b*-values and rates for the uniform seismicity and gridded seismicity approaches are provided in the *PardeeFlt_v3.DAT* fault file and the eight sets of grid files for the gridded seismicity approach for the six source zones (48 total files) are provided in Attachment 2.

2.5 Commentary on ABSMOOTH Calculations and Earthquake Catalog Processing

Because the ABSMOOTH program is not widely used, we describe the program and its implementation briefly below. We also describe the processing of the earthquake catalog used as one of the inputs to the ABSMOOTH program. This commentary is outside the narrow scope of the HID, and may be skipped by the hazard analyst if desired.

For each source zone, we estimated recurrence for background earthquakes for the gridded and the uniform seismicity approaches using the program ABSMOOTH. The ABSMOOTH program was developed by Dr. Gabriel Toro (LCI) for characterizing areal seismic source zones in the Central and Eastern United States (CEUS) as part of a SSHAC Level 3 Project sponsored by the Electric Power Research Institute (EPRI), the U.S. Department of Energy (DOE), and the U.S. Nuclear Regulatory Commission (NRC). Documentation of the software is provided in the CEUS SSHAC Level 3 Report (EPRI/DOE/NRC, 2012). The ABSMOOTH program computes eight realizations that result in eight unique *b*-values applicable to the entire source zone. Then,

ABSMOOTH divides the source zone into cells of a specified size (0.2-degree cells for all source zones except for the Mammoth/Long Valley/Mono-Inyo Volcanic Zone, which used 0.1-degree cells) and calculates the rate of earthquakes of magnitude greater than or equal to M_{min} in each cell. The rate is calculated using the likelihood function of the data in that cell along with penalty functions that smooth the cell-to-cell variation in the rate. The program outputs both the eight realizations of the recurrence parameters and the mean result in order to characterize epistemic uncertainty in both the *b*-value applicable to the source zone and the individual cell rates (EPRI/DOE/NRC, 2012). This approach is based on Markov Chain Monte Carlo techniques to generate multiple realizations from a multi-dimensional probability distribution—in this case, the *b*-value, rate, and uncertainty in those parameters. The eight alternative maps of *b*-value and cell rates are weighted equally (with [0.125] weight each) and represent the central tendency and statistical uncertainty in the recurrence parameters (EPRI/DOE/NRC, 2012).

The *b*-values and total rates (sum of the rates in all cells for a given realization and source zone) are provided in the *PardeeFlt_v3.DAT* fault file for both the gridded and uniform seismicity approaches. In the gridded seismicity approach, total rates are allocated exactly as calculated in the ABSMOOTH program across 0.2 or 0.1-degree grids (Attachment 2). In this approach, although each cell will have the same *b*-value, the rate will differ between cells. In the uniform seismicity approach, the total rates are allocated equally across a given source zone, such that the rate in one part of the zone will equal the rate in any other part of the zone.

The recurrence parameters for the source zones were developed using the historical seismicity record for the period of 1781 through November 2017, spanning almost 237 years. This catalog was assembled from the previous catalog compilations of Felzer (2013) and the USGS Advanced National Seismic Network (ANSS; USGS, 2017). The Felzer (2013) compilation spans the period of 1781 through April 2012, and the USGS ANSS compilation spans the period of May 2012 through November 2017. The majority of the earthquakes in the catalog had magnitudes reported either as duration magnitude (M_D), Richter local magnitude (M_L), or coda magnitude (M_C); other magnitude types in the catalog include moment magnitude (**M**), body wave magnitude (m_b), hand magnitude (M_h), or unknown magnitude type. The magnitudes of all events were converted to a uniform **M** using the same scaling relations applied in APS (2015). In order to account for bias due to rounding of magnitude values (Felzer, 2008), values of N* were calculated for each event in the catalog following Arabasz et al. (2016).

The catalog was declustered using the Gardner and Knopoff (1974) algorithm to remove foreshocks and aftershocks. However, fault-related crustal earthquakes that should be removed to avoid double-counting the resulting hazard was not performed due to the difficulty of identifying such events because of location uncertainty and defining the down-dip geometries of the fault sources. Hence, there is likely some double-counting and the hazard from background earthquakes may be conservative.

The completeness intervals for the catalog in each areal source zone were estimated by considering the completeness intervals of URS (2012) and AMEC (2010), which were estimated

based on settlement history, seismographic installation dates, and by using Stepp plot analyses (Stepp, 1972). Completeness estimates and number of earthquakes within each interval for each areal source zone are listed in Table 2-2. The completeness intervals and an M_{max} uncertainty characterization are required inputs for the ABSMOOTH program.

As stated in Section 2.4, for each source zone, eight realizations of recurrence parameters were calculated, resulting in eight sets of *b*-values and rates (Table 2-3; Figure 2-2). The eight *b*-values and rates are provided in the *PardeeFlt_v3.DAT* fault file and the eight sets of grid files for the six source zones (48 total files) are provided in Attachment 2.

3.0 SPECIAL INSTRUCTIONS AND ADDITIONAL NOTES

This HID does not provide a ground motion characterization model or recommendations on which ground motion models to implement. Therefore, all source zones in the Haz45 fault file are modeled with the same attenuation type. The hazard analyst should therefore review and adjust the atten type parameter accordingly based on the ground motion models selected and implemented in a hazard input file.

In addition to the six source zones, the Haz45 fault file provided as Attachment 1 includes seven fault sources. The seismic source characterization of these fault sources is provided in Section 5 of the main Fault Rupture Hazard and Seismic Source Characterization Report for Pardee Dam.

The background seismic source zones developed for Pardee Dam in this project are part of a site-specific source characterization, in that they are based directly on the observed rates of historical seismicity in the region surrounding Pardee Dam. Site-specific hazard results based on the site-specific source characterization may differ from the results of the National Seismic Hazard Maps (NSHMs) developed for the continental United States by the USGS. The seismic source model for California in the 2014 NSHM is based on the UCERF3 model (Petersen et al., 2014; Field et al., 2013). The equivalent to areal seismic source zones in the UCERF3 model is the gridded seismicity-source model, which is used as a source of hazard from “background” earthquakes in the 2014 NSHMP. This model is an integrated element in the overall UCERF3 model that solves for the historically measured, state-wide rate of earthquakes as a combination of (1) on-fault earthquake rates, with rates determined by the “grand inversion” (Page et al., 2014), and (2) off-fault earthquake rates that are allocated to the gridded seismicity source zone. The overall rates of earthquakes allocated to the gridded source zones, therefore, do not directly depend on the observed historical occurrence and rates of earthquakes from the Pardee Dam vicinity or region (i.e., the observed rates of earthquakes within each areal source zone), but rather are based on a state-wide rate of earthquakes and a state-wide solution of earthquake rates modeled to occur on fault sources. For this reason alone, the 2014 NSHMP gridded seismicity-source model is judged to be inappropriate for use in a site-specific PSHA study in the absence of extensive testing and understanding of how the UCERF3-predicted rates of seismicity compare to observed rates in the Pardee Dam study region.

4.0 REFERENCES CITED

AMEC, 2010, Seismic Hazard Assessment for Northern and Eastern Hydro Divisions, Southern Sierra Nevada, California. Unpublished consulting report submitted to Southern California Edison.

Arabasz, W.J., Pechmann, J.C., and Burlacu, R., 2016, A uniform moment magnitude earthquake catalog and background seismicity rates for the Wasatch Front and surrounding Utah region—Appendix E, in Working Group on Utah Earthquake Probabilities (WGUEP), 2016, Earthquake probabilities for the Wasatch Front region in Utah, Idaho, and Wyoming: Utah Geological Survey Miscellaneous Publication 16-3, p. E1-E126.

Arizona Public Service (APS), 2015, Palo Verde Nuclear Generating Station Seismic Source Characterization, Technical Report prepared by Lettis Consultants International for Westinghouse Electric Company.

EPRI/DOE/NRC (Electric Power Research Institute [EPRI], U.S. Department of Energy [DOE], and U.S. Nuclear Regulatory Commission [NRC]), 2012, Technical report—Central and Eastern United States seismic source characterization for nuclear facilities, v. 1: Palo Alto, California, http://www.ceus-ssc.com/index.htm.

Felzer, K.R., 2008, Calculating California seismicity rates: U.S. Geological Survey Open File Report 2007-1437-I, 41 p.

Felzer, K.R., 2013, The UCERF3 Earthquake Catalog, Appendix K in Field, E.H., Biasi, G.P., Bird, P. et al., eds., Uniform California Earthquake Rupture Forecast, Version 3: U.S. Geological Survey Open-File Report 2013-1165, CGS Special Report 228, and Southern California Earthquake Center Publication 1792.

Field, E.H., Biasi, G.P., Bird, P., Dawson, T.E., Felzer, K.R., Jackson, D.D., Johnson, K.M., Jordan, T.H., Madden, C., Michael, A.J., Milner, K.R., Page, M.T., Parsons, T., Powers, P.M., Shaw, B.E., Thatcher, W.R., Weldon, R.J., II, and Zeng, Y., 2013, Uniform California earthquake rupture forecast, version 3 (UCERF3) - The time-independent model, U.S. Geological Survey Open-File Report 2013–1165, California Geological Survey Special Report 228, and Southern California Earthquake Center Publication 1792, 97 p

Gardner J.K., and Knopoff, L., 1974, Is the sequence of earthquakes in southern California, with aftershocks removed, Poissonian?, Bulletin of the Seismological Society of America, v. 64, p. 1363-1367.

Page, M.T., Field, E.H., Milner, K.R., and Powers, P.M., 2014, The UCERF3 grand inversion: Solving for the long-term rate of ruptures in a fault system: Bulletin of the Seismological Society of America, v. 104, p. 1181–1204.

Petersen, M.D., Moschetti, M.P., Powers, P.M., Mueller, C.S., Haller, K.M., Frankel, A.D., Zeng, Yuehua, Rezaeian, Sanaz, Harmsen, S.C., Boyd, O.S., Field, Ned, Chen, Rui, Rukstales, K.S., Luco, Nico, Wheeler, R.L., Williams, R.A., and Olsen, A.H., 2014, Documentation for the 2014 update of the United States national seismic hazard maps: U.S. Geological Survey Open-File Report 2014–1091, 243 p., https://dx.doi.org/10.3133/ofr20141091.

Stepp, J.C., 1972, Analysis of completeness of the earthquake sample in the Puget Sound area and its effect on statistical estimates of earthquake hazard: Proceedings of the International Conference on Microzonation, v. 2, p. 897-910.

URS Corporation, 2012, Update of the Probabilistic and Deterministic Seismic Hazard Analyses of Success Dam, California, unpublished report submitted to U.S. Army Corps of Engineers.

USGS, 2017, ANSS Comprehensive Earthquake Catalog (ComCat): url https://earthquake.usgs.gov/earthquakes/search/; site accessed 11/30/2017.

TABLES

Table 2-1: Areal (Background) Seismic Source Zones Characterized for Pardee Dam

SOURCE ZONE	UNIQUE ID	STYLE OF FAULTING [FREQUENCY]	SEISMOGENIC THICKNESS	DEPTH TO TOP	M_{MAX} DISTRIBUTION
Coast Ranges	CR	Strike-slip [60%] Normal [0%] Reverse [40%]	10 km [0.3] 13 km [0.4] 16 km [0.3]	2 km [1.0]	6.6 [0.101] 6.8 [0.244] 7.0 [0.310] 7.2 [0.244] 7.4 [0.101]
Coast Ranges-Great Valley Boundary	CRGVB	Strike-slip [33%] Normal [0%] Reverse [67%]	15 km [0.3] 18 km [0.4] 23 km [0.3]	2 km [1.0]	6.6 [0.101] 6.8 [0.244] 7.0 [0.310] 7.2 [0.244] 7.4 [0.101]
Mammoth/Long Valley/Mono-Inyo Volcanic	MLVMI	Strike-slip [50%] Normal [50%] Reverse [0%]	7 km [0.3] 10 km [0.4] 13 km [0.3]	1 km [1.0]	6.5 [0.101] 6.625 [0.244] 6.75 [0.310] 6.875 [0.244] 7.0 [0.101]
Sierra Nevada/Great Valley	SNGV	Strike-slip [40%] Normal [40%] Reverse [20%]	24 km [0.3] 27 km [0.4] 31 km [0.3]	2 km [1.0]	6.0 [0.101] 6.25 [0.244] 6.5 [0.310] 6.75 [0.244] 7.0 [0.101]
Southern Sierra/Tehachapi	SST	Strike-slip [20%] Normal [50%] Reverse [30%]	13 km [0.3] 16 km [0.4] 20 km [0.3]	2 km [1.0]	6.6 [0.101] 6.8 [0.244] 7.0 [0.310] 7.2 [0.244] 7.4 [0.101]
Walker Lane	WL	Strike-slip [67%] Normal [33%] Reverse [0%]	10 km [0.3] 13 km [0.4] 16 km [0.3]	2 km [1.0]	6.6 [0.101] 6.8 [0.244] 7.0 [0.310] 7.2 [0.244] 7.4 [0.101]

Table 2-2: Completeness Estimates and Earthquake Count in Each Magnitude Interval for the Modeled Areal Source Zones

Magnitude Range (M)	Beginning of Usable Period (yr)	Earthquake Count
Coast Ranges Zone		
3.00 – 3.49	1970	550
3.50 – 3.99	1950	197
4.00 – 4.49	1940	187
4.50 – 4.99	1920	75
5.00 – 5.49	1880	22
5.50 – 5.99	1880	19
6.00 – 6.49	1880	10
≥ 6.50	1880	4
Coast Ranges-Great Valley Boundary Zone		
3.00 – 3.49	1970	170
3.50 – 3.99	1950	54
4.00 – 4.49	1940	51
4.50 – 4.99	1920	15
5.00 – 5.49	1880	5
5.50 – 5.99	1880	1
6.00 – 6.49	1880	11
≥ 6.50	1880	1
Mammoth/Long Valley/Mono-Inyo Volcanic Zone		
3.00 – 3.49	1967	91
3.50 – 3.99	1960	39
4.00 – 4.49	1932	19
4.50 – 4.99	1932	4
5.00 – 5.49	1932	3
5.50 – 5.99	1932	2
6.00 – 6.49	1900	1

Magnitude Range (M)	Beginning of Usable Period (yr)	Earthquake Count
Sierra Nevada/Great Valley Zone		
3.00 – 3.49	1964	53
3.50 – 3.99	1964	14
4.00 – 4.49	1964	10
4.50 – 4.99	1932	2
5.00 – 5.49	1900	0
5.50 – 5.99	1870	2
6.00 – 6.49	1850	0
Southern Sierra/Tehachapi Zone		
3.00 – 3.49	1964	131
3.50 – 3.99	1952	49
4.00 – 4.49	1932	35
4.50 – 4.99	1932	19
5.00 – 5.49	1900	9
5.50 – 5.99	1870	5
6.00 – 6.49	1870	1
≥ 6.50	1850	1
Walker Lane Zone		
3.00 – 3.49	1967	463
3.50 – 3.99	1960	222
4.00 – 4.49	1932	197
4.50 – 4.99	1932	78
5.00 – 5.49	1932	46
5.50 – 5.99	1932	11
6.00 – 6.49	1900	12
≥ 6.50	1870	3

Table 2-3: Recurrence Parameters for the Areal Source Zones

REALIZATION	*b*-VALUE	N(M≥5)	WEIGHT
Coast Ranges Zone			
1	0.79	0.46768	[0.125]
2	0.78	0.47191	[0.125]
3	0.80	0.43950	[0.125]
4	0.79	0.47344	[0.125]
5	0.78	0.46023	[0.125]
6	0.76	0.51697	[0.125]
7	0.83	0.38904	[0.125]
8	0.82	0.39502	[0.125]
Coast Ranges-Great Valley Boundary Zone			
1	0.88	0.06275	[0.125]
2	0.83	0.08145	[0.125]
3	0.79	0.09186	[0.125]
4	0.88	0.07020	[0.125]
5	0.83	0.08035	[0.125]
6	0.77	0.09897	[0.125]
7	0.84	0.08079	[0.125]
8	0.76	0.11057	[0.125]
Mammoth/Long Valley/Mono-Inyo Volcanic Zone			
1	0.83	0.05850	[0.125]
2	1.08	0.01920	[0.125]
3	0.95	0.03748	[0.125]
4	0.92	0.04255	[0.125]
5	0.98	0.03167	[0.125]
6	0.91	0.04300	[0.125]
7	0.90	0.04903	[0.125]
8	0.94	0.03379	[0.125]

REALIZATION	*b*-VALUE	N(M≥5)	WEIGHT
Sierra Nevada/Great Valley Zone			
1	0.99	0.01961	[0.125]
2	0.84	0.03232	[0.125]
3	1.21	0.00473	[0.125]
4	0.96	0.01834	[0.125]
5	1.01	0.01429	[0.125]
6	0.93	0.02160	[0.125]
7	1.03	0.01219	[0.125]
8	0.87	0.02589	[0.125]
Southern Sierra/Tehachapi Zone			
1	0.78	0.11506	[0.125]
2	0.79	0.09883	[0.125]
3	0.79	0.09524	[0.125]
4	0.77	0.10360	[0.125]
5	0.78	0.10901	[0.125]
6	0.67	0.19083	[0.125]
7	0.80	0.08824	[0.125]
8	0.71	0.15089	[0.125]
Walker Lane Zone			
1	0.69	0.76822	[0.125]
2	0.70	0.75437	[0.125]
3	0.68	0.75404	[0.125]
4	0.69	0.81534	[0.125]
5	0.67	0.86059	[0.125]
6	0.65	0.87692	[0.125]
7	0.68	0.77292	[0.125]
8	0.68	0.77349	[0.125]

FIGURES

Figure 1-1. Pardee Dam background model study region indicated by 150 km radius bold line.

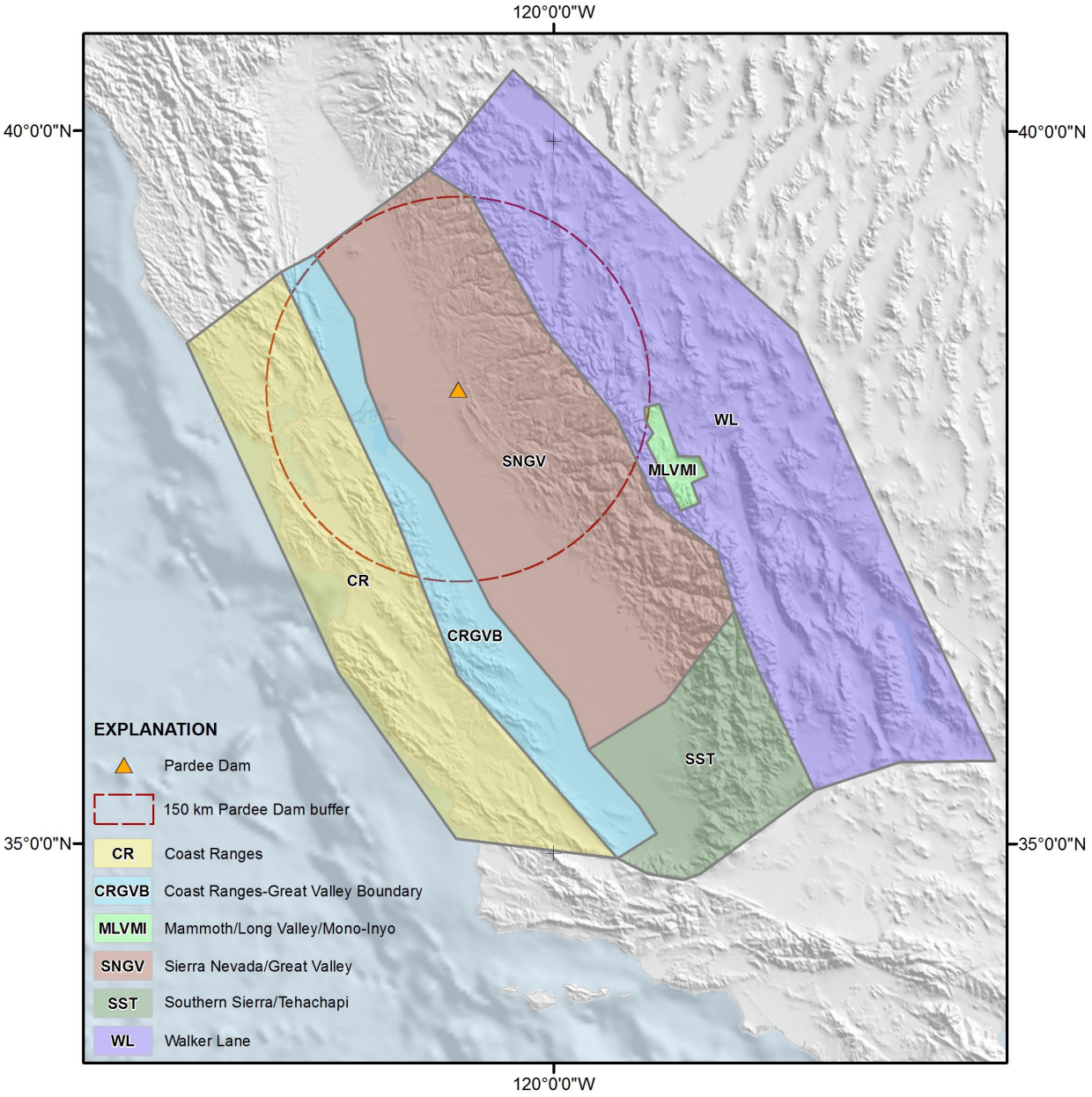

Figure 2-1. Areal (background) seismic source zones modeled for Pardee Dam.

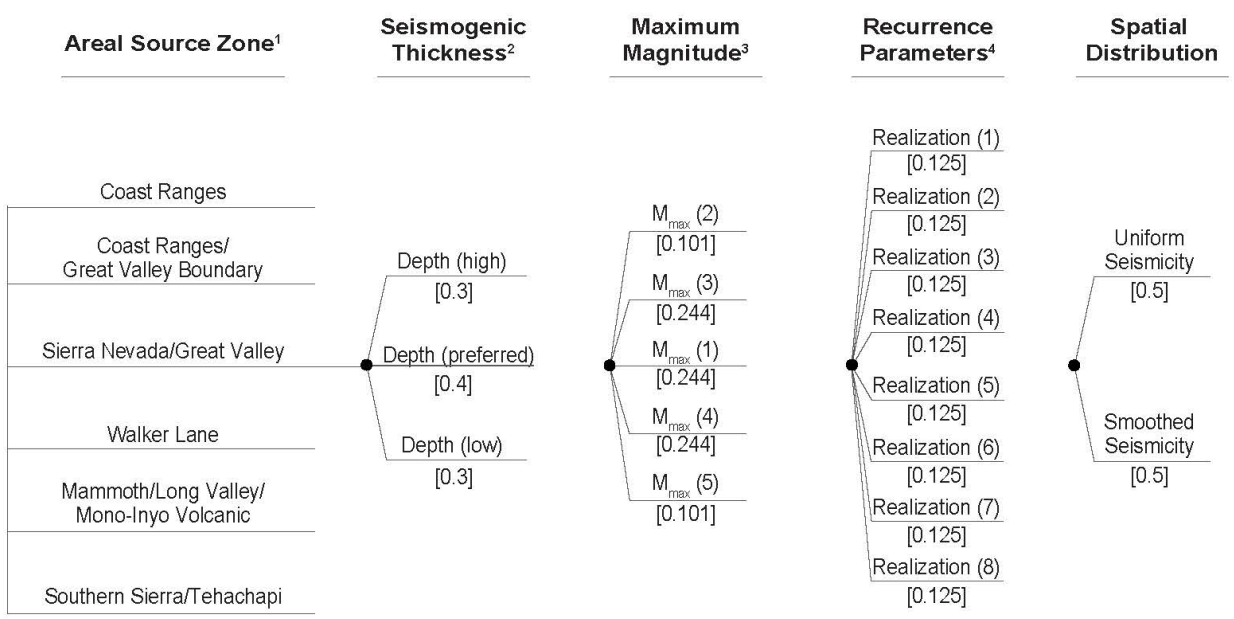

Notes:

[1]See Table 2-1 for style of faulting for each areal source zone.
[2]See Table 2-1 for seismogenic thickness values and depth to top for each areal source zone.
[3]See Table 2-1 for M_{max} values for each areal source zone.
[4]See Table 2-3 for *b*-value and rate (**M**≥5) for each realization and areal source zone.

Figure 2-2. Logic tree structure for the background seismic source zones.

Appendix D

David P. Schwartz, Ph.D.

External Peer Review of Paleoseismic Trenching: Letter Report on Chapter 4 of LCI Pardee Dam Report

To: John Baldwin
Lettis Consultants International, Inc.
1000 Burnett Ave., Suite 350
Concord, CA 94520

From: David P. Schwartz, Ph.D.
1015 McCauley Rd.
Danville, CA 94526

Date: January 10, 20120

Subject: Letter Report on Chapter 4 of LCI Pardee Dam Report

This letter report represents my response to your request to review Chapter 4 of the Lettis Consultants International (LCI) Pardee Dam report to the East Bay Municipal Utility District (EBMUD). This section of the report contains descriptions of the stratigraphy and structure, and their interrelations, in three trenches across the Water Peak fault . I visited trenches LCI-T1 and LCI-T2 (Sites 5 and 6, respectively) on July 24, 2019 and trench LCI-T3 (Site 6) on August 12, 2019.

One of the key questions is the age of deposits either involved in faulting, or overlying the faults, that can be used to date the timing of fault displacement. The Report notes that faulted and unfaulted alluvial and colluvial deposits were sampled for organics (charcoal, seeds) for radiocarbon dating but none was found. The deposits were also sampled for OSL (optical stimulation luminescence) dating, which perhaps could be done at a later date. To date the deposits, LCI developed detailed depositional unit and pedogenic descriptions and correlated these with a well-recognized regional soil chronosequence in the Sierra Nevada Foothills. Comparisons were also made to the deposits and soils in US Army Corps of Engineers (USACE) trench T-3 (Figure 3.2). All correlations are summarized in Table 4.1

Faulting:

The report presents photomosaics showing the stratigraphy and structure, along with descriptions of the alluvial/colluvial units and soils), on the south walls of the three trenches on Plates 1-3. Undrafted logs are provided in Appendix A.

Based on these relations in trenches LCI-T2 and LCI-T3, LCI concludes that the Waters Peak fault at this trench locality is Quaternary-active. To account for uncertainties in trench interpretations three faulting models are developed. These are: a single-event on faults F1 and F2 that displaces unit 200 (Model 1); a single event on fault F2 in trench LCI-2 that displaces units 200 and 500 with fault F1 not clearly extending into Quaternary deposits (Model 2); and a two-event scenario on fault F2 in trench LCI-T2 that displaces all deposits through unit 600, with the vertical displacement of 600 being smaller than the prior event (Model 3). No definitive

evidence of Quaternary of faultng was found in LC-T1; if it had occurred along one of the identified bedrock faults it likely predated unit 500 (the oldest deposit in the trench).

Perspective:

From my perspective the three models cover the range of faulting possibilities that reflects the ambiguities in field relations. The excavation of trench LCI-T3 proved to be important in narrowing the possible faulting sequence. The overall preferred LCI interpretation, which is termed *probable*, is Model 1, a single event (the same rupture) on faults F1 and F2.

Having looked at these relations in the trenches I would lean toward Model 1. Unit 200 was clearly displaced in in LCI-T2 and LCI-T3. There was much discussion in trench LCI-T2 about the possible upward extension of faulting into unit 500 or higher at station 27.75. At the time of my trench visits I could not identify any structural signature that indicated fault slip at that location above unit 200, nor did I observe fault texture features that would suggest recurrent faulting in the Quaternary deposits.

One of the issues discussed in the report was the apparent sense of slip, which was down-to-the west with as suggestion of a reverse component. Based on this observation, the report suggests the possibility of a strike-slip component to the most recent event. I think this is a distinct possibility. There are no historical ruptures in this part of the Foothills for reference and paleoseismic interpretations can have significant uncertainties, so there isn't a hard and fast rule that fault rupture, particularly in the Quaternary, must be purely extensional. The inclusion of a strike-slip component could certainly produce variations in surface rupture geometry.

Overall, the Report is a thorough and detailed effort to define the timing and rupture behavior of the Water Peak fault at sites 5 and 6.

A few editing comments:

1. The inset photo on Plate 2 labels T3 as T2.
2. On Plate 2, why are the upper two strands of F2 queried? Not mentioned in the text. Also what is the queried shear to the east of F2? It should be noted in the text.
3. I've attached a Word file with some additional edits on pages 45-48.